CUKUROVA UNIVERSITY
INSTITUTE OF NATURAL AND APPLIED SCIENCES

MSc THESIS

Upgrading of a Low-grade Iron Ore using a Dry Roll Magnetic Separator

Abdourahman HASSAN BRAHIM FARISS

Mining Engineering Department

June 2023

CUKUROVA UNIVERSITY

INSTITUTE OF NATURAL AND APPLIED SCIENCES

MSc THESIS APPROVAL

Upgrading of a Low-grade Iron Ore using a Dry Roll Magnetic Separator

Abdourahman HASSAN BRAHIM FARISS

Mining Engineering Department

This master's Thesis was evaluated by the following Jury Members on 06/20/2023 and was approved by majority of votes.

Jury : Prof. Dr. Oktay BAYAT …………

: Assoc. Prof. Dr. Mahmut ALTINER (Advisor) …………

: Assist. Prof. Dr. Arman EHSANI …………

This Thesis was written in the Department of Mining Engineering Department, Institute of Natural and Applied Sciences.

Thesis Number:

Prof. Dr. Sadık DİNÇER
Director of the Institute of Natural and Applied Sciences

This work was supported by the Çukurova University Research Fund Project
Project ID: FYL-2022-14903

CONTENTS

CUKUROVA UNIVERSITY
INSTITUTE OF NATURAL AND APPLIED SCIENCES

MSc THESIS

Upgrading of a Low-grade Iron ore using a Dry Roll Magnetic Separator

Abdourahman HASSAN BRAHIM FARISS

Advisor: Assoc. Prof. Dr. Mahmut ALTINER
Co-Advisor: Dr. Ali Can OZDEMIR

Department of Mining Engineering

ABSTRACT

In this thesis, it was aimed to investigate the beneficiation of a low-grade iron ore using a dry-roll magnetic separator. The ore (39.5% Fe content) used herein was collected from Feke/Adana region, Türkiye. The properties of the ore were characterized using Mineral Liberation Analysis (MLA), which determines the following properties: (i) modal mineralogy, (ii) calculated assay, (iii) elemental distribution, and (iv) mineral locking. It was determined that the ore was composed mainly of iron-oxide, quartz, chlorite, muscovite, plagioclase, and other minerals. Goethite and hematite minerals were observed in X-ray diffraction (XRD) measurement. The free surface and liberation degree of iron-oxide mineral detected by MLA were found to be 32.84% and 54.17%, respectively. In the magnetic separation test, the effect of particle size (-1+0.500mm, -0.500+0.300 mm, and -0.300+0.125 mm), splitter position (43° and 58°), cleaning stage (1 and 2), magnetic field (0.2 T and 0.4 T) on the recovery of the magnetic product from the ore was investigated. It was understood from the experimental results that the magnetic product (-1+0.500 mm) with an iron content of 67.67% can be obtained, but its recovery was not acceptable value (<30%). There was an inverse relationship determined between iron content and recovery value in the magnetic separation test. As such, an increase in the speed of conveyor led to an increase in the iron content in the magnetic product, and a decrease its recovery. The iron content of the magnetic product (-0.500+0.300 and -0.300+0.125 mm) cannot be reached to desired levels (>56% of Fe and >70% of recovery). The experimental results were evaluated by artificial neural network (ANN) method to determine the efficiency of the parameters on the beneficiation test. The Pearson (Pc) correlation showed that the parameters were ordered as follows: conveyor speed, particle size, and splitter position for iron content. Different scenarios were carried out to obtain the magnetic product with desired properties (>56% Fe). It was tried to conduct microwave treatment to increase the magnetic susceptibility (MH) of the ore. It was found that there was no need to perform microwave treatment on the ore with a size of <0.500 mm. Microwave treatment played a key role on the ore with a size of -1+0.500 mm and its MH value increased to 4.30 emu/g from 0.16 emu/g. However, the change in the ore with a size of <0.500 mm was negligible. Finally, a flowsheet was proposed to obtain a magnetic product (-1+0.500 mm) containing 56.65% iron and 90.01% of recovery, whereas the iron content of the mixed magnetic product (-0.500+0.300 mm and -0.300+0.125 mm) was 51.11% and recoveries over 90%.

Keywords: Artificial Neural Network (ANN), Dry-Roll Magnetic Separation, Low-grade Iron Ore, Mineral Liberation Analysis (MLA), Microwave Treatment

ÇUKUROVA ÜNİVERSİTESİ
FEN BİLİMLERİ ENSTİTÜSÜ

YÜKSEK LİSANS TEZİ

Düşük Tenörlü Demir Cevherinin Kuru-Roll Manyetik Ayırıcı ile Zenginleştirilmesi

Abdourahman HASSAN BRAHIM FARISS

Danışman: Doç. Dr. Mahmut ALTINER
İkinci Danışman: Dr. Ali Can ÖZDEMİR

Maden Mühendisliği Anabilim Dalı

ÖZ

Bu tez çalışmasında, düşük tenörlü demir cevherinin kuru manyetik ayırıcı ile zenginleştirilmesi amaçlanmıştır. Çalışmada kullanılan cevher (%39.5 Fe içeren) Feke/Adana bölgesinden alınmıştır. Mineral Serbestleşme Analizi (MLA) ile cevherin özellikleri karakterize edilmiştir: (i) modal mineraloji, (ii) hesaplanmış içerik, (iii) elementel dağılım, (iv) mineral bağlılığı. Cevherin başlıca olarak demir-oksit, kuvars, klorit, müskovit, plajiyoklaz ve diğer minerallerden oluştuğu belirlenmiştir. X-ışını difraksiyon (XRD) ölçümlerinde götit ve hematit mineralleri gözlenmiştir. MLA tarafından tespit edilen serbest yüzey ve özgürleşme derecesi demir-oxit minerali için sırasıyla %32,84 ve %54,17 olarak bulunmuştur. Manyetik ayırma deneylerinde, tane boyutu boyutu (-1+0,500 mm, -0,500+0,300 mm ve -0,300+0,125 mm), ayırıcı pozisyonu (43° ve 58°), temizleme aşaması (1 ve 2) ve manyetik alan şiddeti (0,2 T ve 0,4 T) gibi değişkenlerin etkisi araştırılmıştır. Deneysel sonuçlardan, %67.67 demir içeriğine sahip olan manyetik ürünün (-1+0.500 mm) elde edilebileceği, ancak geri kazanımının kabul edilebilir değer (<%30) olmadığı anlaşılmıştır. Manyetik ayırma deneyinde demir içeriği ile geri kazanım değeri arasında ters ilişki belirlenmiştir. Bu nedenle, konveyör hızının artması manyetik üründeki demir içeriğini artırırken geri kazanımını azaltmaktadır. Manyetik ürünün (-0,500+0,300 mm ve -0,300+0,125 mm) demir içeriği istenen seviyelere (>%56 Fe ve >%70 kazanım) ulaşamamıştır. Elde edilen deneysel sonuçlar, zenginleştirme testinde parametrelerin etkinliğini belirlemek için yapay sinir ağı (ANN) yöntemiyle değerlendirilmiştir. Pearson (Pc) korelasyonu, parametrelerin elde edilen manyetik ürünün demir içeriğine etkisi sırasıyla besleme hızı, parçacık boyutu ve ayırıcı pozisyonu şeklinde sıralandığını göstermiştir. Ayrıca, istenilen özelliklere sahip manyetik ürünü (>%56 Fe) elde etmek için farklı senaryolar denenmiştir. Cevherin manyetik duyarlılığını (MH) artırmak için mikrodalga işlemi uygulanmıştır. Tane boyutu 0.500 mm'nin altındaki cevherler üzerinde mikrodalga işlemi yapmanın gerekli olmadığı, buna karşın mikrodalga işlemi ile -1+0,500 mm boyutundaki cevherin MH değeri 0.16 emu/g'dan 4.30 emu/g'ya yükselmiştir.. Sonuç olarak, -1+0.500 mm boyutunda %56.65 demir ve %90.01 kazanım oranı içeren manyetik bir ürün elde etmek için bir akış şeması önerilmiştir. Ayrıca, karışık manyetik ürünün (-0,500+0,300 mm ve -0,300+0,125 mm) demir içeriği %51,11 ve >%90 kazanım verimi olarak belirlenmiştir.

Anahtar Kelimeler: Yapay Sinir Ağı (ANN), Kuru-Roll Manyetik Ayırma, Düşük Tenörlü Demir Cevheri, Mineral Serbestleşme Analizi (MLA), Mikrodalga Uygulama

GENİŞLETİLMİŞ ÖZET

Demir (Fe), Dünya kabuğunun %5'ine karşılık gelen en bol kaya oluşturan elementlerden biridir. Demir'nin diğer metallerle kolayca alaşım yapabilme özelliğinden dolayı güçlü bir metal olarak sınıflandırılabildiği iyi bilinmektedir. Bu nedenle, demir içeren alaşımlar otomobil, raptiyeler, demiryolları, binalar vb. gibi birçok üründe şekil verebilir. Dahası, çelik olarak demir metalinin kullanımı, diğer tüm metallerle karşılaştırıldığında yirmi kat daha fazladır. Demir oldukça yumuşak ve kolay işlenebilir, ancak erime noktası 1538 °C ve yoğunluğu 7.87 g/cm^3'tür. Karbonun indirgeme aşamasındaki varlığı, demir'i daha sert ve son derece çok yönlü olan çelik haline getirir.

Demir oksit içeren birçok mineral bulunmaktadır, örneğin hematit (%70, Fe_2O_3), goetit (%63, α-FeO(OH)), manyetit (%72, Fe_3O_4), limonit ($2Fe_2O_3 \cdot 2H_2O$) ve siderit (%48 Fe, $FeCO_3$). Bu minerallerden hematit ve manyetit demir ve çelik endüstrilerinde yaygın olarak kullanılmaktadır. Türkiye'de ithal edilen demir içeriği %50-62 aralığında olduğundan, zenginleştirme işlemlerine gerek yoktur. Kırma ve sınıflandırma işlemlerinden sonra bu demirler çelik üretim endüstrisinde kullanılmak üzere hazırdır. Bu bölgeler dışında, değerli demir ürünleri elde etmek için yüksek demir ve düşük kirletici madde içerikleriyle zenginleştirme stratejileri uygulanması gereklidir.

Her ne kadar Dünya genelinde yüksek maden üretimi olsa da, ilerleyen yıllarda demir konsantre talebini karşılamak için düşük kaliteli cevherler, atıklar ve atık kaya gibi çeşitli kaynaklardan demir cevheri çıkarılması ve geri kazanılması gerekmektedir. Yüksek kaliteli demir cevheri yatakları giderek daha az bulunur hale gelirken, düşük kaliteli demir cevheri yatakları daha bol ve yaygındır. Bu düşük kaliteli yataklar genellikle önemli miktarda demir içermekte, ancak diğer mineraller ve kirleticilerle karışık olduklarından geleneksel yöntemlerle işlenmeleri zor ve maliyetlidir.

Düşük kaliteli cevherden istenen özelliklere (yüksek demir ve düşük kirleticiler) sahip demir konsantresi elde etmek için birçok çalışma yapılmaktadır. Bu çalışmalarda, sürtünme ve yıkama, hidrosiklon, jig, yoğun ortam tamburları (DMD'ler), sallantılı masa ve Humphrey spiral gibi çeşitli yöntemler önerilmiştir. Bu yöntemlerle yüksek demir (%57'den yüksek) ve düşük kirletici içerikler (örneğin, Al, Si, Na, K, P) gibi gereksinimlere uygun demir konsantreleri hazırlanabilir. Bu yöntemlere ek olarak ve manyetik ayırma, manyetik özellik gösteren parçacıkları cevherden ayırmak için en basit yöntemlerden biridir.

Tüm bu bilgiler ışığında, bu tez çalışmasında Adana ili Feke ilçesinde bulunan eski bir demir madenin zenginleştirilmesi çalışmaları gerçekleştirilmiştir. Yaklaşık 100 kg numune ilgili sahadan alınarak maden bölümü laboratuvarlarına getirilmiştir. Alınan numune Feke'deki çalışması durdurulmuş olan bir maden ocağın depo sahasından farklı kısımlardan alınmıştır. Kırma, eleme, sınıflandırma işlemlerini takiben çalışmada kullanılmak üzere üç farklı (-1+0,500 mm, -0,500+0,300 mm, -0,300+0,125 mm) boyut dağılımına sahip temsili numuneler manyetik zenginleştirme testleri için hazırlanmıştır. Tane boyut dağılımına bağlı olarak hazırlanan numunelerin demir içerikleri sırasıyla %39,20 (-1+0,500 mm), %41.91 (-0,500+0,300 mm) ve %39,59 (-0,300+0,125 mm)'dir.

Zenginleştirme testleri öncesinde cevherin karakteristik özelliği mineral serbestleşme analizi (MLA) yapılarak belirlenmiştir. MLA analizine göre cevherin içerdiği demir değeri %40 olarak belirlenmiştir. Analiz ile cevherin içerdiği hematit ve götit mineralleri varlığı ayrı ayrı belirlenememiş olup, toplam demir-oksit değeri olarak hesaplanabilmiştir. XRD analizine göre cevherdeki hematit ve götit varlıkları tespit edilmiştir. Ayrıca, kuvars, apatit, kaolinit, muskovit, zirkon, klorit, Al_silikat, rutil, spinel_kromit ve plajioklaz gibi minerallerin varlığı da tespit edilmiştir. Cevherin bünyesindeki demir varlığının demir -oksit mineralleri ile ilgili olduğu, ancak az miktarda demir içeren klorit ve ilmenit minerallerinin tespit edilmiştir (toplam miktar: %1,79). Si açısından değerlendirildiğinde ise, Si içeren ana mineraller kuvars (%82,58) ve plajioklas (%10,44) olarak tespit edilmiştir. Demir-oksit mineralinin serbest yüzey miktarı %32,84 olarak belirlenmiştir. Serbestleşme derecesi ise %54,17'dir.

Kuru ortamda gerçekleştirilen manyetik zenginleştirme testlerinde bıçak açısı, bant hızı, tane boyutu, temizleme sayısı, manyetik alan şiddeti gibi parametrelerin etkileri ortaya konmuştur. İki farklı manyetik alanda (0,2 T ve 0,4 T) testler gerçekleştirilmiştir. Elde edilen sonuçlar, yüksek demir içeren manyetik ürün elde edilmesi durumunda verimin oldukça düşük olacağına işaret etmektedir. Ayrıca temizleme aşamasının manyetik ürünün demir içeriğinde ve geri kazanımında azalmaya neden olduğu ve bu nedenle temizleme aşaması işleminin gereksiz bir aşama olduğu belirlenmiştir. Ayrıca, manyetik alanın 0.2 T olduğu durumda -1+0.500 mm boyutunda %64 demir içeriğine sahip manyetik ürün elde edilmiştir, ancak verimi %30'un altında olmuştur. Deneysel sonuçlar konveyör hızındaki artış, manyetik ürünün demir içeriğini artırdığını göstermektedir. Beklendiği gibi, konveyör hızının artmasıyla kazanma verimi düşmeye başlamıştır. Tane boyut dağılımı -0.500+0.300 mm olan cevherden >56% demir içeriğine sahip ve yüksek geri kazanıma sahip manyetik ürün elde etmek için uygulanacak deneysel parametreler: "Temizleme aşaması: 1, Manyetik alan: 0.4 T, bant hızı: 7 Hz, ayırıcı konumu: 43° olarak belirlenmiştir. Ancak, kazanma verimi %35,25 olarak belirlenmiştir. Benzer sonuçlar -0.300+0.125 mm boyutundaki örnekle manyetik ayırma testi yapıldığında benzer sonuçlar elde edilmiştir.

Öncelikle parametreler arasındaki ilişkinin incelenmesi için Pearson korelasyon analizi gerçekleştirilmiştir. Elde edilen sonuçlara göre, parametrelerin demir içeriği üzerindeki etkisini şu sıraya göre sıralanmıştır: (en yüksekten en düşüğe) (i) Konveyör hızı, (ii) parçacık boyutu ve (iii) ayırıcı konumu. Daha sonra, manyetik ayırma testinde demir içeriği ve geri kazanımı parametrelerinin verimliliği yapay sinir ağı (ANN) yöntemi kullanılarak tahmin edilmiştir. Bu aşamada, Bayesian Lineer Regresyon (BR), Levenberg-Marquard (LM) ve Scaled Conjection Gradient (SCG) olmak üzere üç farklı eğitim algoritması kullanılmıştır.

Demir değeri tahmini için LM ve SCG modellerinde sırasıyla en yüksek korelasyon katsayısı R (0.996), en düşük Karekök ortalama hata RMSE (0.582), en düşük Ortalama Karesel Hata MSE

(0.339) ve en düşük Ortalama Mutlak Hata MAE (0.194) eğitim aşaması görülmüştür. Ancak test aşamasındaki tahmin başarısı değerlendirildiğinde, BR modelinin en yüksek korelasyon katsayısı R'ye (0.887), en düşük Karekök ortalama hata RMSE'ye (4.230), en düşük Ortalama Karesel Hata MSE'ye (17.889) ve en düşük Ortalama Mutlak Hata MAE'ye (3.477) sahip olduğu anlaşılmıştır. Tartışılan istatistiksel parametrelere dayanarak, eğitim aşamasında LM ve SCG modelleri, test aşamasında ise BR modeli, demir değerini tahmin etmede daha iyi performans göstermiştir.

Kazanma veriminin tahmini için LM ve SCG modelleri eğitim aşamasında sırasıyla en yüksek korelasyon katsayısı R'ye (0.998), en düşük Karekök ortalama hata RMSE'ye (1.695), en düşük Ortalama Karesel Hata MSE'ye (2.872) ve en düşük Ortalama Mutlak Hata MAE'ye (0.582) sahiptir. Ancak test aşamasındaki tahmin başarısı değerlendirildiğinde, BR modelinin en yüksek korelasyon katsayısı R'ye (0.972), en düşük Karekök ortalama hata RMSE'ye (6.729), en düşük Ortalama Karesel Hata MSE'ye (45.286) ve en düşük Ortalama Mutlak Hata MAE'ye (5.418) sahip olduğu anlaşılmıştır. Tartışılan istatistiksel parametrelere dayalı olarak, eğitim aşamasında LM ve SCG modelleri, test aşamasında ise BR modeli, geri kazanım değerini tahmin etmede daha iyi performans göstermiştir.

Geliştirilen modellerin performansını daha iyi değerlendirmek için tahmin edilen değerler ile ölçülen değerler karşılaştırılmıştır. Burada, demir tahmini için tüm modellerden elde edilen tahmin değerleri ile gerçek değerlerin eğilimleri birbirine benzer görünmektedir. Ancak, BR modelinin diğer modellere nispeten daha yakın bir eğilim gösterdiği anlaşılmaktadır. Geri kazanım tahmini için tüm modellerin tahmin sonuçları ile ölçülen değerlerin örtüştüğü görülmektedir. Ancak, BR modelinin sonuçlarının deneysel veri noktalarına diğer modellere göre daha iyi uyduğu görülmektedir.

Son aşamada; çalışmada hem kazanma veriminin yüksek olması hem de demir oranında istenilen seviyeye çıkması için farklı senaryolar tasarlanmış ve uygulanmıştır. Bu aşamada, sadece bant hızı ve ayırıcı bıçakların açısı değiştirilmiştir. Deneylerde manyetik alanı yüksek olanı seçilip elde edilen manyetik olmayan ürün parametreleri değiştirerek tekrar beslenmiş ve içerdiği değerli demir'in kazanımı sağlanmıştır. Toplam verim hesaplanmıştır. Ancak, tane boyutları -0,500+0,300 mm ve -0,300+0,125 mm olan numunelerde hedeflenen sonuçlar elde edilmemiştir. Ama -1+0,500500 mm tane boyutlarındaki numuneden manyetik Zenginleştirme işlemi neticesinde %56,22 demir içeren manyetik ürün %90,01 kazanma verimi ile elde edilmiştir.

İnce boyutlarda (-0,500 mm) cevherin manyetik özelliğinin artırılmasının kazanma verimine etkisi olabileceği düşünülmüş ve mikrodalga ile ön ısıtma testleri gerçekleştirilmiştir. Yapılan işlemler neticesinde cevherin bünyesinde bulunan hematit minerallerinin manyetit mineraline dönüştüğü, götit mineralinin ise hematit mineraline dönüştüğü tespit edilmiştir. Ancak, cevherin manyetik duyarlılık özelliğindeki değişiklikler tane boyutu -0,500+0,300 mm ve -0,300+0,125 mm için kayda değer şekilde yüksek olmamıştır, buna karşın -1+0.500 mm boyutundaki örneğin üzerinde güçlü bir etkiye sahipti. Mikrodalga ile işlenen örneğin manyetik duyarlılığının 0,16 emu/g'den 4,30 emu/g'ye yükselmiştir.

Elde edilen tüm deneysel sonuçlar göz önüne alındığında, düşük kaliteli cevherden manyetik ürün elde etmek için bir akış şeması önerilmiştir. Önerilen manyetik ayırma sürecinde 100 kg cevher kullanıldığında, -1+0,500 mm boyutundaki manyetik ürünün demir içeriği %56,65 olarak bulundu ve ağırlığı 19,62 kg olarak hesaplandı. Bununla birlikte, kuru manyetik ayırma testinden elde edilen sonuçlar, 0,500 mm'nin altında bir boyuta sahip örnekte tatmin edici olmamıştır ve -0,500 mm boyutundaki nihai manyetik ürünün %51,14 demir içerdiği ve ağırlığının 34,08 kg olduğu belirlenmiştir.

Gelecekteki çalışmalar için aşağıdaki konular önerilmektedir: (i) Manyetik parçacıkların manyetik ayırıcı üzerindeki davranışının modellenmesi incelenebilir. (ii) <0,500 mm boyutunda örneğin bir değirmende öğütülmesi ve ıslak manyetik ayırıcıyla zenginleştirilmesi araştırılabilir.

ACKNOWLEDGEMENTS

I would like to express my endless gratitude to my advisor, Assoc. Prof. Dr. Mahmut ALTINER, to the head of the Mining Engineering Department, Prof. Dr. Ahmet DAĞ, who allowed me to use the facilities of the department, to Res. Assist. Dr. Ali Can ÖZDEMİR and to the Department Staff who made this possible.

Thanks to Assoc. Dr. Mahmut ALTINER, who directed and put all his ressources and knowledge at my disposal and to Res. Assist. Dr. Ali Can ÖZDEMİR, a faculty member of the Department of Mining Engineering, who shared his experiences with me during the use of MATLAB software.

Also, I would like to express my endless gratitude and respect to Mr. Ahmed and Zayanou, who are studying at Çukurova University Mining Engineering Department, for helping me with the laboratory experiments. I would like thank Cukurova University Research Fund (project ID: FYL-2022-14903) for providing budget to perform necessary analyses and to buy required equipment in our laboratory.

LIST OF TABLES

LIST OF FIGURES

SYMBOLS AND ABBREVIATIONS

AAS	: Atomic Absorption Spectrometer
ANN	: Artificial Neural Network
AOGMS	: Air-pulsated Oil Gravity Separation
BR	: Bayesian Regression
BSE	: Back Scattered Electron
EDS	: Energy Dispersive Spectrometry
HGMS	: High Gradient Magnetic Separation
kW	: Kilowatt
LM	: Levenberg-Marquardt
MAE	: Mean Absolute Error
MH	: Magnetic Hysteresis
MLA	: Mineral Liberation Analysis
Mo	: Molybdenum
MSE	: Mean Squared Error
Ni	: Nickel
Pc	: Pearson Correlation
R	: Coefficient of Correlation
RER	: Rare Earth Roll
RMSE	: Root Mean Squared Error
SCG	: Scaled Conjugate Gradient
SEM	: Scanning Electron Microscope
T	: Tesla
TGA	: Thermo-Gravimetric Analyzer
WHIMS	: Wet High Intensity Magnetic Separator
XRD	: X-ray Diffraction
XRF	: X-ray Fluorescence
GAUSS	: Gs (1Tesla = 10000gs)
HPGR	: High Pressure Grinding Rolls

1. INTRODUCTION

Iron (Fe) is one of the most abundant rock-forming elements, corresponding to 5% of the Earth's crust. It is well known that iron can be classified as a powerful metal due to its easy alloying property with other metals. Therefore, iron-containing alloys can be shaped in many products including, car, pins, railways, buildings etc. Moreover, the use of iron metal in the form of steel is twenty times as high as compared to all other metals. Iron is quite soft and easily worked, but its melting point is 1538 °C and its density 7.87 g/cm^3. The presence of carbon in the reduction stage makes iron into steel, which is harder and extremely versatile. In addition, many types of steel containing Cr, Mn, Ni and Mo can be prepared as stainless steel. Table 1.1 summarizes the use of iron compounds in our daily life (Summerfield, 2020).

Table 1.1. Iron compounds and their use in our daily life (Summerfield, 2020)

Iron compound	**Component**	**Properties**	**Uses**
Cast Iron	Fe + up to 5% carbon	Hard, brittle	Camp ovens, woks
Galvanized iron	Zn-coated Fe	Resists rusting malleable	Roofing, motor vehicle bodies, boats
Tin plate	Ti-coated Fe	Resists rusting	Tin cans for food preservation
Steel	Fe + <1% C	Hard, strong, malleable,	Building, machinery, transportation, cans & container
Stainless steel	Fe + C + Ni + Cr	Doesn't rust malleable	Cutlery, hospital equipment, motor vehicle parts
Tool steel	Fe + C + V + Cr + W or Mo	Very hard, very brittle	Metal cutting tools

In addition, steel's desirable properties make it the main structural metal in engineering and building projects, accounting for about 90% of all metal used each year, 60% of iron and steel products are evaluated in transportation and construction, and 20% in machinery manufacture. Table 1.2. shows the use of iron products in daily life (Summerfield, 2020).

Table 1.2. The use of iron in daily life (Summerfield, 2020).

Use	Description
Transportation	Steel railway, ships, car frames
Construction	Steel buildings, bridges, reinforcing in concrete buildings, roofing
Machinery	Steel engines, pumps, cranes
Wire products	Steel wire fences, ships' cables, door screens
Storage	Container, storage tanks
Oil and gas	Drill rods, casing, pipelines
Appliance and equipment	Steel refrigerators, washing machines, dishwashers, hospital equipment
Health	Animals need iron for making energy and carrying blood around the body. Essential for people to treat patients who were pale, lacking in energy and suffering from anaemia

There are many minerals of iron oxide such as, hematite (70%, Fe_2O_3), goethite (63%, α-FeO(OH)), magnetite (72%, Fe_3O_4), limonite ($2Fe_2O_3 \cdot 2H_2O$), and siderite (48% Fe, $FeCO_3$) for the extraction of iron economically. Among them, hematite and magnetite are widely used in the iron and steel industries. Figure 1.1. shows the iron ore reserves in Türkiye maps. Mining operations to extract iron ores from the mining area are carried out in all regions. Iron ores in Sivas, Malatya, and Erzican regions are directly used in the industry due to their high iron and low impurity contents. As iron content is in a range of 50-62%, there is no need to perform beneficiation processes. These irons after crushing and classification are ready for use in the steelmaking industry. Apart from these regions, beneficiation strategies should be investigated to obtain valuable iron products with high iron and low impurity contents (Tuncel et al., 2017).

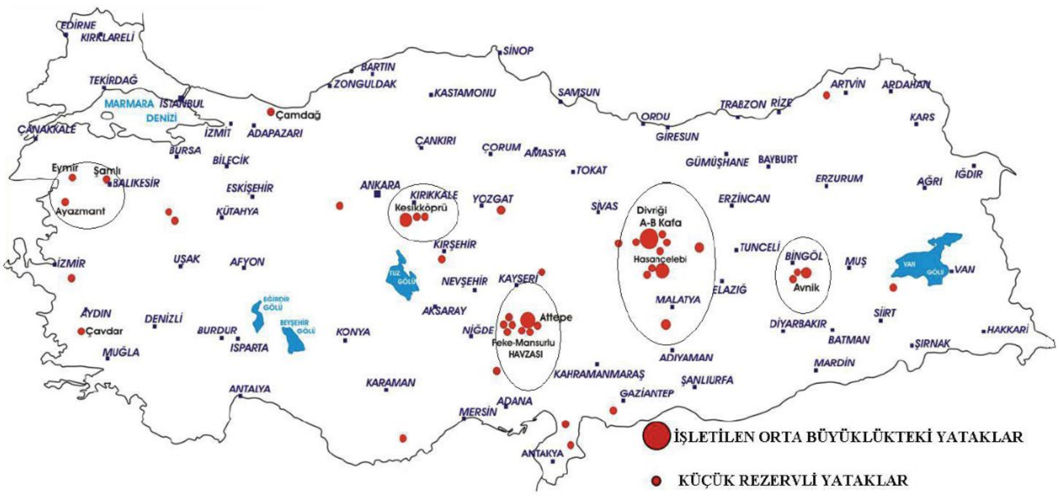

Figure 1.1. Mining areas where iron ores are extracted for use (Tuncel et al., 2017)

The demand for the iron ore continues to grow as the world economy expands. As of 2023, mine production and iron ore reserves worldwide are listed in Table. 1.3.

Table 1.3. Mine production and iron reserves in the world (USGS Minerals Commodity, 2023).

Country	**Mine Production**				**Reserves (million metric tons)**	
	Usable ore		**Iron content**			
	2021	**2022**	**2021**	**2022**	**Crude ore**	**Iron content**
United States	47,500	46,000	30,100	29,000	3,000	1,000
Australia	912,000	880,000	565,000	540,000	51,000	27,000
Brazil	431,000	410,000	273,000	260,000	34,000	15,000
Canada	57,500	58,000	34,500	35,000	6,000	2,300
Chile	17,700	16,000	11,200	10,000	NA	NA
China	394,000	380,000	246,000	240,000	20,000	6,900
India	273,000	290,000	169,000	180,000	5,500	3,400
Iran	72,900	75,000	47,900	49,000	2,700	1,500
Kazakhstan	64,100	66,000	13,100	14,000	2,500	900
Mauritania	12,800	13,000	8,000	8,100	NA	NA
Mexico	10,800	11,000	6,810	6,900	NA	NA
Peru	18,100	17,000	12,100	11,000	2,600	1,200
Russia	96,000	90,000	66,700	63,000	29,000	14,000
South Africa	73,100	76,000	46,500	48,000	1,000	670
Sweden	40,200	39,000	28,600	28,000	1,300	600
Türkiye	**16,100**	**17,000**	**9,710**	**10,000**	**130**	**38**
Ukraine	83,800	76,000	52,400	47,000	6,500	2,300
Other countries	56,700	59,000	4,900	5,000	18,000	9,500
World total (rounded)	2,680,000	2,600,000	1,630,000	1,600,000	180,000	85,000

Although there is high mine production worldwide, it is necessary to extract and recover iron ore from various sources, including low-grade ores, tailings, and waste rock to meet the iron concentrate demand from the industry. It is obvious that low-grade iron ore is important because it represents a significant resource that can be extracted and processed into high-quality iron ore products. While high-grade iron ore deposits are becoming increasingly scarce, low-grade iron ore deposits are more abundant and widespread. These low-grade deposits often contain a significant amount of iron but are also mixed with other minerals and impurities that make them difficult and expensive to process using traditional methods. (Tuncel et al., 2017)

To obtain iron concentrate with desired properties (high Fe and low impurity content) from the low-grade ore, many studies have been investigated (Dwari et al. 2013; Tripathy et al. 2017; Messai et al. 2020; Nunna et al. 2020; Nunna et al. 2021). Various methods, including scrubbing and washing, hydro-cyclone, jig, dense medium drums (DMDs), shaking table, and Humphrey spiral were suggested to prepare iron concentrates with the required properties, such as high iron (>56%) and low impurity contents (e.g., Al, Si, Na, K, P). (Tripathy et al. 2017). In addition to these methods, magnetic separation is one of the simplest methods to separate particles showing magnetic properties from the ore (Singh et al. 2013). The working principle of dry roll magnetic separator is explained in detail in the following section.

1.1. Working Principle of a Dry Roll Magnetic Separator

Magnetic separators work based on the difference in magnetic properties between minerals. By applying a magnetic field to the ore, the magnetic particles are attracted to the magnetic surface, while the non-magnetic particles are repelled and remain in suspension. This allows for the separation of magnetic particles from non-magnetic particles, resulting in a concentrate with a high iron content. Some of the most common types of magnetic separators include drum separators, roll separators, and wet high-intensity magnetic separators. Among them, roll magnetic separator is a type of magnetic separator used to separate magnetic and non-magnetic particles from a mixture. Two types of roll magnetic separator have been used (i) electromagnetic induction roll and (ii) permanent roll magnetic separator. Magnet composed of NdFeB has superior advantages compared to the electromagnetic separator. These advantages are: (i) energy efficiency, (ii) lower operating cost, (iii) higher separation efficiency, (iv) greater flexibility, and (v) reduced environmental impact. Figure 1.2. shows the development of the materials that create the constant magnetic field from 1880 to date (Xie et al. 2022). The working principle of these separators was reviewed in detail by Xie et al. (2022) and some magnetic separators can be seen in Figure 1.3.

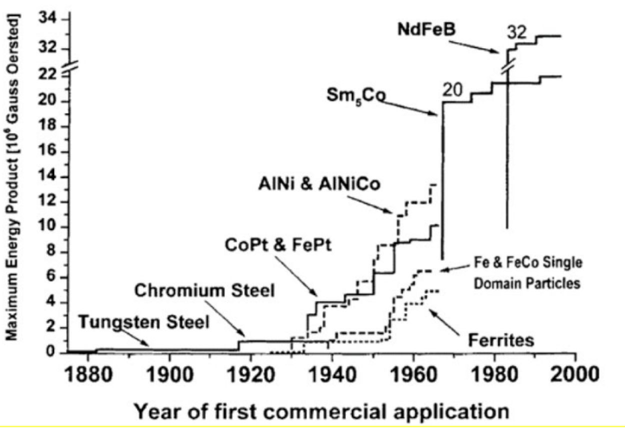

Figure 1.2. The development of materials for use in permanent rare earth roll (RER) magnetic separator. (Xie et al., 2022)

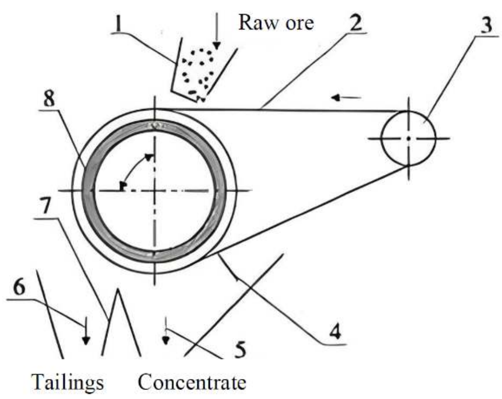

(a) Working principle of CTFG dry magnetic separator for fine ore (Wang et al. 2017)

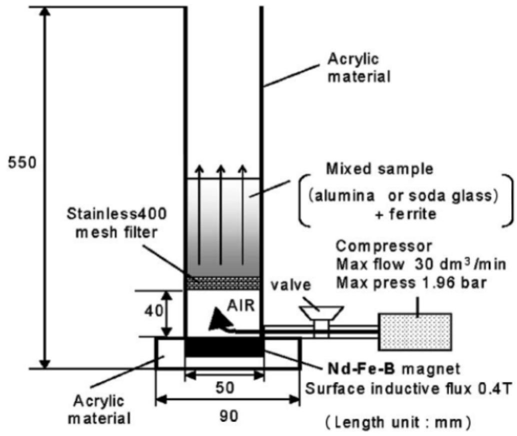

(b) An open gradient magnetic separator (Mishima et al. 2004)

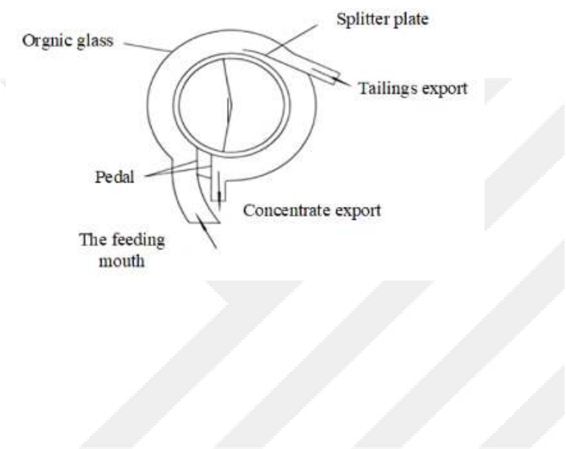

(c) Air suspension dry magnetic separator(Cheng 2007)

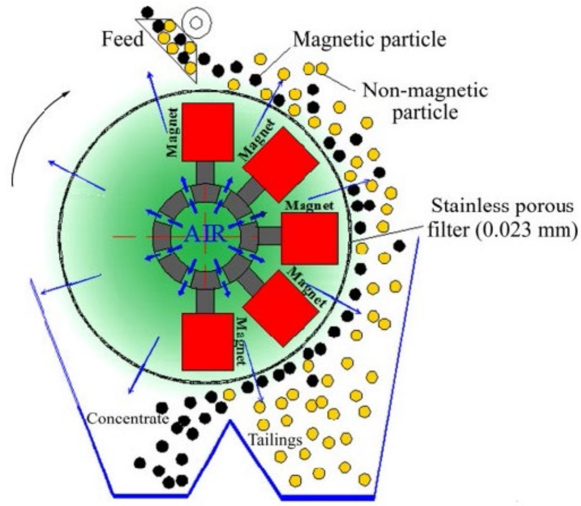

(d) New type of wind dry-type magnetic separator(Liu, Lu et al. 2020)

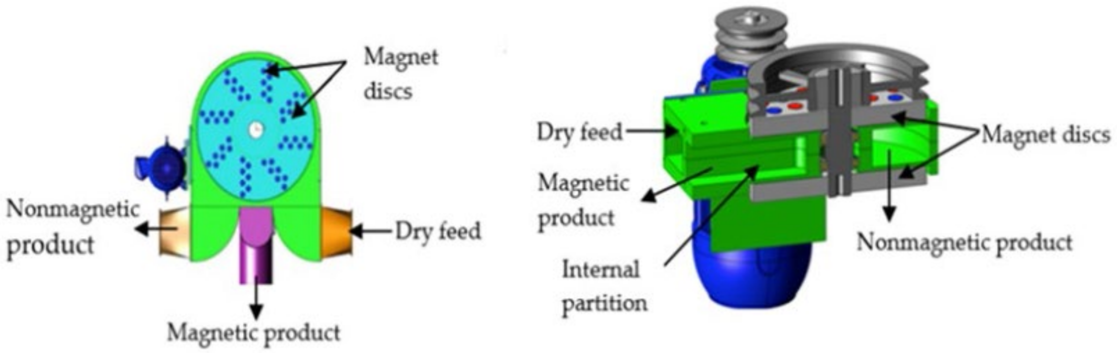

(e) Novel pneumatic planer magnetic separator

Figure 1.3. Magnetic separators that are designed for different resources to be beneficiated (Xie et al., 2022)

The roll comprising magnet discs and mild steel discs can be seen in Figure 1.4. The roll magnetic separator is often used with a conveyor belt with different thickness that affects the magnetic field strength. A schematic of the rare earth roll (RER) separator is seen in Figure 1.5 (Dobbins et al. 2009).

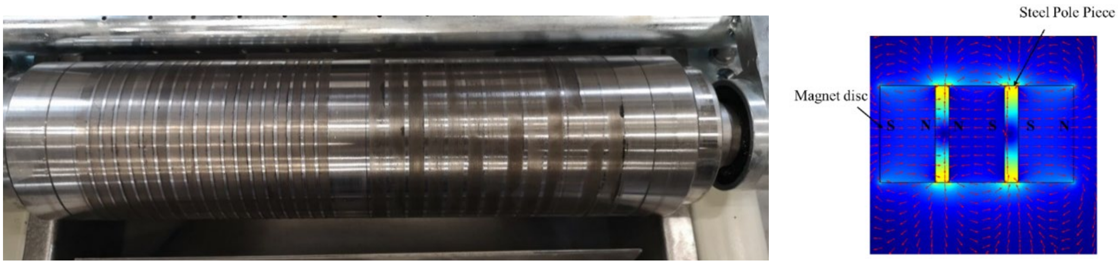

Figure 1.4. Roll comprising magnet discs with mild steel discs

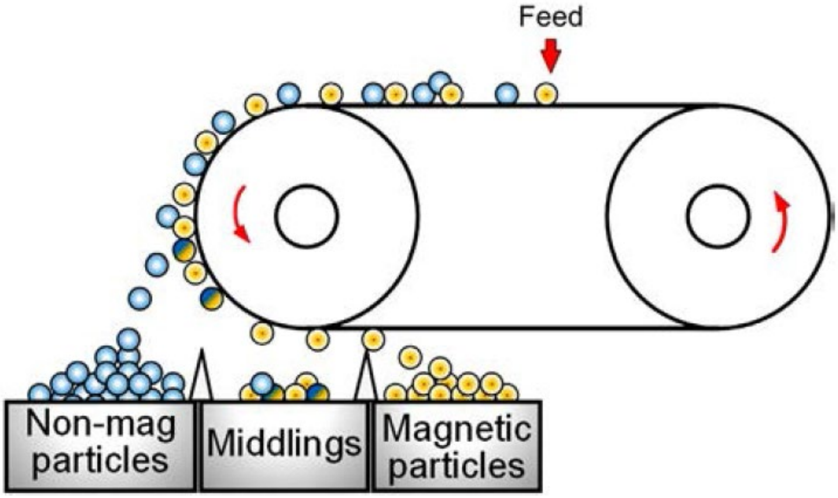

Figure 1.5. The picture of a RER separator (Dobbins et al. 2009)

The roll magnetic separator consists of a roll-shaped magnet, typically made of rare-earth materials, mounted on a stationary shaft. The magnet rotates at a high speed, creating a strong magnetic field around the roll. The material to be separated is fed onto the roll and passes through the magnetic field. Magnetic particles are attracted to the roll and are carried along with it, while non-magnetic particles are not affected and fall off at the end of the roll. There are various forces including: a magnetic force (F_m), a gravitational force (F_g), a drag force (F_d), which play a key role in the behavior of a particle in the magnetic field (Figure 1.6). (Jan Svoboda. 2004)

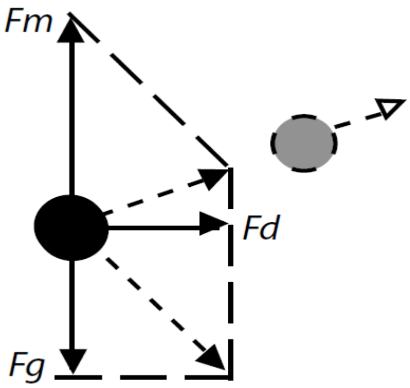

Figure 1.6. Forces that have strong effects on the behavior of particle on the magnetic field area (Dobbins et al. 2009).

$F_m > F_g + F_d$; the particles are attracted to the roll,

$F_m < F_g + F_d$; the particles are not affected and fall off at the end of the roll

$$F_m = V \times X \times H \times \text{grad } H \qquad (1.1)$$

Where, F_m is the magnetic attraction force, V is the volume of the particle, X is the magnetic susceptibility, H is the magnetic field, grade H is the magnetic field gradient.

Moreover, the working parameters of the RER separator have a great influence on the separation efficiency of the magnetic product from the ore. These parameters are magnetic field strength, roll speed, feed rate, particle size, splitter position, magnetic properties of the material, and thickness of the conveyor belt.

1.2. Purpose of the Research

In this thesis, we investigated the recovery of a valuable iron content from a low-grade iron ore (a mixture of goethite and hematite) using a dry roll magnetic separator (Miknatis Ar-Ge). The ore obtained from a mining area (Feke/Adana, Türkiye) was characterized using mineral liberation analysis (MLA) techniques, which provide the following properties: (i) modal mineralogy, (ii) calculated assay, (iii) elemental distribution, and (iv) mineral locking. In the magnetic separation test, the effects of magnetic field strength, splitter position, conveyor speed, particle size, and cleaning stage on the iron content and the recovery of the magnetic product from the ore were investigated. The obtained experimental findings were further evaluated by ANN methods to determine the effect of each working parameter on the iron content of magnetic product and its recovery. After all, different scenarios were investigated to increase the recovery and also improve the feasibility of the magnetic separation process. Furthermore, the effect of microwave treatment on the magnetic separation test was studied. Considering all results, flowsheet was proposed to obtain an iron concentrate with high iron content and recoveries from the ore.

2. PRELIMINARY WORK

High-grade ores have been depleted with the increase of industrialization in countries, and therefore low-grade ores should be evaluated in a sustainable and cost-effective manner. Many studies have focused on designing new equipment that can be used in the beneficiation of low-grade ores. As such, dry and wet magnetic separators with a high intensity magnetic field have been suggested for separating paramagnetic minerals, including goethite and hematite. However, many parameters, including the working principle of a magnetic separator and the mineralogical property of an ore should be considered. Tripathy et al. (2017) revealed that the splitter position of the magnetic separator played a key role in the separation mechanism of the roll magnetic separator, as shown in Figure 2.1. Furthermore, the conveyor speed had great effects on the selectivity of the minerals. It was determined that an increase in the conveyor speed results in a decrease in the amount of magnetic material content in the magnetic product, as reported in a previous study (Naik, 2002).

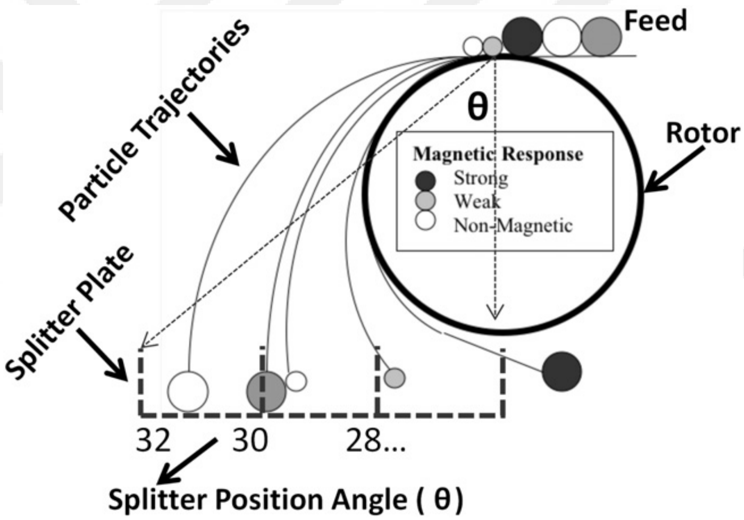

Figure 2.1. Effect of splitter position on the behavior of the particles in the magnetic separation process (Tripathy et al. 2017)

It was possible to obtain a magnetic product with a iron content of 53.1% and a recovery of 36.8% using the RER magnetic separator. Based on these findings, it can be concluded that conveyor speed and splitter position are key parameters for achieving optimal results. These findings were in good agreement with those of a previous study, which the iron content in the middling and non-magnetic fractions started to increase with the increase of conveyor speed. This phenomenon was explained by the dominance of centrifugal force affecting particles on the roll (Mohanraj et al. 2021). Furthermore, it was determined that the design of the magnetic roll (magnet-to-steel disk thickness) was one of the most important parameters for achieving high efficiency in magnetic separation.

Ku et al. analyzed the dynamic separation process of a dry magnetic separator using the finite element method. The following factors: the bulk size and shape, magnetic permeability property, and forces (magnetic force, magnetic particle-particle attraction, and gravity) acting on the ore particles are used in the dynamic simulation and it was found that separation predictions were strongly dependent on these factors: (i) particle size had a great influence on the forces acting on magnetic bulks, (ii) the magnetic permeability of bulks affected both its movement trajectory (as the speed of conveyor belt) and the separation efficiency. However, the shape size and splitter position had no effect on their movement trajectory and separation efficiency. Quast and Skinner (2020) investigated the effects of magnetic field magnitude, matrices, and particle sizes on the recovery of hematite particles to the magnetic fraction. The recovery of hematite particles to magnetic fraction are influenced by their mineralogical characteristics and particle sizes. The use of a fine expanded metal matrix with sharp edges and corners enhances the localized magnetic field intensity and leads to much higher recoveries of hematite. The study also suggests that quantitative analysis of the effects of the matrix could improve the performance of commercial high-intensity magnetic separators. (Ku, Lei et al. 2021)

Messai et al. (2020) carried out a study to characterize and enhance low-grade iron ores from the Rouina deposit (Ain Defla). The low-grade iron ore (%30.85 Fe) sample was upgraded using procedures that included classification, washing, and dry high-intensity magnetic separation to make it viable as a commercial product. After the sample had been ground, each closed-size sieve fraction was washed, dried, and then subjected to dry high-intensity magnetic separation, where it was discovered that only limited improvement was possible. With a magnetic field intensity of 2.4 T at the size fraction of [-0.125 +0.063 mm], it was possible to produce a magnetic concentrate of 54.09% with a recovery percentage of 89.30% and yield of 62.82%.

Liu et al. (2020) explained the fundamental principle of Air-pulsated Oil Gravity Separation (AOGMS), and a perpetually operating laboratory scaled AOGMS was evaluated for its efficacy in the separation of magnetite particles from raw material with a particle size smaller than 3 mm and an unsettled liberation degree. An inquiry was conducted into the impact of pivotal factors, including the intensity of the magnetic field, the velocity of air flow, and the rate of rotation of the roles, on the efficacy of separation. According to the findings, the performance is particularly influenced by the intensity of the magnetic field and the rate of airflow. An increase in airflow rate can greatly improve concentrate grade with just a little change in iron recovery when there is a magnetic intensity field of 1250 Gs on the roller surface because it accelerates the removal of quartz and mica containing SiO_2 and Al_2O_3. The AOGMS technique might offer the necessary competitiveness in dry separation process, enabling the effective removal of trapped particles and small non-magnetic particles. This further demonstrates how the separation efficiency of complicated iron ore may be successfully strengthened by reasonable matching of various force fields.

In industrial practice, improving the recovery of ultrafine magnetic particles by using HGMS is a challenging problem. Particle capture in Higher gradient magnetic separator (HGMS) is described mathematically, and several analytical models for regular shape matrices—only circular and elliptic—under ideal circumstances (ideal potential flow) have been developed. Matrix structures with irregular shapes offer superior magnetic properties and can improve HGMS particle recovery. However, it is impossible to build analytical models for matrices with irregular shape, and instead, qualitative assessments were frequently carried out, which can scarcely be considered accurate and compelling. It is crucial to create procedures for conducting quantitative studies on matrices with irregular shapes. Xue et al. (2020) used axial HGMS to examine particle capture by irregular matrices using 3D numerical simulation. For axial HGMS, a simulation model was developed that included a particle group and magnetic matrices with circular, elliptic, square, and diamond cross-sections. The four different types of matrices were used to specifically show the evolution of particle groups in HGMS system. The particle motion trajectories were depicted, and the comparison of particle capture cross-section area were calculated. Under a modest induction range, elliptic and diamond matrices outperform circular and square matrices in terms of particle capture performance and can be used to improve ultrafine particle recovery. The numerical simulation results agree with earlier theoretical investigations using analytical models and matrix experimentation. The results of the current study also suggests that there should be optimum diamond matrix aspect ratios and optimum tooth angles for grooved plates used in HGMS.

Tripathy et al. (2020) presented an artificial neural network (ANN) model to forecast the operation of an induced roll high-intensity magnetic separator while upgrading low-grade iron ore fines. The network input for an induced roll magnetic separator includes important process variables such as applied current, rotor speed, splitter location, particle size, and feed rate. An induced roll magnetic separator's separation performance (iron content, silica content, iron recovery, and silica rejection of the magnetic product) may be predicted using a feedforward ANN with one hidden layer and units ranging from 9 to 40. With an R^2 value of 0.95 in both training and testing phases, the simulated results produced by neural network modeling are highly comparable to the actual outcomes. Further analysis of the researched variables' sensitivity is done using the generated models. It is discovered that the impacts of rotor speed and splitter positions are more sensitive to the separation. Additionally, a solution that has been optimized is created to forecast the optimum grade-recovery curve that can be obtained for this preconcentration.

Liu and Lei (2022) suggested an innovative technique of "ultra-crushing in High Pressure Grinding Rolls (HPGR) - classified separation in order to increase grinding efficiency and minimize over-grinding throughout the whole grinding process. Particle size distribution, liberation traits, and separation features were all discussed in relation to the novel method. There was no discernible change in the size of the coarse particles between HPGR and the traditional impact crusher. The tiny particles (0.18 mm), which are featured by a greater fines content (a yield of 38.43%), a larger specific surface area, a higher quartz liberation, etc., are where the "Particle Bed Breakage" features of HPGR products are mostly focused. It is important to note that in HPGR, finely dispersed iron particles separate from quartz minerals under high compressive stress, which is more conducive to the subsequent separation. The HPGR (0.18 mm) tailings had the lowest grade (7.29%) according to magnetic separation tests, which is around one percentage point lower than coarse grinding products. The novel method with a 0.18 mm prescreens size for an Anshan type hematite ore is practical based on the study presented above.

For beneficiating low-grade complex iron ores, several combinations of separation technologies have been combined. Numerous researchers have reported data on the performance of separation technologies, allowing comparisons between traditional and novel technologies. A study made by Nunna et al (2022) attest that as higher-grade ores become depleted, a greater emphasis will be placed on developing suitable beneficiation strategies for low-grade hematite-goethite ores containing higher levels of impurities such as silica and alumina. The techniques chosen to reduce impurity levels in these lower-grade iron ores will be determined by the ore mineralogy, which consists of hydrated hematite (e.g., goethite or limonite) and iron carbonates (e.g., siderite), with gangue minerals such as quartzite, complex aluminum silicates (e.g., kaolinite, chlorite and phlogopite), and aluminum oxides (e.g. gibbsite); as well as a full understanding of the separation process dynamics. Magnetic separation, wet and dry heavy media separation, and air-pulsed jigging are the main concentration processes that can be used to upgrade lower-grade lump iron ores. Wet and dry gravity and magnetic separation, flotation, and roasting followed by magnetic separation are among the technologies that can be used to benefit iron ore fines. A summary of separation technologies applicable to the processing of lump iron ore and iron ore fines and ultra-fines is given in Table 2.1.

Table 2.1. Processing technologies and application options for low-grade iron ore (Nunna et G.J., 2021)

Product (size range)	Technology	Applications	Selection principles
Lump (−31.5 + 6.3 mm)	Scrubbing or washing	Drum scrubber, log washing	The technology has great potential for desliming porous lower grade Pilbara iron ores (e.g. limonite/goethite and hematite-goethite ores), which carry ultrafine clayey kaolin and/or gibbsite minerals in the pores.
	Gravity separation	HMS, LARCODEMS, Tri-Flo separators	- Processing of some ores may result in slime buildup in the separating suspension, and the medium viscosity may increase to the point where separation efficiency is adversely affected. - Media (magnetite or ferrosilicon) is lost in the processing. It may be difficult or costly to obtain in some regions for treating low-grade porous ore minerals
		Jigging	Jigging is a promising technology for upgrading lower-grade hematite BIF ores and other difficult-to-treat ores. The technique should be investigated by conducting tests on selected samples.
	Magnetic separation	RED (Rare Earth Drum) magnetic separators	- RED magnetic separators can be used to pre-concentrate coarse particles ranging in size up to 75 mm. Established applications include hematite and martite-type iron ores - The possible application of roasting followed by RED magnetic separation technology to low-grade iron ore processing is considered as a prospective option for study and evaluation
Coarse fines (-6.3 + 1.0/0.5 mm)	Scrubbing or washing	Attrition scrubbers	- High-intensity conditioning can liberate aggregate minerals from slime coatings, disintegrate clay agglomerates, clean, and polish mineral grains. - Depending upon the nature of the clayey minerals, attrition scrubbing is generally applicable for particles of −10 mm size. The actual scrubbing time depends on the residence time in the attrition scrubber, which is usually operated at densities of 70–80% solids.
	Gravity separation	HMS, jigging	Similar to Lump processing (see above).
	Magnetic separation	RED, RER (Rare Earth Roll) magnetic separators	Similar to Lump processing (see above)
Ultra-fines (−1.0/0.5 mm+75/45 µm) and slimes (−75/45 µm)	Sizing/ classification/ gravity separation	Hydro cyclones, fine screens	- Supplementary processes like scrubbers, fine screens, and cyclones have potential applications in integrating beneficiation processes. - Separating an aggregate of mixed particles into groups according to size ahead of separation is essential to increase the efficiency of the subsequent gravity/magnetic/flotation separation processes.

		Spirals, TBS (teeter-bed separator)	Spirals and TBS are widely used in iron ore processing with benefits including reduced floor space and labor requirements and operational simplicity
	Magnetic separation	Matrix magnets, WHIMS, HGMS	This technology might work satisfactorily on specific size fractions that are well liberated, but it is unlikely that adequate product grade and recovery would be obtained for lower-grade ultra fines and slimes.
	Flotation	Direct, reverse anionic and reverse cationic flotation; column flotation	The separation of kaolinite and gibbsite in iron ores is challenging due to the similarities in their surface properties. New reagent regimes may give better separations.
Dry beneficiation options (an effective alternative for upgrading low-grade iron hydroxide ores)	Sizing/ classification	Circulating air classifiers, dust cyclones	Air scrubbing and classification can be employed as feed preparation. A sharp separation from −10 mm size with a cut size as fine as 20–38 μm is achievable depending upon the characteristics of the material.
	Roasting followed by magnetic separation	Conventional and microwave roasting and dry magnetic separators	- The goethite-containing ores have a low magnetic susceptibility compared with hematite ores. Thermal and microwave-assisted magnetizing or neutral air roasting followed by magnetic separation using RED/RER magnetic separators are potential alternative pathways for achieving good separation and recoveries. - Depending upon ore characteristics, the rejection of gangue minerals plus an upgrade of 4–6 wt% Fe by the expulsion of the combined water can be achievable

It was determined that microwave heating had superior advantages on the magnetic properties of iron ores compared to the traditional method. Omran et al. (2014) examined the impact of microwave treatment on Egyptian iron ore samples. Several methods were used to examine how changing the microwave exposure time and power would affect the magnetic characteristics of iron ore both before and after the microwave pretreatment. With higher particle sizes and longer exposure times for a fixed value of the applied power intensity, microwave therapy was shown to be more effective. Iron recovery increased from 39.54% in the untreated sample to 97.95% in the microwave-treated sample, according to magnetic separation of microwave-treated and untreated iron ore. According to the findings, microwave radiation significantly affects hematite's magnetic characteristics by creating new, more magnetic phases that make it easier to separate them from non-magnetic minerals and achieve high recovery rates of up to 98%. Investigations were done into how microwave radiation affected the pace of heating, the magnetic characteristics, and the magnetic separation of iron ore. The findings showed that:

- For samples with smaller particle sizes, more energy is needed to raise the sample temperature.
- The magnetism saturation of hematite rose from 0.50 to 2.48 emu/g by extending the exposure period from 0 to 90 s, which may be related to phase shifts on the mineral particles' surfaces.
- With longer exposure times comes a higher magnetic recovery ratio. For samples treated for 90 s at 900 W of microwave radiation and separated using 1 T of magnetic field intensity, an iron ore recovery of around 98% could be achieved. Microwave radiation's augmentation of the magnetic characteristics of weak magnetic minerals by changing the mineral surface to more magnetic phases are responsible for the improvement in recovery.

-

3. MATERIAL AND METHOD

3.1. Material

The raw material used in this study was collected from an old mining area located in Feke/Adana, Türkiye. Approximately 100 kg of the sample, with a size of -100 mm, was brought to our laboratory for use in the beneficiation test. The chemical composition of the sample determined by XRF (PANalytical Mini Pal) analyses are listed in Table 3.1.

Table 3.1. The chemical composition of the raw ore used in this thesis

Element	Content %
Al_2O_3	9.12
CaO	3.12
SiO_2	19.01
Fe	**41.01**
K_2O	0.185
MgO	0.62
TiO_2	1.29
Na_2O	0.32

* it was determined at a temperature of 1000 °C under air atmosphere using a TGA analyzer (Mettler Toledo, TGA 3+)

3.2. Method

3.2.1. Sample Preparation

First, the sample was dried at 105 °C in an oven (Memmert). In a follow up, the sample was crushed to below -1 mm by using a lab-scale jaw crusher. The sample was classified using a dry screener (Retsch) in the following sizes: -1+0.500 mm, -0.500+0.300 mm, and -0.300+0.125 mm. Table 3.2 shows the amount of the ore in each range.

Table 3.2. The distribution of the ore after dry sieving (%)

Particle size (mm)	Weight (%)
-1+0.500	35.55
-0.500+0.300	30.12
-0.300+0.125	25.24
-0.125	**9.09***

* The sub sample below 0.125 mm was not used in the magnetic separation test.

The chemical composition of the sample with different sizes were determined by the aforementioned methods. For each magnetic separation test, 1 kg of the sample (for each particle size) was prepared.

3.2.2. Mineral Liberation Analysis (MLA)

The representative sample with a size of -0.500+0.300 mm was prepared using a rotary micro riffler (Quanta chrome). After the sample was frozen with resin, its surface was polished in eight stages by abrasion and polishing processes. The surface of the polished sample was then coated with carbon. Mineral Liberation Analysis (MLA, FEI Quanta 400 MLA) was used to determine the mineral boundaries in the polished sample using backscattered electron (BSE) images and energy dispersive spectrometry (EDS, Bruker X-flash 6030 Dual EDS) spectra. MLA Suite 3.1 software was used for the characterization of the obtained results in MLA. Furthermore, the phase properties of the sample were identified using a PANalytical EMPYREAN in the 2ø range of 5°–85° with a 0.02 step size, and the patterns were evaluated using a PDXL software for mineral identification.

3.2.3. Magnetic Separation

A dry magnetic (RARE EARTH) separation test was carried out using a lab-scale dry roll magnetic separator (Miknatis Ar-Ge), which is seen in Figure 3.1. The equipment comprises several parts: (1) sample feeder, (2) conveyor (3) splitter, (4) two magnetic zones, (5) board used to control the speed of the conveyor. Additionally, the magnet array can be seen in Figure 3.1.

The conveyor with a different thickness can be adapted to the equipment, and various magnetic areas can be provided. In this thesis, the conveyor with a thickness of 2 mm was used to create the following magnetic fields: Zone-1 (0.2 T) and Zone-2 (0.4 T), which was measured by the Gauss meter.

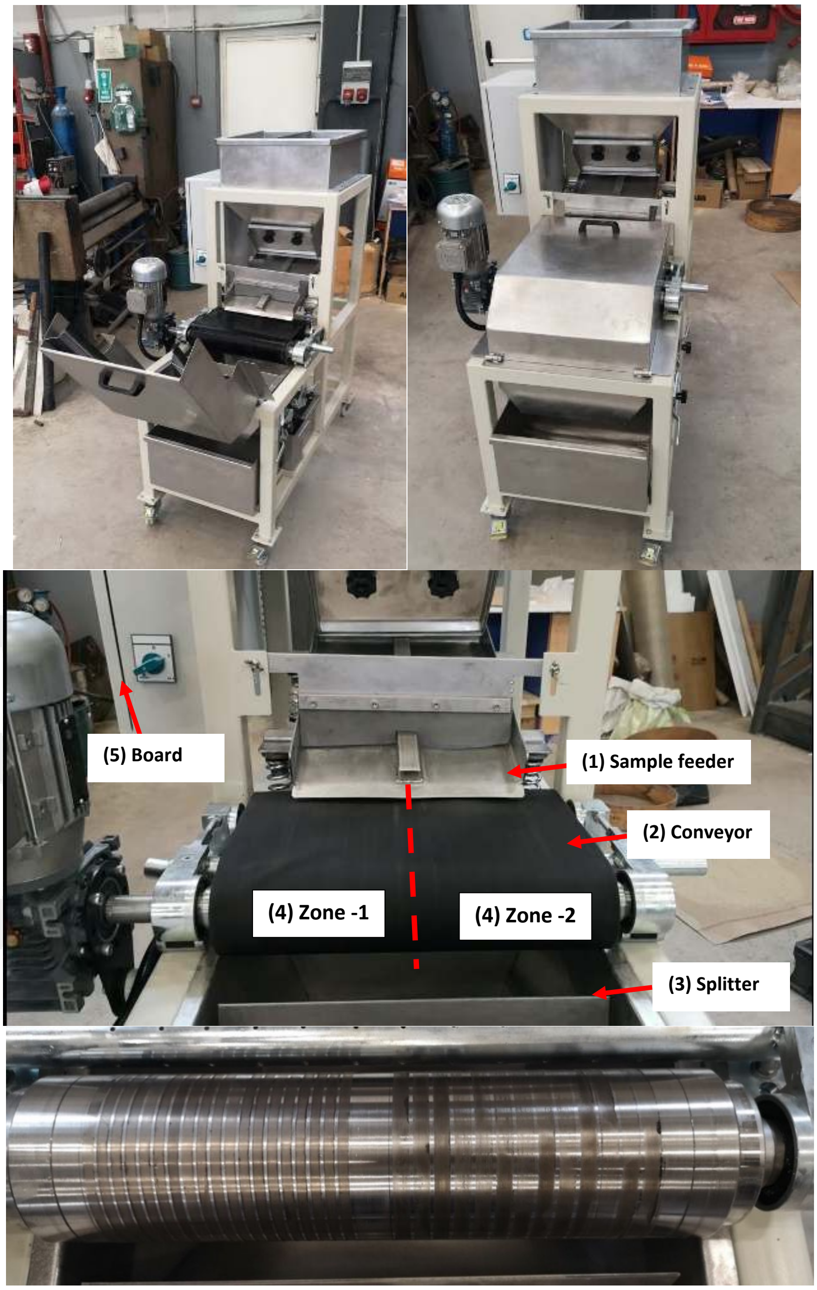

Figure 3.1. The photograph of a lab-scale dry roll-magnetic separator min proc lab, Çukurova University

Three products including magnetic, middling, and non-magnetic were obtained based on the splitter edge. However, there was no need to obtain a middling product, and therefore the edge was adjusted to obtain two different products: non-magnetic and magnetic products after the magnetic separation test. The experimental conditions that were investigated are listed in Table 3.3.

Table 3.3. The operations used during the experiments.

No	Particle size (mm)	Splitter Angle (°)	Speed (Hz)	Magnetic Field (T)	Cleaning stage
No1	-1+0.500	43	5	0.4 T	1
No2	-1+0.500				2
No3	-0.500+0.300				1
No4	-0.500+0.300				2
No5	-0.300+0.125				1
No6	-0.300+0.125				2
No7	-1+0.500			0.2 T	1
No8	-1+0.500				2
No9	-0.500+0.300				1
No10	-0.500+0.300				2
No11	-0.300+0.125				1
No12	-0.300+0.125				2
No13	-1+0.500	43	3	0.4 T	1
No14	-0.500+0.300				1
No15	-0.300+0.125				1
No16	-1+0.500		5		1
No17	-0.500+0.300				1
No18	-0.300+0.125				1
No19	-1+0.500		7		1
No20	-0.500+0.300				1
No21	-0.300+0.125				1
No22	-1+0.500	58	3		1
No23	-0.500+0.300				1
No24	-0.300+0.125				1
No25	-1+0.500		5		1
No26	-0.500+0.300				1
No27	-0.300+0.125				1
No28	-1+0.500		7		1
No29	-0.500+0.300				1
No30	-0.300+0.125				1

The obtained products (magnetic and non-magnetic) were weighed, and their chemical compositions were determined by XRF. Afterwards, the recovery of iron in the magnetic product was calculated using Equation 3.1.

$$X = \frac{c(f-t)}{f(c-t)} \times 100 \quad (3.1)$$

Where, X is the recovery of iron from the sample, c is the weight of the magnetic product after the magnetic separation test, (c-f) is the iron content in the magnetic product, f is the initial weight of the sample, (c-t) is the iron content in the feed.

3.2.4. Modeling of Magnetic Separation Test Results

ANN method, which is widely preferred in different sciences, was used in modeling the experimental results obtained (Govindaraju, 2000). This method can generate a solution on complex or imprecise data and detect trends that are very complex. Parallel distributed structure and generalization ability constitute the computation and information processing power of ANN. ANN is basically a method that tries to imitate the learning process of the human brain. An ANN contains a group of interconnected cells called neurons, which are interconnected via weighted synapses. The ANN structure includes a training layer created according to the input layer parameters and carries out the learning process. The information contained here is transmitted to the next neuron in the form of neural connections. The input and output layers contain neurons representing the input and output variables, respectively. The hidden layer, on the other hand, consists of a set of specific neurons and provides the connection between the two layers above (Yilmaz and Yuksek, 2009; Ravi Kiran and Rajput, 2011; Hayer and Khosravi, 2014; Gharaei-Manesh et. al, 2016). The structure of the ANN network can be seen in Figure 3.2.

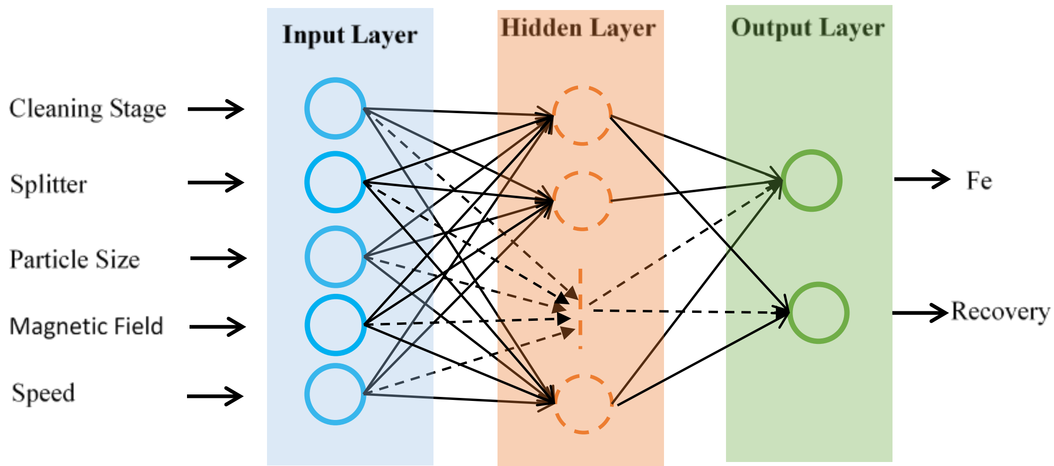

Figure 3.2. The structure of the ANN network (Gharaei-Manesh et. al, 2016)

In this study, using the ANN model, it was possible to determine the effect of working condition parameters (i.e. cleaning stage, splitter position, particle size, and magnetic field) on the iron content and the recovery of iron from the ore. The following three different training algorithms were used in the modeling stage. (i) Bayesian Regression (BR), (ii) Levenberg-Marquardt (ML), and (iii) Scaled Conjugate Gradient (SCG).

3.2.4.1 Training Algorithms Used to Predict the Magnetic Separation Test Results

Bayesian Linear Regression: Insufficient data or data with a bad distribution can be dealt with effectively using Bayesian linear regression. It enables you to apply a prior to the noise and coefficients, allowing the priors to assume control in the absence of data. What's more, you can inquire of Bayesian linear regression as to which aspects of its data-fitting capabilities it is confident in, and which aspects are questionable (perhaps based just on the priors). You can specifically ask it:

- What is the whole posterior distribution on the estimated linear relationship, what is the confidence in that relationship, and what is the estimated linear relationship?
- What are the estimated noise parameters and noise posterior distribution?
- What is the estimated gradient and the associated posterior distribution?

The Bayesian perspective uses probability distributions to formulate linear regression. The response, y, is supposed to be chosen from a probability distribution rather than being evaluated as a single number. The response is sampled from a normal distribution in the Bayesian Linear Regression model, and it is given by Equation (3.2):

$$y \sim N(\beta^T X, \sigma^2 I) \tag{3.2}$$

A normal distribution with a mean and variance produces the result, y. The weight matrix is transposed by the predictor matrix, and the result is the mean for linear regression. The variance is calculated by multiplying the identity matrix by the square of the standard deviation.

In addition to the model parameters also coming from a distribution, the response is also generated from a probability distribution. The training inputs and outputs affect the posterior probability of the model parameters in the following ways (Equation 3.3)

$$P(A/B) = \frac{P(B|A) * P(A)}{P(B)} \tag{3.3}$$

P(A) is the probability of event A occurring, also known as the prior probability.
P(A|B) is the conditional probability of event A occurring, given that B is true. This is the posterior probability due to its variable dependency on B. This assumes that event A is not independent of B.
P(A|B) is the conditional probability of event A occurring, given that B is true. This is the posterior probability due to its variable dependency on B. This assumes that event A is not independent of B.
P(B) is the probability of event B occurring.

Given the inputs and outputs, P(A/B) represents the posterior probability distribution of the model parameters. This is equal to the prior probability of the parameters multiplied by the likelihood of the data, P (B), and divided by a normalization constant (Equation 3.4)

$$\text{Posterior} = \frac{\text{Liklihood} * \text{Prior}}{\text{Normalization}} \tag{3.4}$$

Here, we can observe the two benefits of Bayesian Linear Regression:

- Priors: If we have knowledge (or a guess for what the model parameters should be), we can include them in our model. If we don't have any estimates ahead of time, we can use non-informative priors for the parameters, such as a normal distribution.
- Posterior: The result of performing Bayesian Linear Regression is a distribution of possible model parameters based on the data and the prior. This allows us to quantify our uncertainty about the model. If we have fewer data points, the posterior distribution will be more spread out.

When there are infinite data points, the outputs for the parameters converge to the values obtained by ordinary Least Squares (OLS), since the probability washes out the prior as the number of data points increases.

Levenberg-Marquardt: The algorithm called Levenberg–Marquardt algorithm was developed by Kenneth Levenberg and Donald Marquardt (Levenberg, 1944; Marquardt, 1963). A multivariate function can be written as the sum of squares of non-linear real-valued functions, and the Levenberg-Marquardt (LM) algorithm iteratively locates its minimum. It has been widely embraced across a wide range of fields and has emerged as the standard approach for non-linear least-squares issues. The Gauss-Newton method and the steepest descent can both be compared to LM. The technique operates like a steepest descent method when the current answer is very different from the correct one: it is slow but will eventually converge. It turns into a Gauss-Newton method when the present answer is reasonably near to the ideal one. This algorithm consists of the following four steps: steepest descent algorithm, Newton method, Gauss–Newton algorithm and Levenberg–Marquardt algorithm (Yu and Wilamowski, 2011).

The steepest descent algorithm can be written as follows:

$$w_{k+1} = w_k - \propto g_k \tag{3.5}$$

where

w is the weight vector;

k is the index of iterations;

∝ is the learning constant;

g is the total error function.

Newton's method is the second step as follows:

$$w_{k+1} = w_k - {H_k}^{-1} g_k \tag{3.6}$$

where H is a Hessian matrix.

The third step is the Gauss–Newton algorithm:

$$w_{k+1} = w_k - (J_k^T J_k)^{-1} J_k e_k \tag{3.7}$$

where

J is a Jacobian matrix;

e is an error vector.

The relationship between the Hessian matrix and the Jacobian matrix is given in Equation 3.8.

$$H \approx J^T J + \mu I \tag{3.8}$$

where

μ is always positive and called the combination coefficient;

I is the identity matrix.

Finally, the Levenberg–Marquardt algorithm is given below:

$$w_{k+1} = w_k - (J_k^T J_k + \mu I)^{-1} J_k e_k \tag{3.9}$$

Scaled Conjugate Gradient: The best algorithm should be used to ensure that the system gives the best training and test efficiency in the shortest amount of time, which is to supply the system with the fastest intelligence, in order to reduce experiment time and money waste. As a second order training procedure for neural networks, the scaled conjugate gradient algorithm is employed. With outstanding test efficiency, it offers quicker training. Information is used as input. From each parameter, some significant and trustworthy features are extracted and used as training input for a neural network. Weights are accepted for testing when the error level reaches a satisfactory level. Finally, the minor misclassification issues are resolved by a lexical matching technique.

It is possible to use another approach in estimating the step size than the line-search technique. The idea is to estimate the term δk = E"(Wk) Pk in Conjugate Gradient with a nonsymmetric approximation of the form:

- $\delta k = E''(W_k) P_k$ (3.10)

- $\delta k = \frac{E'(Wk + \sigma k\, Pk) - E'(Wk)}{\sigma k}$, $0 < \sigma_k < 1$. (3.11)

where, W is weight vector in space R^n, E(w) is the global error function, E' (w) is the gradient of error, $E'_{qw}(y1)$ is the quadratic approximation of error function, p1, p2....pk be the set of non-zero weight vectors.

where, λk is a scalar and is adjusted each time according to the sign of S_k.

The step size,

- $\alpha k = \frac{\mu k}{\delta k} = \frac{-pjT\, E'qw(y1)}{pjT\, E''(w)pj}$ (3.12)

Additional magnetic separation tests were carried out for use in the modeling to strengthen the prediction accuracy. Information about these tests is given in Table 3.4.

Table 3.4. Experimental conditions (size, splitter, speed, magnetic field and cleaning stage) for additional magnetic separation tests

No	Particle size (mm)	Splitter Angle (°)	Speed (Hz)	Magnetic Field (T)	Cleaning stage
M1	-0.500+0.300	43	5	0.4	2
M2	-0.300+0.125	43	5	0.4	2
M3	-0.300+0.125	43	7	0.4	2
M4	-0.500+0.300	43	7	0.4	2
M5	-0.300+0.125	43	7	0.4	2
M6	-0.300+0.125	58	3	0.4	2
M7	-0.500+0.300	58	3	0.2	2
M8	-0.300+0.125	58	3	0.2	2
M9	-0.300+0.125	58	5	0.2	2
M10	-0.500+0.300	58	5	0.2	2
M11	-0.300+0.125	58	5	0.2	2
M12	-0.300+0.125	58	7	0.2	2
M13	-0.500+0.300	58	7	0.4	2
M14	-0.300+0.125	58	7	0.4	2

3.2.4.2 Criteria for Performance Evaluation

To evaluate the validation of developed models, four performance assessment indicators comprised the Coefficient of correlation (R), Root Mean Squared Error (RMSE), Mean Square Error (MSE), and Mean Absolute Error (MAE) were used.

The coefficient of correlation (R) is a statistical measure of how well unknown data are predicted relative to known data. R takes a value between 0 and 1, and the closer to 1, the higher the prediction accuracy (Ceryan, 2014). How much error is made while estimating new data is measured with the mean absolute error (MAE) indicator. The lower the value, the more accurate the model (Kabiru et al., 2014). Mean square error (MSE) and root mean square error (RSME) are indicators of the quality of a regression model. MSE is the mean of the square of the error and RMSE is the square root of the MSE. When MSE and RMSE values approach zero, it means that the accuracy of the model increases (Gilan et al., 2012). R, MAE, MSE and RMSE are calculated by the following Equations:

$$R = \sqrt{\frac{\sum_{i=1}^{n}(y_{mi}-\bar{y}_m)^2-\sum_{i=1}^{n}\left(y_{mi}-y_{pi}\right)^2}{\sum_{i=1}^{n}(y_{mi}-\bar{y}_m)^2}} \tag{3.13}$$

$$MAE = \frac{\sum_{i=1}^{n}|y_{mi}-y_{pi}|}{n} \tag{3.14}$$

$$MSE = \frac{1}{n}\sum_{i=1}^{n}\left(y_{mi}-y_{pi}\right)^2 \tag{3.15}$$

$$RMSE = \sqrt{\frac{1}{n}\sum_{i=1}^{n}\left(y_{mi}-y_{pi}\right)^2} \tag{3.16}$$

where y_{mi} and y_{pi} are the ith observation of the actual data and predicted data, respectively, $\bar{y}_m$ is the mean of the actual data and n is the number of observations.

3.2.5. Different Scenarios for Magnetic Separation Tests

Two different scenarios were investigated to obtain the magnetic product with a high iron content and high recovery. Additional separation tests were carried out on the sample obtained as the non-magnetic product in the magnetic separation test (Figure 3.3).

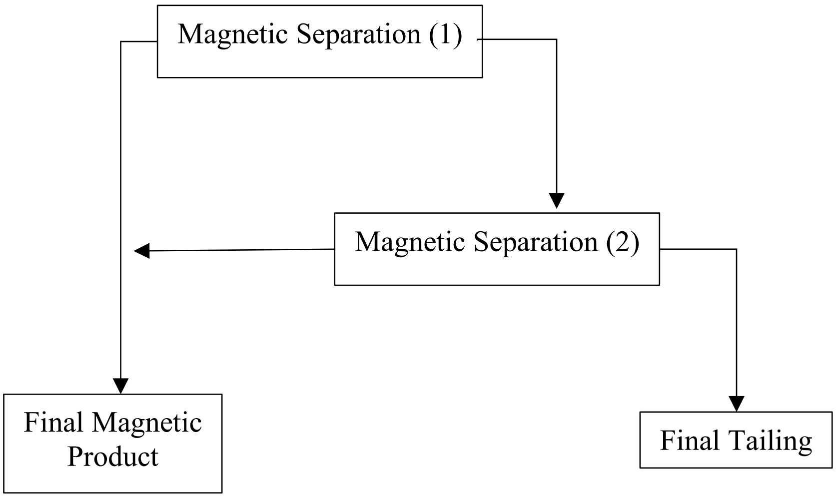

Figure 3.3. Scenario for magnetic separation test

3.2.6. Microwave Treatment

To improve the recovery of iron from the ore, samples with different sizes were exposed to microwave treatment at a field of 1800 W for different times to experiment microwave-assisted reduction roasting of hematite. The surface temperature of each sample was measured using a thermal camera (Testo 865). The effect of microwave treatment on the properties of the sample was investigated by using various instrumental techniques including, optical microscope (Leica), XRD (PANalytical EMPYREAN), and magnetic hystheris (Quantum Design, PPMS DynaCool-9).

4. RESULTS AND DISCUSSIONS

4.1. Mineral Liberation Analysis (MLA) of the Ore

The detailed mineral liberation (MLA) analysis was carried out to determine various properties of the ore: (i) modal mineralogy, (ii) calculated assay, (iii) elemental distribution, and (iv) mineral locking. As EDS detector that is available in MLA equipment cannot measure elements (i.e. H^{+}) having a lower than 7 atomic number, it was not possible to detect the amount of hematite and goethite minerals separately and these minerals were named as iron-oxide minerals during the analysis. Many particles representing iron-oxide minerals were detected by the MLA analysis (Figure 4.1).

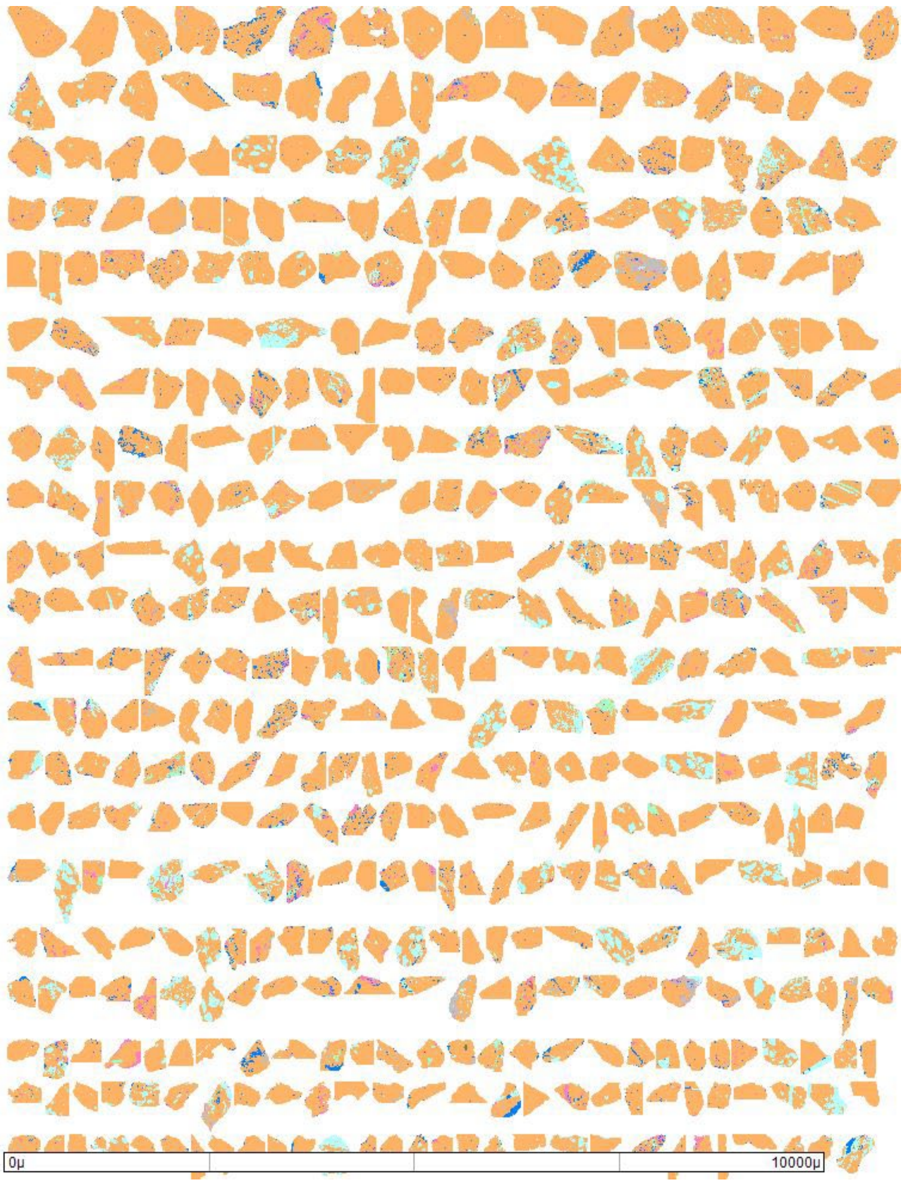

Figure 4.1. MLA classified images showing iron-oxide in the sample

The calculated elemental content by MLA was shown in Figure 4.2. It is clearly seen that the sample contained 40% iron, %5.45 Si, and %10.95 others, which are in good agreement with the chemical results detected by AAS analysis (can be seen in Table 3.1).

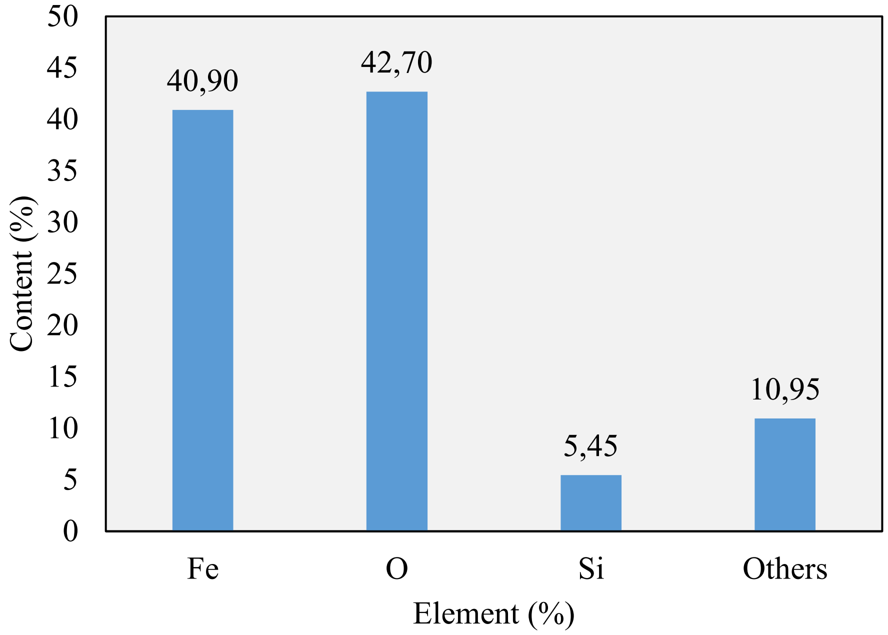

Figure 4.2. Calculated elemental content by MLA.

Figure 4.3 shows the modal distribution of the sample used in this study. The detailed mineralogical analysis indicated that the sample was mainly composed of iron-oxide minerals as major content, and quartz (SiO_2), chlorite ($(Mg,Fe)_3(Si,Al)_4O_{10}(OH)_2{\cdot}(Mg,Fe)_3(OH)_6$), ilmenite ($Fe^{2+}TiO_3$), kaolinite ($Al_2Si_2O_5(OH)_4$), apatite ($Ca_5(PO_4)(F,Cl,OH)$), muscovite ($KAl_3Si_3O_{10}(OH)_{1.9}F_{0.1}$) , zircon ($ZrSiO_4$), Al-silicate ($Al_2SiO_5$), rutile ($TiO_2$), calcite ($CaCO_3$), spinel-chromite ($(Fe^{2+},Mg)Cr_2O_4$) , and plagioclase ($Na_{0.5}Ca_{0.5}Si_3AlO_8$) minerals as minor content. iron-oxide minerals detected by X-ray diffraction (XRD, PANalytical Empyrean) analyses were hematite and goethite minerals (Figure 4.3.b), but other minerals cannot be determined due to the detection limit of the XRD analysis (<5%).

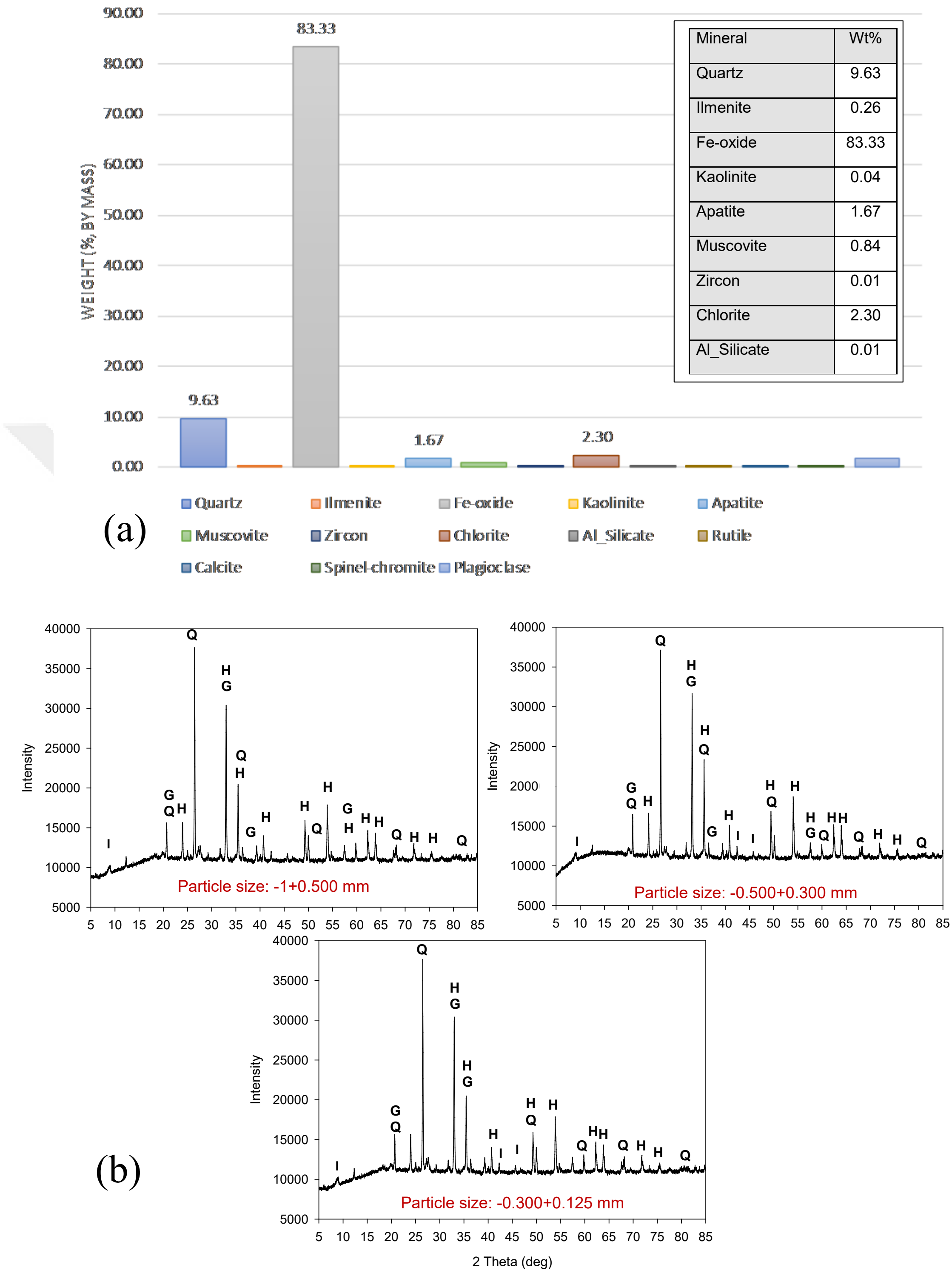

Mineral	Wt%
Quartz	9.63
Ilmenite	0.26
Fe-oxide	83.33
Kaolinite	0.04
Apatite	1.67
Muscovite	0.84
Zircon	0.01
Chlorite	2.30
Al_Silicate	0.01

Figure 4.3. (a) Modal mineral distribution of the sample (by mass), (b) XRD pattern of the raw ore in different particle size ranges (G: Goethite “96-100-8768”, Q: Quartz “96-500-0036”, H: Hematite “96-900-0140”)

Figure 4.4 shows the elemental distribution of the sample based on the mineral content and it was determined that approximately 98.21% of iron was found in iron-oxide minerals, whereas 1.79% of iron was determined in chlorite and ilmenite minerals. The presence of Si in quartz, plagioclase, and other minerals was found to be 82.58%, 10.44%, and 6.94%, respectively. Al-bearing minerals were as follows: plagioclase (33.05% Al), muscovite (29.86% Al), chlorite (32.78% Al), and others (2.24% Al). In addition, the detailed findings related to the elemental distribution of the ore can be seen in Table 4.1.

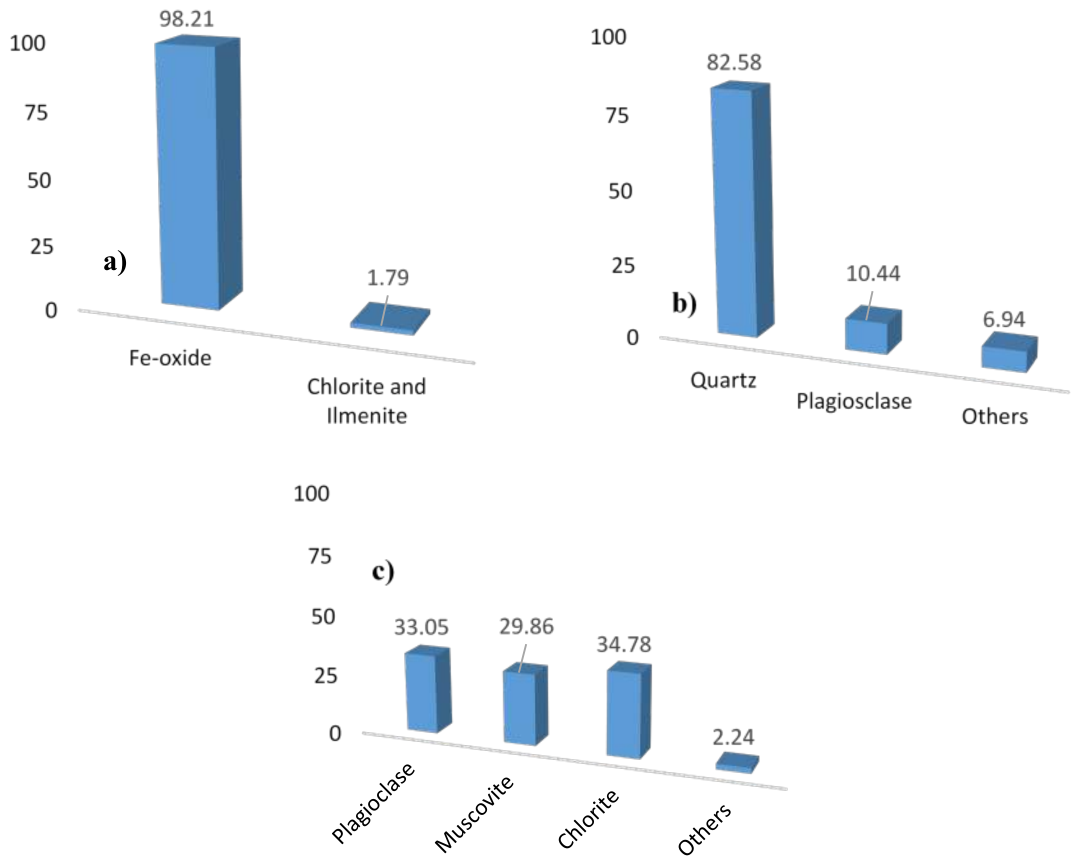

Figure 4.4. Elemental distribution based on mineral content (by mass) a) Fe, b) Si, and c) Al

Table 4.1. Elemental distribution of the raw ore based on mineral content.

Mineral	Al (%)	C (%)	Ca (%)	Cl (%)	Cr (%)	F (%)	Fe (%)	H (%)	K (%)
Quartz	0.00	0.00	0.00	0.00	0.00	0.00	0.00	0.00	0.00
Ilmenite	0.00	0.00	0.00	0.00	0.00	0.00	**0.24**	0.00	0.00
Fe-oxide	0.00	99.96	0.00	0.00	0.00	0.00	**98.21**	0.00	0.00
Kaolinite	**1.58**	0.00	0.00	0.00	0.00	0.00	0.00	1.90	0.00
Apatite	0.00	0.00	81.58	100.00	0.00	72.06	0.00	2.94	0.00
Muscovite	**29.86**	0.00	0.00	0.00	0.00	27.94	0.09	11.14	100.00
Zircon	0.00	0.00	0.00	0.00	0.00	0.00	0.00	0.00	0.00
Chlorite	**34.78**	0.00	0.00	0.00	0.00	0.00	**1.46**	84.02	0.00
Al_Silicate	**0.66**	0.00	0.00	0.00	0.00	0.00	0.00	0.00	0.00
Rutile	0.00	0.00	0.00	0.00	0.00	0.00	0.00	0.00	0.00
Calcite	0.00	0.04	1.60	0.00	0.00	0.00	0.00	0.00	0.00
Spinel-chromite	0.07	0.00	0.00	0.00	100.00	0.00	0.00	0.00	0.00
Plagioclase	**33.05**	0.00	16.82	0.00	0.00	0.00	0.00	0.00	0.00

Mineral	Mg (%)	Mn (%)	Na (%)	O (%)	P (%)	Si (%)	Ti (%)	Zr (%)
Quartz	0.00	0.00	0.00	12.01	0.00	**82.58**	0.00	0.00
Ilmenite	0.00	100.00	0.00	0.19	0.00	0.00	74.35	0.00
Fe-oxide	0.00	0.00	0.00	80.85	0.00	0.00	0.00	0.00
Kaolinite	0.00	0.00	0.00	0.05	0.00	0.17	0.00	0.00
Apatite	0.00	0.00	0.00	1.51	100.00	0.00	0.00	0.00
Muscovite	3.06	0.00	0.00	0.85	0.00	**3.07**	7.07	0.00
Zircon	0.00	0.00	0.00	0.01	0.00	0.04	0.00	100.00
Chlorite	96.85	0.00	0.00	2.40	0.00	**3.66**	0.00	0.00
Al_Silicate	0.00	0.00	0.00	0.01	0.00	0.03	0.00	0.00
Rutile	0.00	0.00	0.00	0.03	0.00	0.00	18.54	0.00
Calcite	0.00	0.00	0.00	0.04	0.00	0.00	0.00	0.00
Spinel-chromite	0.09	0.00	0.00	0.00	0.00	0.00	0.04	0.00
Plagioclase	0.00	0.00	100.00	2.03	0.00	**10.44**	0.00	0.00

Free iron-oxide particle, a particle that is composed of iron-oxide and quartz, and a particle containing many minerals were determined in SEM-EDS and MLA images, respectively (Figure 4.5. 4.6 and 4.7). It was clearly seen that iron-oxide particles occurred as binary or ternary associations with different quartz, plagioclase, muscovite, apatite, chlorite and other mineral phases and the free surface of iron-oxide was only 32.84%, as shown in Figure 4.8. The amount of the liberated iron-oxide mineral was found to be 54.17%, whereas the rests occurred 37.47% binary particle and 8.36% ternary particle. Table 4.2 summarizes the distribution of iron-oxide mineral and its liberation degree in the ore.

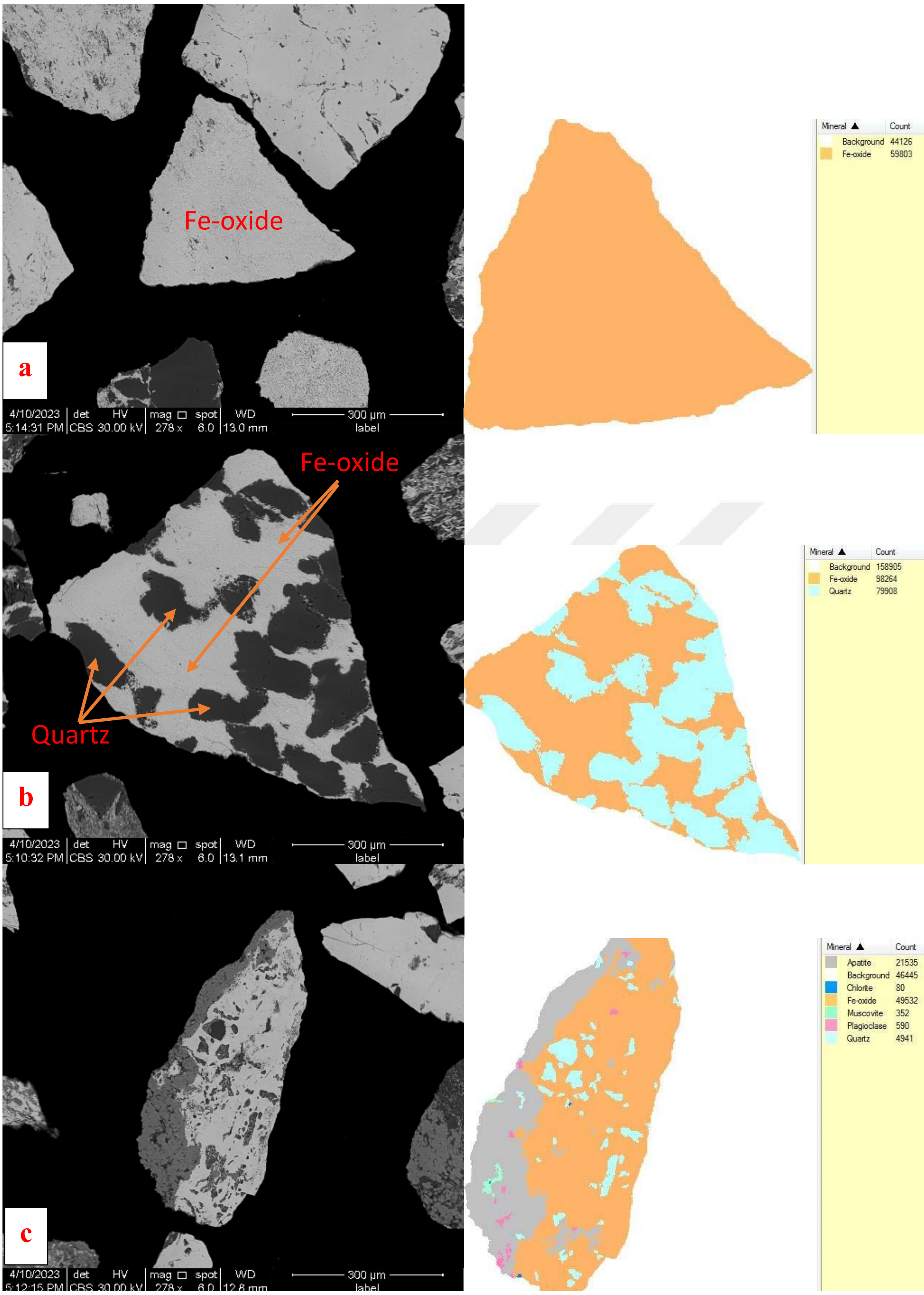

Figure 4.5. SEM and BSE images (a) free iron-oxide particle, (b) particle that is composed of quartz and iron-oxide, (c) particle that is composed of many minerals; apatite, chlorite, iron-oxide, muscovite, plagioclase, and quartz

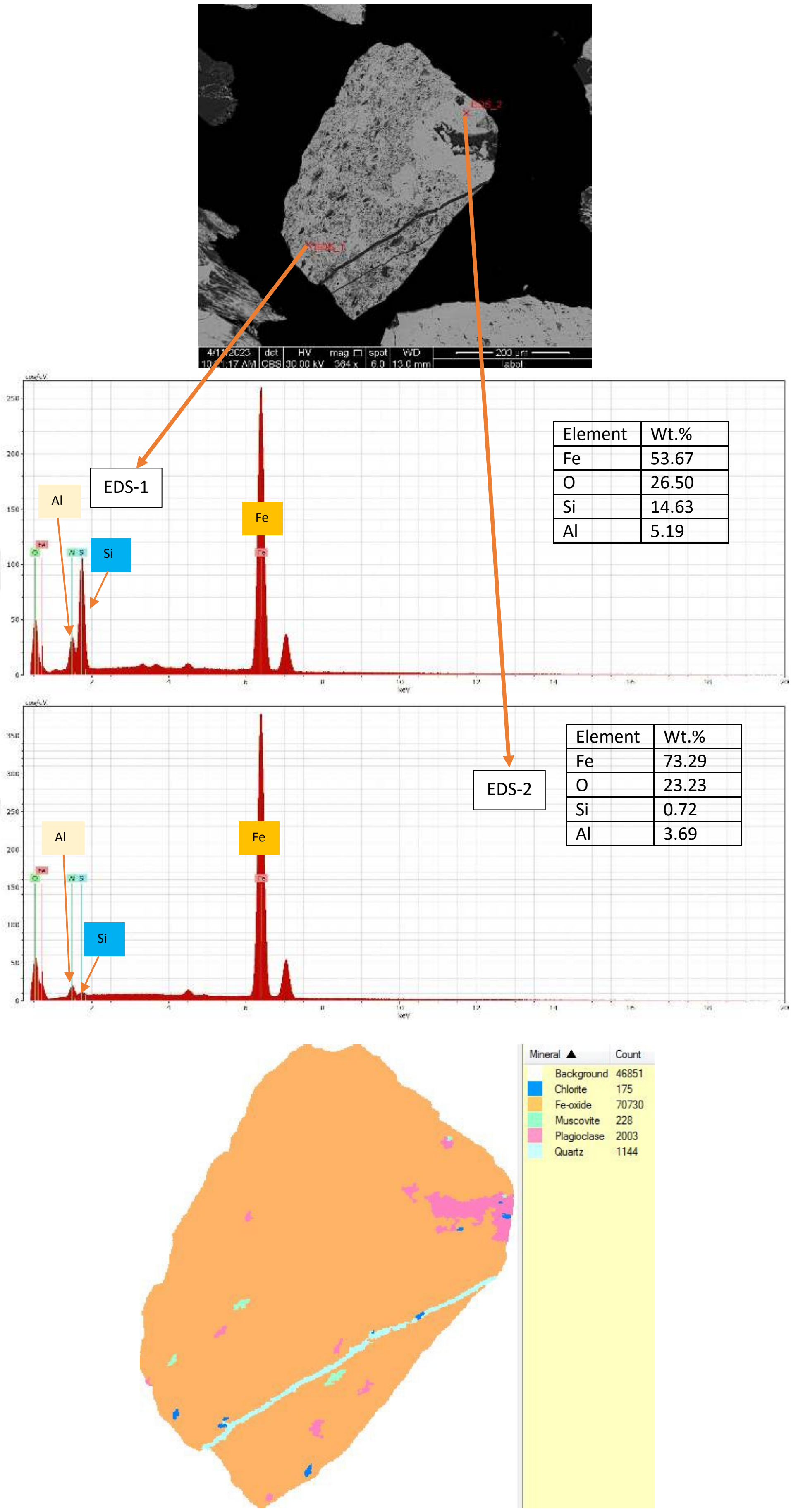

Figure 4.6. EDS spectrums of a particle that is composed of Al, Fe, Si, and O element

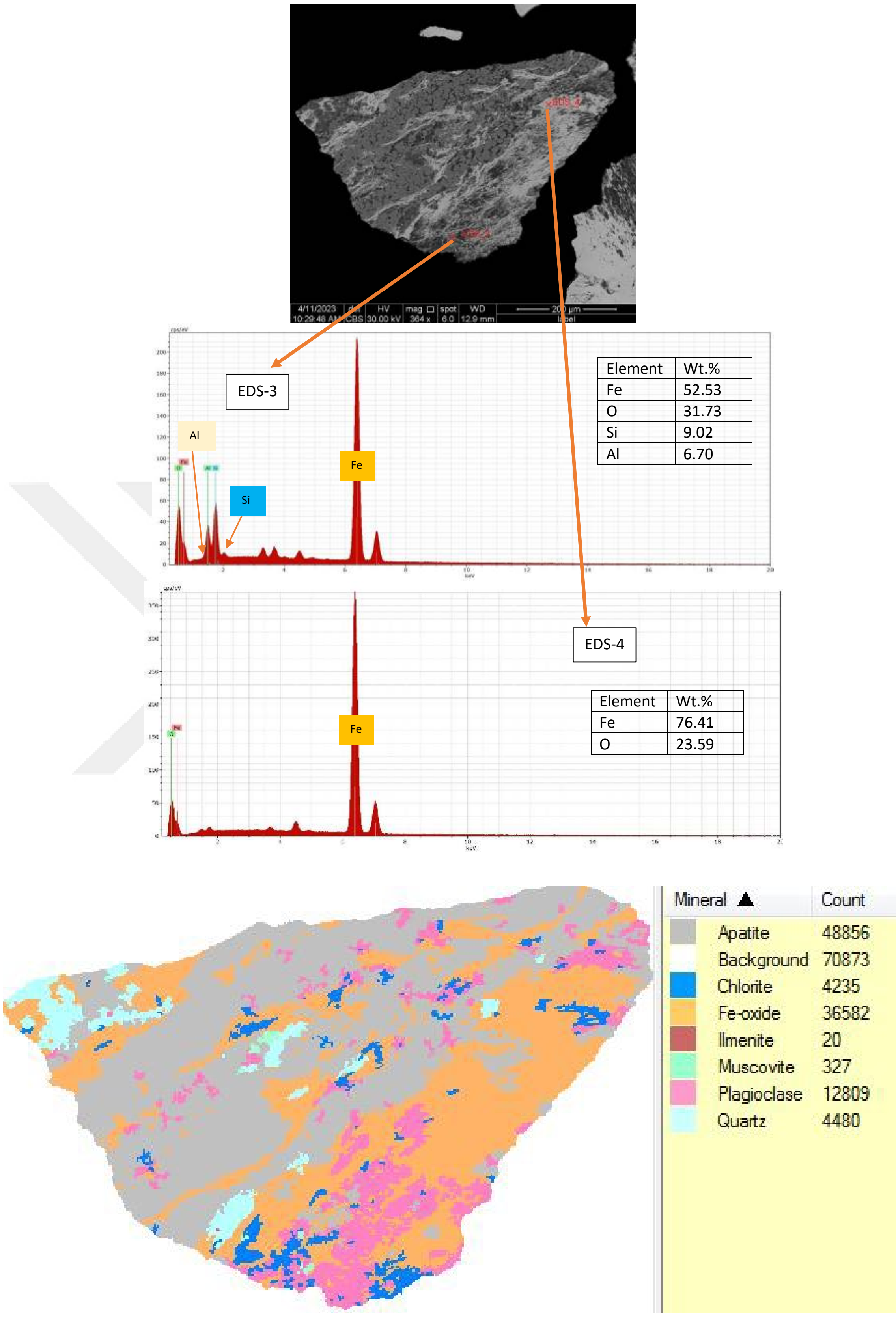

Figure 4.7. EDS spectrums of different particles that are composed of Al, Fe, Si, and O elements

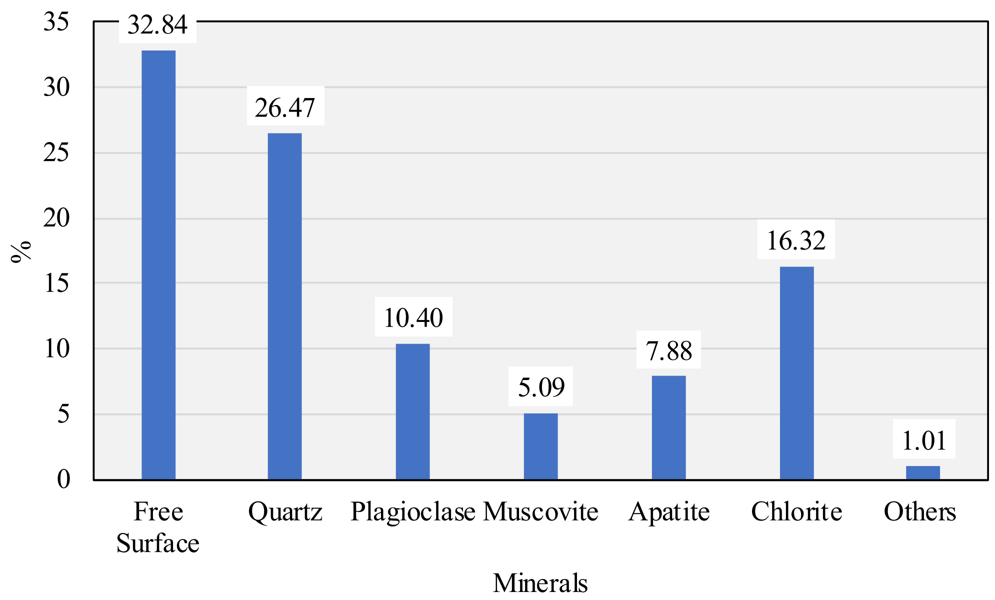

Figure 4.8. Locking of iron-oxide minerals in the ore

Table 4.2. Mineral associations for iron-oxide minerals (binary particle: A particle containing two phase, ternary particle: A particle containing at least three phases) and liberation degree of iron-oxide minerals

iron-oxide Weight% locked in...	**Binary Particle (%)**	**Ternary+ Particle (%)**
Quartz	20.62	2.25
Ilmenite	0.10	0.17
Kaolinite	0.00	0.01
Apatite	4.44	1.33
Muscovite	1.82	0.73
Zircon	0.00	0.02
Chlorite	6.21	2.02
Al-Silicate	0.00	0.00
Rutile	0.07	0.03
Calcite	0.00	0.00
Spinel-chromite	0.00	0.00
Plagioclase	4.22	1.79
iron-oxide distribution summary (%)		
Liberated (%)	54.17	
Total Binary (%)	37.47	
Total Ternary (%)	8.36	
Total Lib+Bin (%)	91.64	
Total Lib+Bin+Tern (%)	100.00	
Liberated (%)	54.17	

4.2. Magnetic Separation Tests

4.2.1. The large particle sample (with a size of -1+0.500 mm)

The prepared sample was tested in two different magnetic fields (0.2 and 0.4T) then cleaned in two steps. Having been passed on a 0.2T, the sample shows an increase of iron (%) which was 39.5% but a considerable decrease in the recovery; in the other part we can observe a decrease in both with a 0.4T. It is clearly seen from Table 4.3 that there is an opposite reaction between the iron recovery and the iron that allow as to say that with a high magnetic field we can obtain a higher recovery of 67.67% but 56.32% of iron by contrast we are able to obtain a high iron of 66.17% but a recovery of 19.07% with a low magnetic field and 2 cleaning stages.

Table 4.3. Effect of cleaning stage on the recovery of iron from the sample prepared in -1+0.500 mm (experimental parameters that were kept constant in this stage are as follows: conveyor speed: 5 Hz, splitter position: 43°)

Exp. No	Magnetic Field (T)	Cleaning stage	Magnetic product				Fe recovery (%)	Fe (%)*
			Amount (%)	Fe (%)	SiO_2 (%)	Al_2O_3 (%)		
No1	0.4	1	47.10	56.32	7	6.4	67.67	23.96
No2		2	32.40	53.03	5	14	43.83	32.57
No7	0.2	1	19.75	64.51	3.01	0.12	32.50	32.97
No8		2	11.30	66.17	1.01	0.1	19.07	35.76

* is the iron content of the non-magnetic product.

Figure 4.9 illustrates a low recovery on both high and low magnetic fields and a quite same obtainment of iron with the cleaning steps. Therefore, the cleaning steps with a -1+0.500 mm of the sample was not efficient.

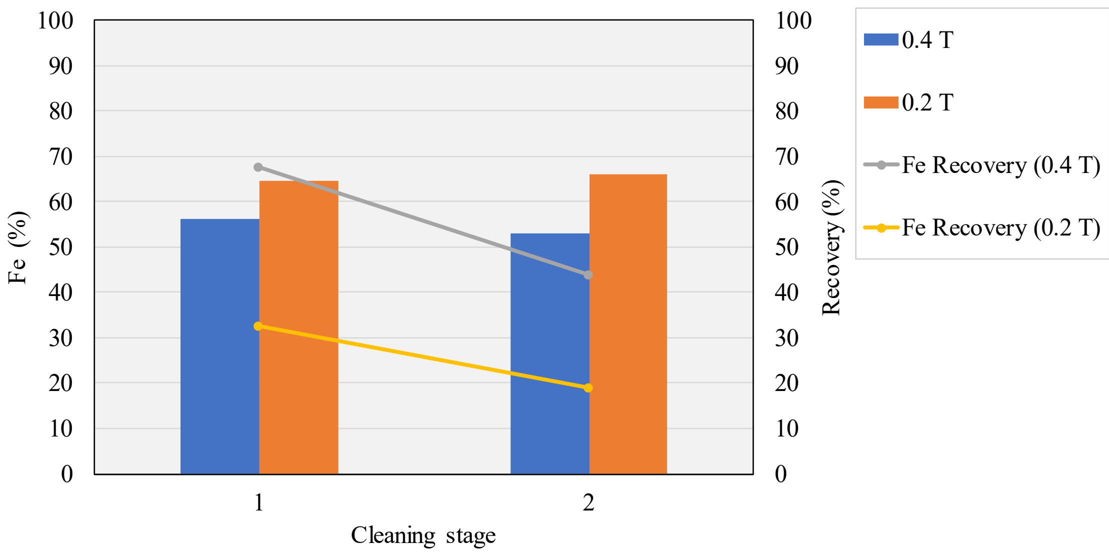

Figure 4.9. Effect of cleaning stage on the recovery of iron (-1+0.500 mm)

Table 4.4 shows the result of magnetic separation based on one cleaning stage, a high magnetic field, two different splitter positions (43 and 58°) and convey speed for the sample. Taking the splitters result and the convey speed into consideration, the quantity of iron increases efficiently with both splitters while the convey speeds. However, there is a remarkable withdraw for the recovery with the speed. From the result we can conclude that the speed sends even some magnetic particles to the non-magnetic section which explains that we have a higher iron of 67.59 and 65.49% but recovery of 14.10 and 28.9%. The higher recovery of 94.43% is observed with the splitter at 58° and 3 Hz of speed but the iron is seen with the splitter at 43° with 7 Hz of speed.

Table 4.4. Effect of splitter position on the recovery of iron from the sample prepared in -1+0.500 mm of particle size (experimental parameters that were kept constant in this stage are as follows: cleaning stage: 1, magnetic field: 0.4 T)

Exp. No	**Splitter (°)**	**Conveyor speed (Hz)**	**Magnetic product**				**Fe recovery (%)**	**Fe (%)***
			Amount (%)	**Fe (%)**	**SiO_2 (%)**	**Al_2O_3 (%)**		
No13	43	3	65.63	52.93	8.8	8.6	88.62	12.98
No16		5	38.25	56.34	6	8.8	54.97	28.59
No19		7	8.18	**67.59**	**1.4**	**0.9**	**14.10**	36.67
No22	58	3	86.35	42.87	13	10.1	94.43	16.00
No25		5	63.63	53.23	8	9.3	80.81	14.66
No28		7	17.30	**65.49**	**1.3**	**0.6**	**28.90**	33.70

* is the iron content of the non-magnetic product.

Figure 4.10 illustrates the relation between the convey speed and the splitter positions. It is remarked that as the speed increase the recovery decreases which is the opposite of the iron content at its turn increases with the speed.

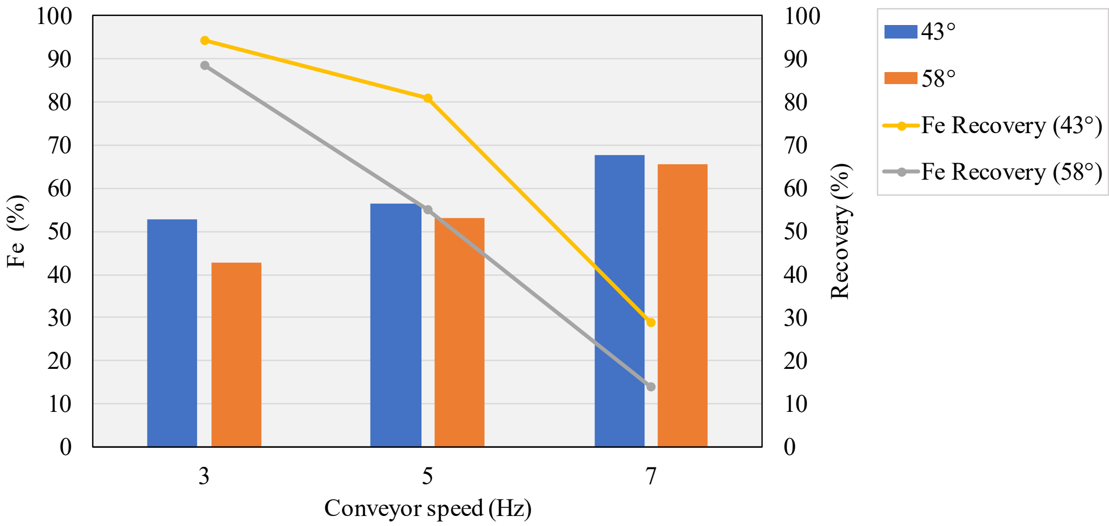

Figure 4.10. Effect of splitter position on the recovery of iron (-1+0.500 mm)

4.2.2. The mid particle sample (with a size of -0.500+0.300 mm)

Another 2 steps cleaning with 5Hz of convey speed, 2 different magnetic fields and 43° of splitter was experimented for the sample -0.500+0.300. For both magnetic fields, the iron content slightly increased from 48.27 to 52.96% and from 48.55 to 50.94% but the recovery is dramatically decreasing from 77.54 to 64.96% and from 54.12 to 37.35% with the cleaning stages. There is an important amount of iron in the non-magnetic product (Table 4.5). These experiments couldn't satisfy the purpose aimed by this study which is to have a iron content of at least 56% with a recovery over 70%.

Table 4.5. Effect of cleaning stage on the recovery of iron from the sample prepared in -0.500+0.300 mm (experimental parameters that were kept constant in this stage are as follows: conveyor speed: 5 Hz, splitter position: 43°)

Exp. No	Magnetic Field (T)	Cleaning stage	Magnetic product				Fe recovery (%)	Fe (%)*
			Amount (%)	Fe (%)	SiO_2 (%)	Al_2O_3 (%)		
No3	0.4	1	67.33	48.27	14	9	77.54	28.81
No4		2	51.40	52.96	9.9	8.3	64.96	30.22
No9	0.2	1	46.73	48.55	14	8.3	54.12	36.09
No10		2	30.73	50.94	12	8.1	37.35	37.90

* is the iron content of the non-magnetic product.

Summarizing Table 4.5, we can obtain the graph in Figure 4.11 which presents a slump on the recovery with the 2nd cleaning stage.

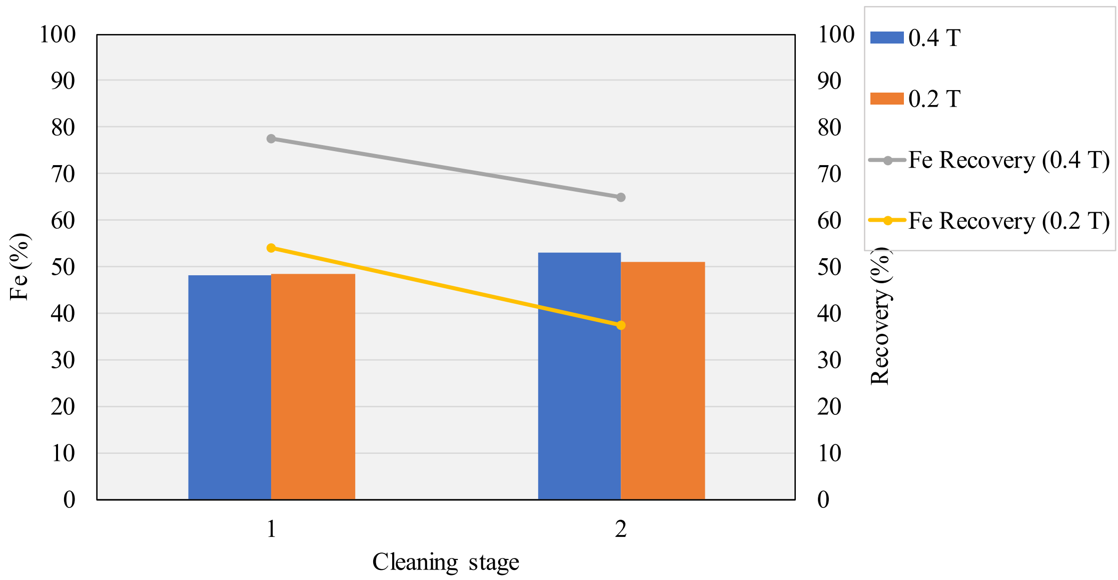

Figure 4.11. Effect of cleaning stage on the recovery of iron (-0.500+0.300 mm).

An increase in the rotation speed of roller improves the concentrate grade but reduces the iron recovery for both splitters. As the rotation speed of roller increases, the centrifugal force upon particles increases, so that more non-magnetic particles and fine magnetic particles were discarded out of the magnetic field, resulting in improvement of concentrate grade at the expense of recovery. The higher recovery of 98.43% is observed with the splitter at 58° with less iron in the non-magnetic and 45.48% of iron in the magnetic product. While the speed increases, we obtained higher amount of iron which extended up to 63.74% but the recovery was inacceptable. (Table 4.6). These findings are consistent with those of a previous study (Zhang et al. 2015).

Table 4.6. Effect of splitter position on the recovery of iron from the sample prepared in -0.500+0.300 mm (experimental parameters that were kept constant in this stage are as follows: cleaning stage: 1, magnetic field: 0.4 T)

Exp. No	Splitter (°)	Conveyor speed (Hz)	Magnetic product				Fe recovery (%)	Fe (%)*
			Amount (%)	Fe (%)	SiO_2 (%)	Al_2O_3 (%)		
No14	43	3	77.93	46.83	14.01	10.7	87.08	24.54
No17		5	56.98	52.49	9.6	9.3	71.36	27.89
No20		7	23.18	**63.74**	1.5	0.9	**35.25**	35.32
No23	58	3	90.70	45.48	15.01	10.1	98.43	7.09
No26		5	75.10	49.29	11.9	9.2	88.32	19.66
No29		7	34.90	53.99	8.3	8.2	44.96	35.43
* is the iron content of the non-magnetic product.								

Figure 4.12 illustrates the result shown in Table 4.6 which is a low recovery while increasing the roller speed.

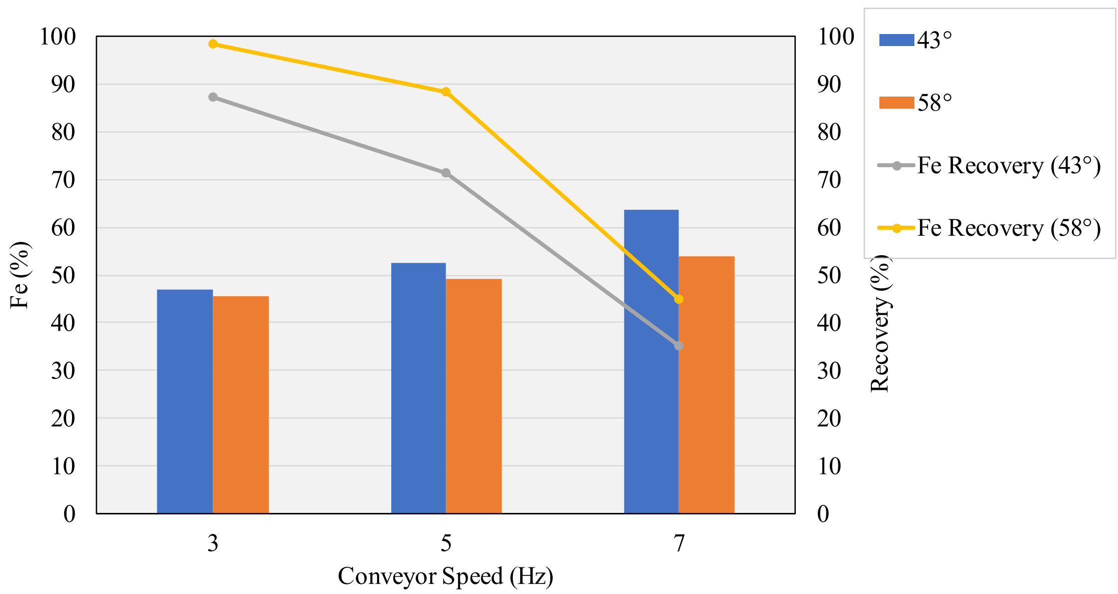

Figure 4.12. Effect of splitter position on the recovery of iron (-0.500+0.300 mm)

4.2.3. The fine particle sample (with a size of -0.300+0.125 mm)

Table 4.6 shows a finer product which was experimented with 2 different magnetic fields, 2 cleaning stages, 5Hz of speed and 43° of splitter. There are no considerable decreases with the cleaning stages but a slight increase with the magnetic fields (Figure 4.13). The higher magnetic field allows us to obtain a higher recovery of 90.27% whereas the amount of iron in the magnetic product is seen to be same for both magnetic fields. The cleaning stages have no significant impact on the product. Having seen the result, there might be an effect if we adjust the speed of the rollers.

Table 4.7. Effect of cleaning stage on the recovery of iron from the sample prepared in -300+0.125 mm (experimental parameters that were kept constant in this stage are as follows: conveyor speed: 5 Hz, splitter position: 43°)

Exp. No	**Magnetic Field (T)**	**Cleaning stage**	**Magnetic product**				**Fe recovery (%)**	**Fe (%)***
			Amount (%)	**Fe (%)**	**SiO_2 (%)**	**Al_2O_3 (%)**		
No5	0.4	1	77.78	45.96	15	9.9	90.27	17.33
No6		2	65.83	48.33	13	9.5	80.35	22.77
No11	0.2	1	72.20	45.63	15	10.2	83.22	23.90
No12		2	50.18	48.48	13	9.4	61.43	30.65

* is the iron content of the non-magnetic product.

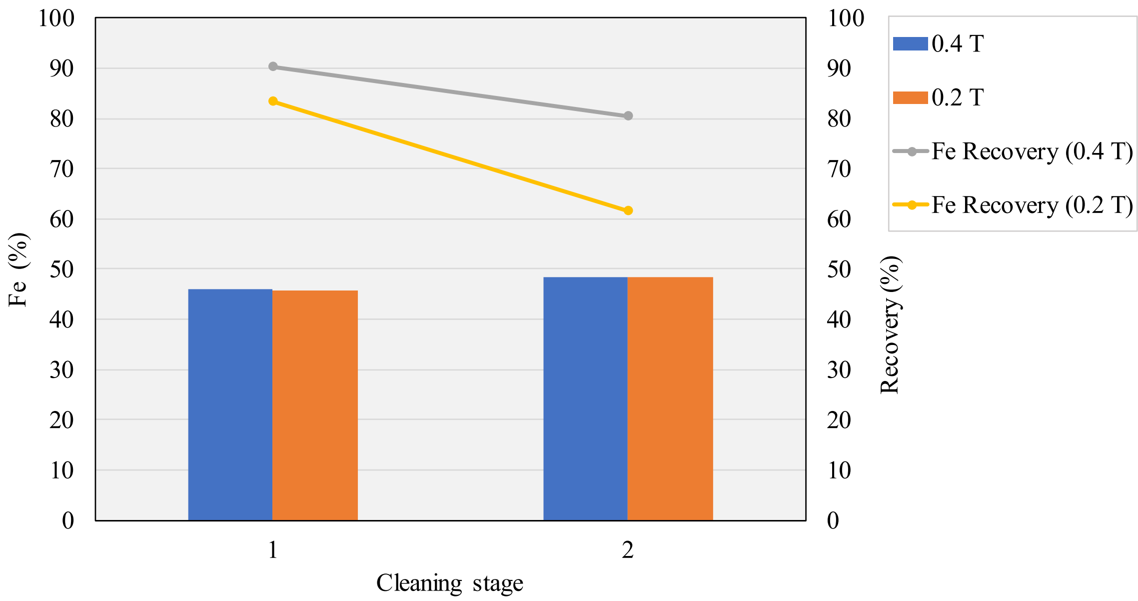

Figure 4.13. Effect of cleaning stage on the recovery of iron (-300+0.125 mm)

Table 4.6 shows that an opposite reaction is seen while testing the fine product with 2 different splitters at 43 and 58° in the iron content on the magnetic product compared to the recovery. The previous test allows to set the magnetic field to 0.4T and choose one cleaning stage due to the higher recovery and a quite same amount of iron in the magnetic product. It was decided to change the splitter position and increase the roller speed to see if we can obtain a better result. With the chosen parameters the iron increases to 51.00% with the higher speed of 7Hz while the recovery decreases considerably to 50.94% from 93.87%, as shown in Figure 4.14.

Table 4.8. Effect of splitter position on the recovery of iron from the sample prepared in -0.300+0.125 mm (other parameters that were kept as constant: cleaning stage: 1, magnetic field: 0.4 T)

Exp. No	**Splitter (°)**	**Convery speed (Hz)**	**Magnetic product**				**Fe recovery (%)**	**Fe (%)***
			Amount (%)	**Fe (%)**	**SiO_2 (%)**	**Al_2O_3 (%)**		
No15	43	3	83.65	44.43	16.01	10.5	93.87	14.84
No18		5	70.78	46.09	16	9.3	82.39	23.86
No21		7	39.55	51.00	11.1	8.6	50.94	32.13
No24	58	3	94.85	40.22	15.01	10.1	96.36	27.99
No27		5	83.45	44.10	17	10.5	87.81	16.86
No30		7	50.18	50.43	10.7	9.8	63.91	28.68
* is the iron content of the non-magnetic product.								

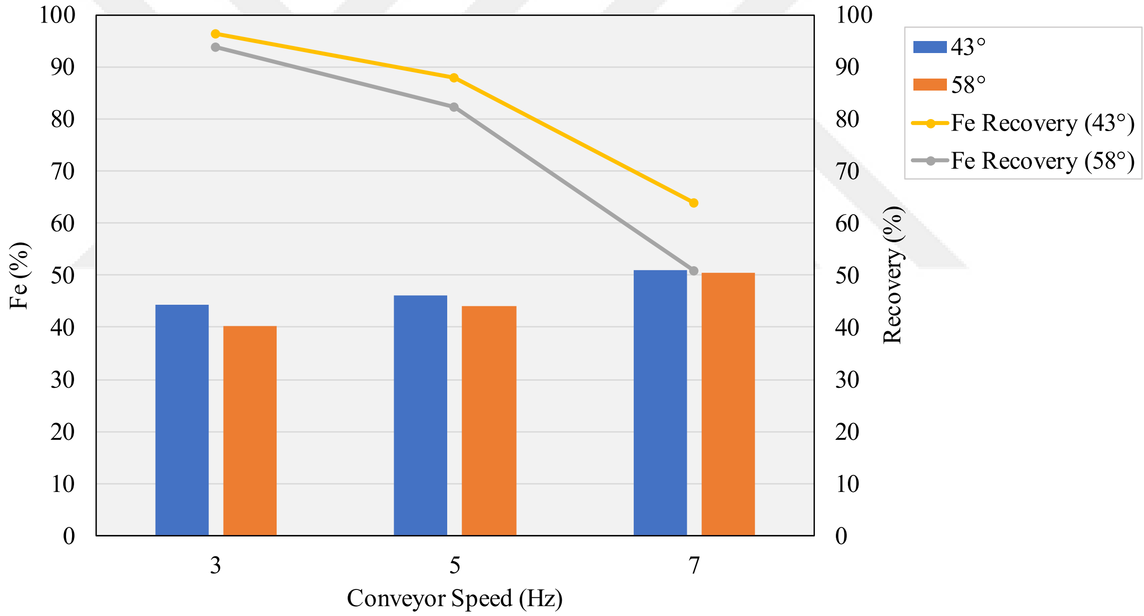

Figure 4.14. Effect of splitter position on the recovery of iron (-0.300+0.125 mm)

4.3. Modeling

All experimental results used in the modeling are listed in Table 4.9. To obtain an adequate result from iron processing methods, the most important parameters are iron and the recovery. The direct analysis of the recovery in the laboratory causes losses of both electrical grade and time. Also, performing this analysis by manual methods may lead to experimental errors. To overcome these problems, the iron and recovery were estimated based on the data set from experiments. By recording the experimental results, a data set consisting of 44 data was created and the same data set was used in all modeling studies. For the robustness of algorithms, the data were split into two sets, namely, training sets and test sets in a random manner. While training sets consisted of 80% of the all data set, the test set formed 20% of it.

Table 4.9. Experimental results used in the modeling test (1: -1+0.500 mm, 2: -0.500+0.300 µm, and 3: -0.300+0.125 µm)

Test No	Particle size	Splitter (°)	Speed (Hz)	Magnetic Field (T)	Cleaning stage	Fe (%)	Recovery (%)
No1	1	43	5	0.4	1	56.32	67.67
No2	1	43	5	0.4	2	53.02	43.83
No3	2	43	5	0.4	1	48.26	77.54
No4	2	43	5	0.4	2	52.96	64.96
No5	3	43	5	0.4	1	45.95	90.27
No6	3	43	5	0.4	2	48.32	80.35
No7	1	43	5	0.2	1	64.51	32.50
No8	1	43	5	0.2	2	66.17	19.07
No9	2	43	5	0.2	1	48.54	54.12
No10	2	43	5	0.2	2	50.93	37.35
No11	3	43	5	0.2	1	45.63	83.22
No12	3	43	5	0.2	2	48.47	61.43
No13	1	43	3	0.4	1	52.93	88.62
No14	2	43	3	0.4	1	46.83	87.08
No15	3	43	3	0.4	1	44.42	93.87
No16	1	43	5	0.4	1	56.33	54.97
No17	2	43	5	0.4	1	52.49	76.30
No18	3	43	5	0.4	1	46.08	77.83
No19	1	43	7	0.4	1	67.59	14.10
No20	2	43	7	0.4	1	63.74	35.25
No21	3	43	7	0.4	1	50.99	50.94
No22	1	58	3	0.4	1	42.86	94.43
No23	2	58	3	0.4	1	45.47	98.43
No24	3	58	3	0.4	1	40.22	96.36
No25	1	58	5	0.4	1	53.22	86.39
No26	2	58	5	0.4	1	49.28	88.32
No27	3	58	5	0.4	1	44.1	92.95
No28	1	58	7	0.4	1	65.49	28.90
No29	2	58	7	0.4	1	53.99	44.96
No30	3	58	7	0.4	1	50.42	63.91
No S1	2	43	5	0.4	2	50.55	71.65
No S2	3	43	5	0.4	2	44.6	74.21
No S3	1	43	7	0.4	2	64.56	12.65
No S4	2	43	7	0.4	2	61.09	33.65
No S5	3	43	7	0.4	2	49.60	48.22
No S6	1	58	3	0.4	2	41.65	93.56
No S7	2	58	3	0.2	2	44.65	97.65
No S8	3	58	3	0.2	2	40.01	96.02
No S9	1	58	5	0.2	2	51.65	81.46
No S10	2	58	5	0.2	2	47.56	86.05
No S11	3	58	5	0.2	2	43.01	90.05
No S12	1	58	7	0.2	2	64.01	25.65
No S13	2	58	7	4000	2	50.65	39.65
No S14	3	58	7	4000	2	48.65	59.65

Before estimating the iron and the Recovery between the input and output variables, the Pearson correlation (Pc) was calculated. The Pearson correlation graph given in Figure 4.15 shows that the effect of the parameters on the iron content was ordered as follows: highest linear correlation: conveyor speed and highest inverse correlation: particle size. The cleaning stage did not play a curial role in the magnetic separation process. Moreover, the Pearson correlation graph for iron recovery indicates that the conveyor speed was the most important parameter affecting the iron recovery (Figure 4.16). When the results obtained for Recovery are examined, the variables that Recovery has the highest linear correlation among all input variables are respectively the Particle size and splitter, and the variables with the highest inverse correlation are respectively the speed and cleaning stage. It was observed that there was a relatively low correlation between other variables.

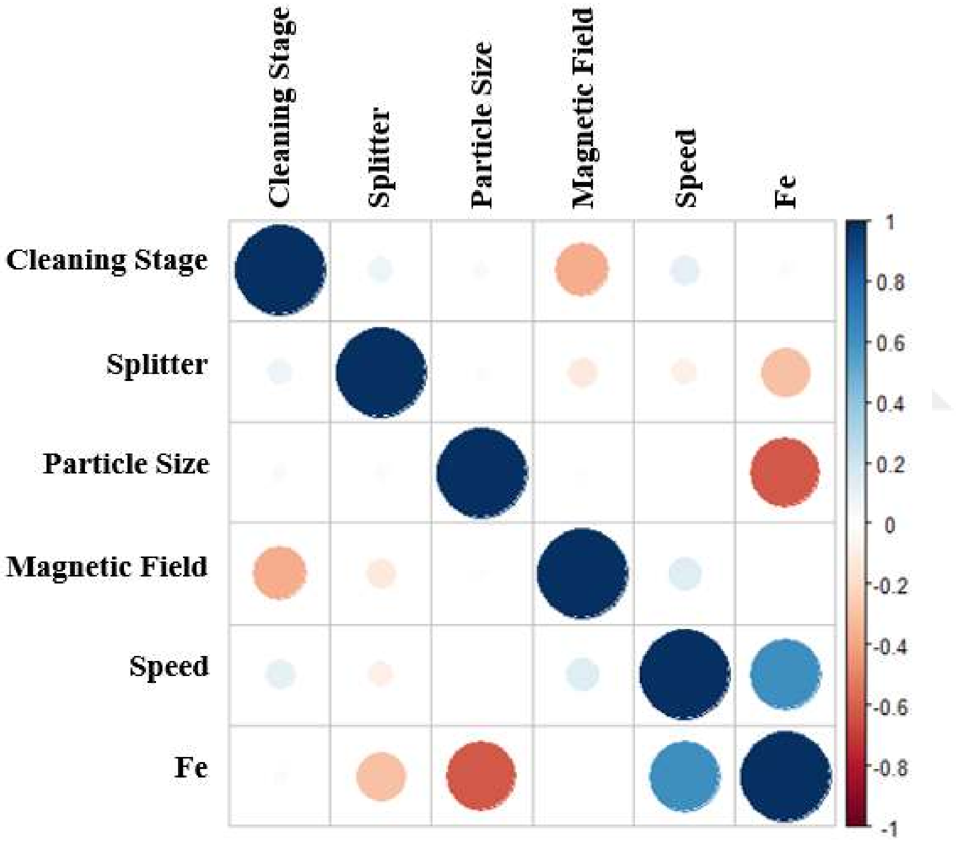

Figure 4.15. The Pearson correlation of input and output (Fe) data.

In this thesis, MATLAB software was used in all modeling studies. Herein, 3 different training algorithms were applied: (i) Levenberg-Marquardt algorithm, (ii) Bayesian regularization and (iii) scaled conjugate gradient algorithm. Figures 4.17 and 4.18 show a graph of training and test errors for iron and recovery, respectively. The results appear to be reasonable given the small final mean square error. It is seen that the best performance occurs in different iterations for each training algorithm.

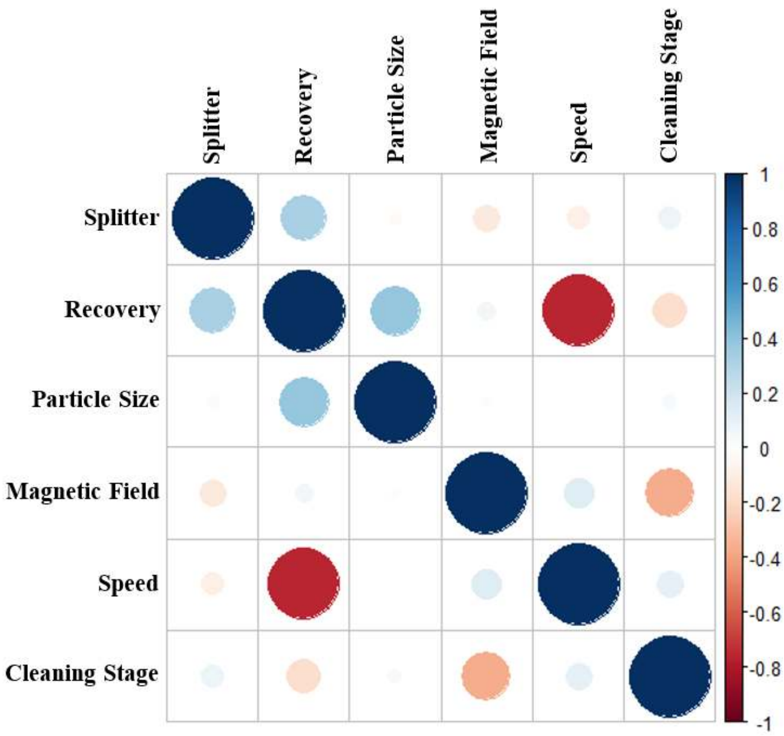

Figure 4.16. The Pearson correlation of input and output (Recovery) data.

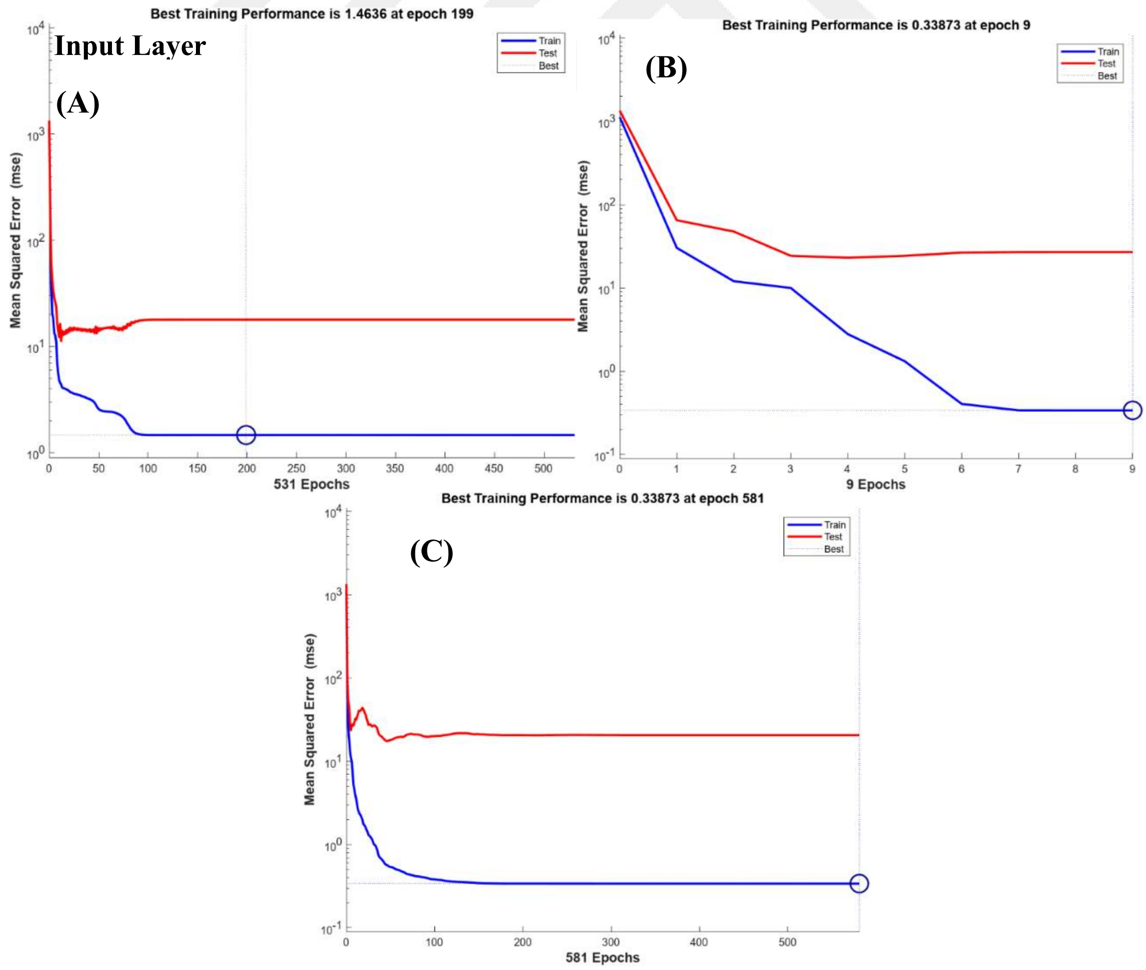

Figure 4.17. Performance change with different epochs for iron prediction. A: BR; B: LM; C: SCG.

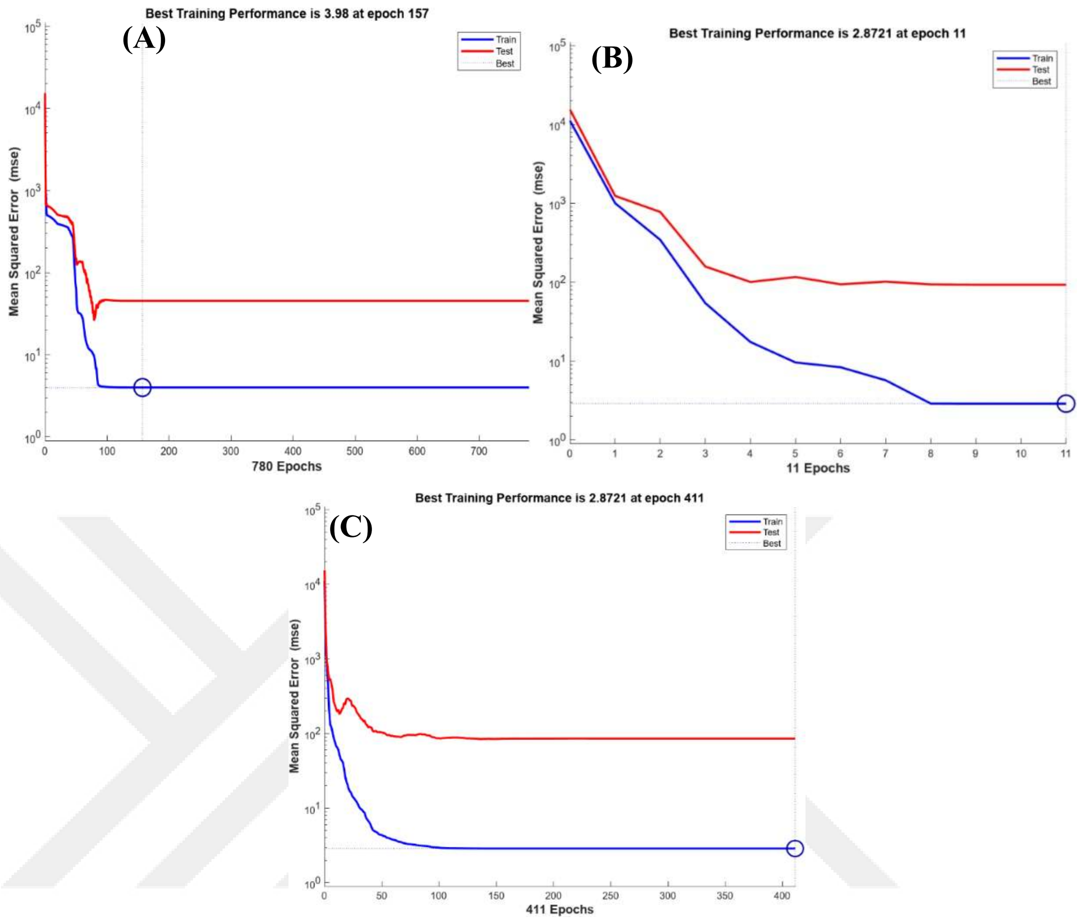

Figure 4.18. Performance change with different epochs for iron prediction. A: BR; B: LM; A: SCG.

A scatter plot was used to visually understand the relationship between actual and predicted values. In these graphs, the closer the data is to the regression line in the scatterplot, the more accurate the prediction is [48], [70]. For the developed models, the distribution graph of the measured and predicted values for iron and Recovery in both training (a) and test (b) stages are respectively given in Figure 4.19. and 4.20.

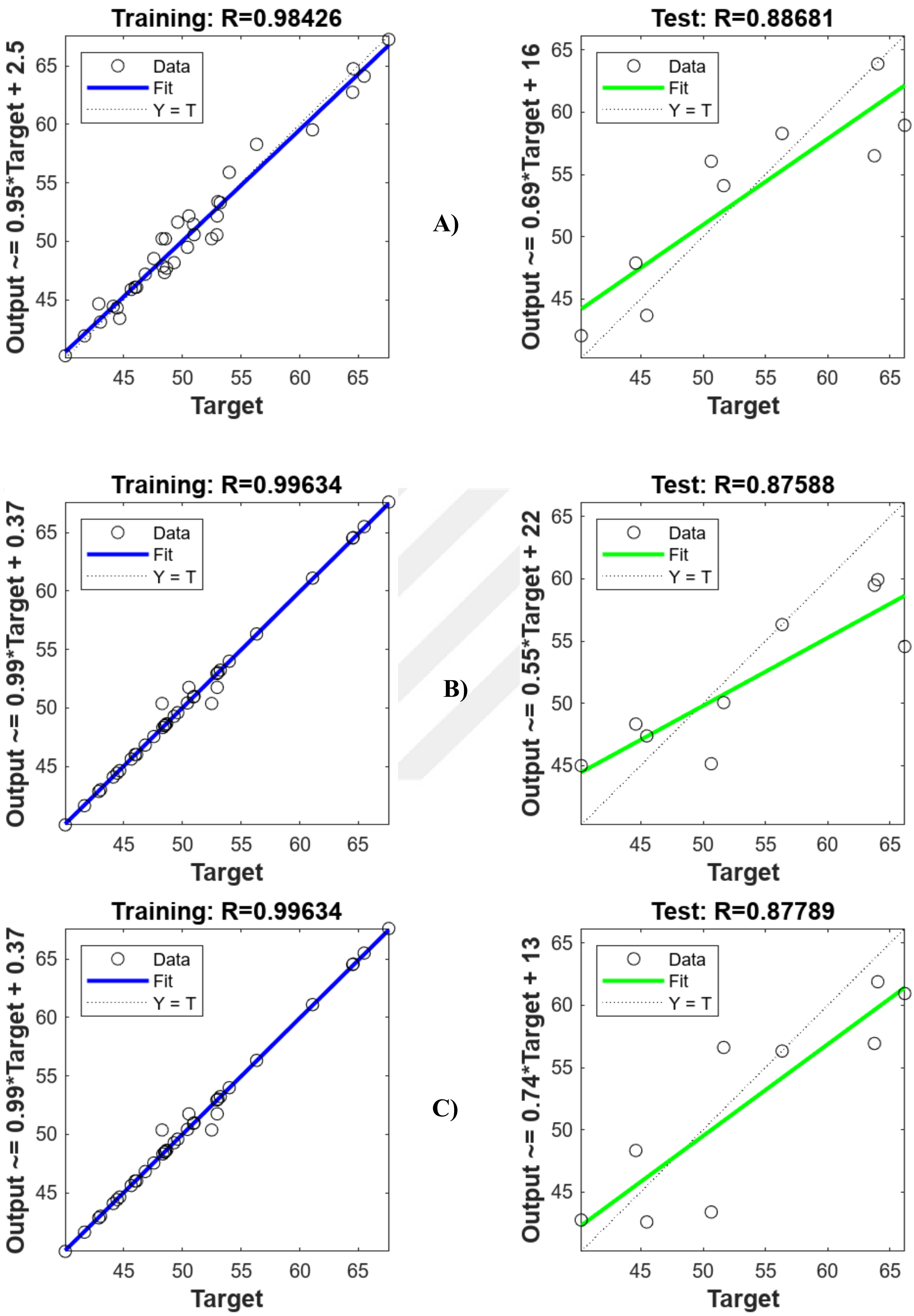

Figure 4.19. Comparison of experimental and predicted iron values. A: BR; B: LM; C: SCG.

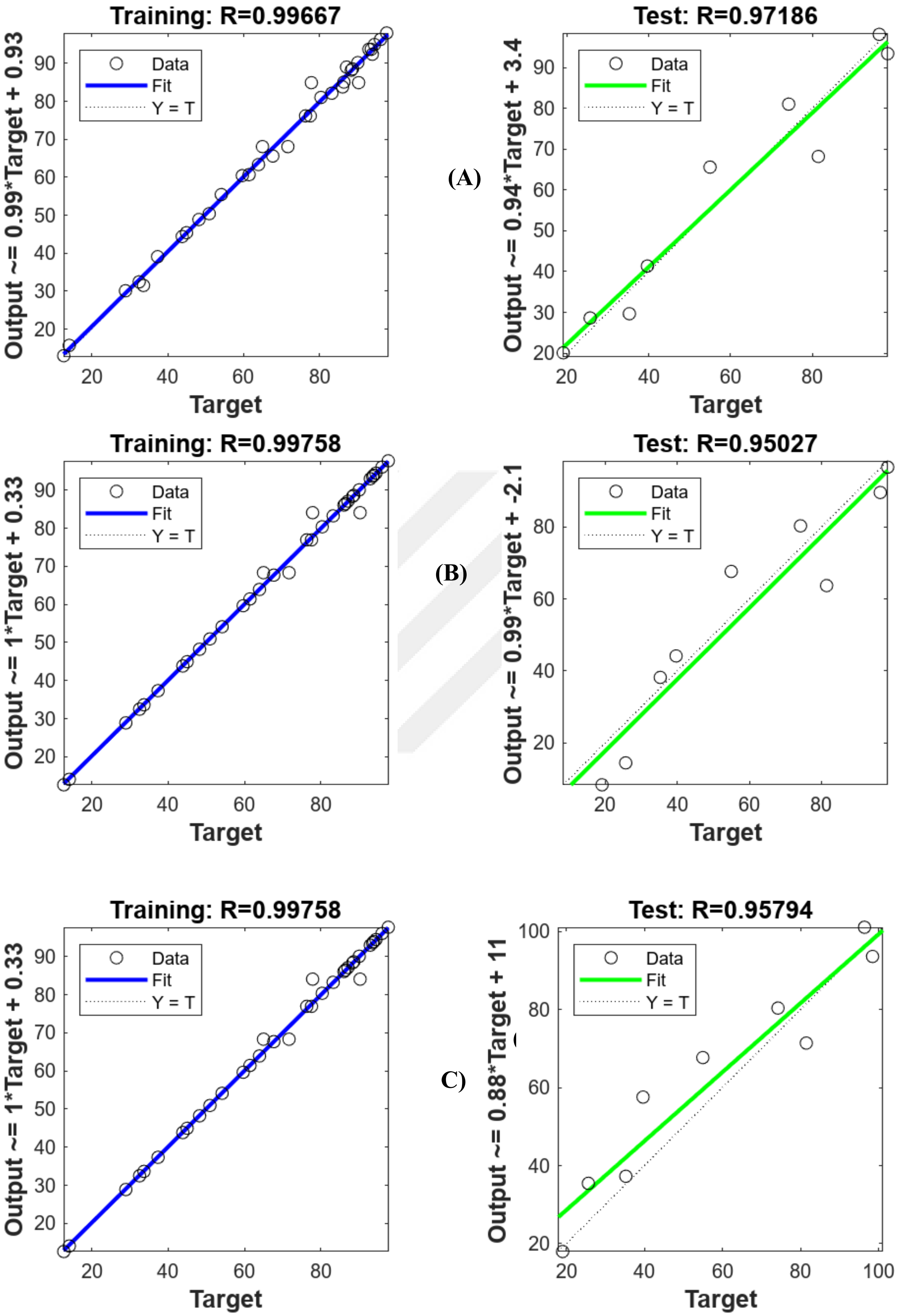

Figure 4.20. Comparison of experimental and predicted Recovery values. A: BR; B: LM; C: SCG.

For iron estimation, LM and SCG models gave the highest correlation coefficient at the training stage (R=0.996). In the test phase, the data points with the closest distribution to the Regression line were obtained with the BR model (R=0.886). For recovery prediction, LM and SCG models gave the highest correlation coefficient during the training phase (R=0.997). In the test phase, the data points with the closest distribution to the Regression line were obtained with the BR model (R=0.972). In this study, BR, LM and SCG models, which are training models used in machine learning, were used to predict iron and Recovery values. In order to evaluate the prediction performance of the developed models, performance evaluation criteria were calculated, and the results were presented in Table 4.9 for iron content and Table 4.10 for iron Recovery.

Table 4.10. The validation of the prediction model for iron

		BR	LM	SCG
Training	R	0.984	0.996	0.996
	RMSE	1.210	0.582	0.582
	MSE	1.464	0.339	0.339
	MAE	0.960	0.194	0.194
Testing	R	0.887	0.876	0.878
	RMSE	4.230	5.193	4.524
	MSE	17.889	26.964	20.464
	MAE	3.477	4.161	3.948

It is clearly seen in Table 4.10 that the LM and SCG models for the estimation of iron value had respectively the highest R (0.996), the lowest RMSE (0.582), the lowest MSE (0.339), and the lowest MAE (0.194) at the training stage. However, when the prediction success in the test phase was evaluated, it was understood that the BR model had the highest R (0.887), the lowest RMSE (4.230), the lowest MSE (17.889) and the lowest MAE (3.477). Based on the statistical parameters discussed, the LM and SCG models in the training phase and the BR model in the testing phase outperformed in estimating the iron value.

From Table 4.11, the LM and SCG models for the estimation of the Recovery value had respectively the highest R (0.998), lowest RMSE (1.695), lowest MSE (2.872), and lowest MAE (0.582) at the training stage. However, when the prediction success in the test phase was evaluated, it was understood that the BR model had the highest R (0.972), the lowest RMSE (6.729), the lowest MSE (45.286) and the lowest MAE (5.418). Based on the statistical parameters discussed, the LM and SCG models in the training phase and the BR model in the testing phase outperformed in estimating the recovery value.

Table 4.11. The validation of the prediction model for Recovery

		BR	LM	SCG
Training	R	0.997	0.998	0.998
	RMSE	1.995	1.695	1.695
	MSE	3.980	2.872	2.872
	MAE	1.328	0.582	0.582
Testing	R	0.972	0.950	0.958
	RMSE	6.729	9.622	9.237
	MSE	45.286	92.583	85.314
	MAE	5.418	8.280	7.696

In order to better evaluate the performance of the developed models, the estimated values and the variation of the measured values were compared (Figure 4.21). Here, the predicted values obtained from all models for the estimation of iron seem to be similar to the true value trend. However, it is understood that the BR model tends to be relatively closer to other models. For the recovery estimation (Figure 4.22), it is seen that the estimation results of all models and the measured values overlap. However, it appears that the results of the BR model fit the experimental data points better than the other models.

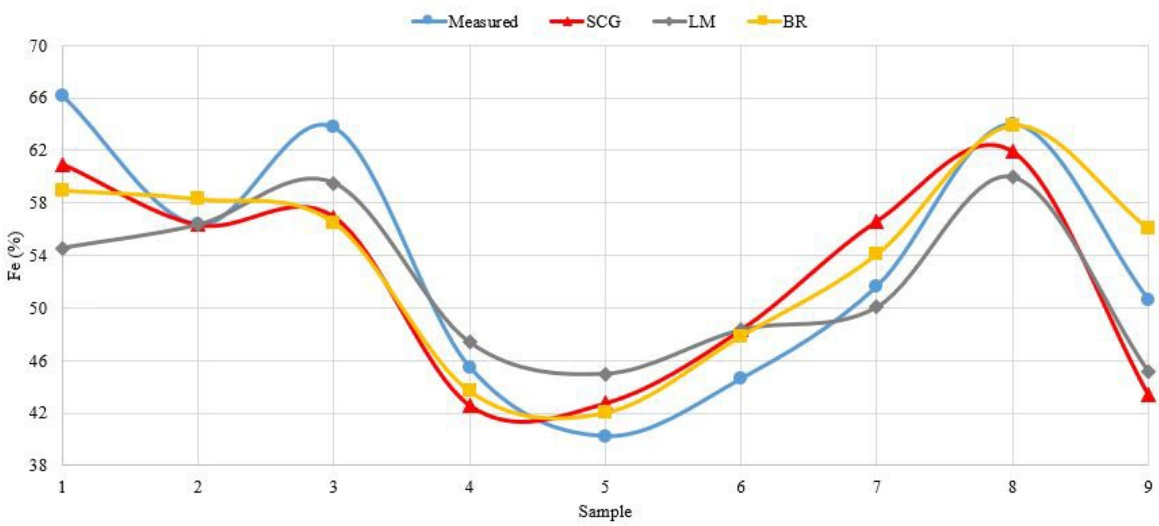

Figure 4.21. The Pearson correlation of input and output (Fe) data.

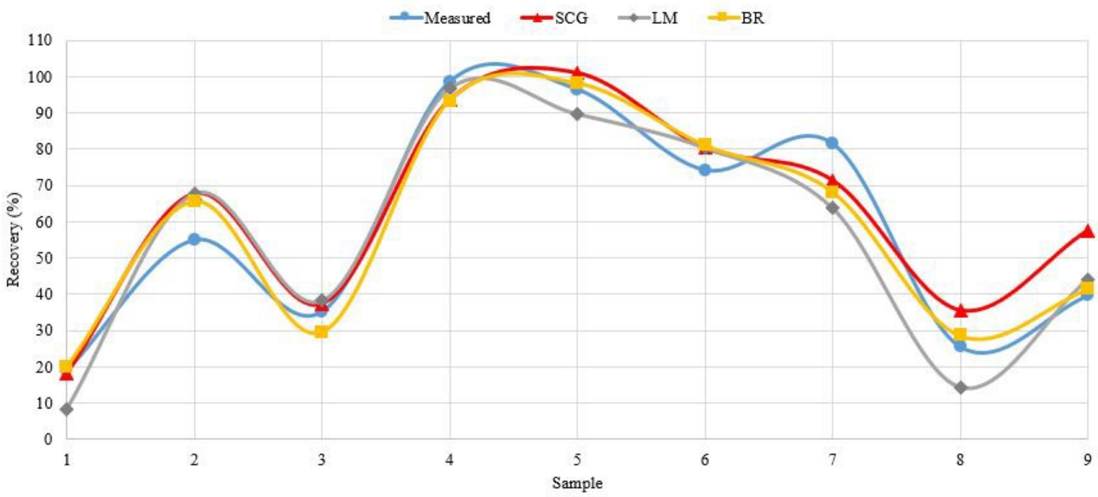

Figure 4.22. The Pearson correlation of input and output (Recovery) data.

4.4. Different Magnetic Separation Tests

Although magnetic separation studies were carried out under different working conditions, The obtained results from the previous experiments were not satisfying; therefore it was decided to create multiple scenarios to see if we can reach the optimum goal set which is to get iron higher than 56% and a recovery higher than 70% by using the roll magnetic separator (0.4T) by varying the main process parameters, including rotor speed, splitter position and the results are discussed in further sections.

4.4.1. Scenario – 1: [particle size: -1+0.500 mm]

For this scenario, it was decided to adjust the speed using the same sample (-1+0.500 mm) while keeping the splitter position constant. Then, the splitter position and speed were adjusted using the same sample to determine if it is possible to achieve an optimal iron content and recovery. The obtained results are summarized in Table 4.12. Figure 4.23 shows the effect of splitter position under different working conditions of the magnetic separator. Sample No31 was used for an initial experiment, and the resulting concentrate was then utilized for a second experiment with a reduced speed while maintaining the same splitter position (43°). It was observed that at a speed of 5Hz, an iron content of 56.34% was obtained, although the recovery was low. However, when the speed was decreased, the recovery increased while the iron content decreased. The combination of these two experiments resulted in a total iron content of 53% and a recovery rate of 95.97%. Further experimentation was conducted on the concentrate obtained from sample 31 at the same speed (5Hz), yielding a total iron content of 56.06% and a recovery rate of 71.54% when combined with the concentrate from experiment 33. These parameters produced satisfactory results. Additionally, the same concentrate from sample 31 was tested with an increased speed of 7 Hz, resulting in a total iron content of 56.50% and a recovery rate of 54.33%.

Table 4.12. The results obtained from Scenario - 1

Exp. No	Splitter (°)	Conveyor speed (Hz)	Magnetic product		Fe recovery (%)
			Amount (%)	Fe (%)	
No31	43	5	36.98	56.34	53.14
No32*		3	33.67	49.86	67.95
Total magnetic product (%)		**Total Fe (%)**		**Overall Recovery (%)**	
70.65		53.25		95.97	
* the non-magnetic product obtained in the magnetic separation test (No.31) was used as the feed material in No32 test to increase the Fe recovery.					
Exp. No	**Splitter (°)**	**Conveyor speed (Hz)**	**Magnetic product Amount (%)**	**Magnetic product Fe (%)**	**Fe recovery (%)**
No31	43	5	36.98	56.34	53.14
No33*		5	13.04	55.28	29.19
Total magnetic product (%)		**Total Fe (%)**		**Overall Recovery (%)**	
50.02		56.06		71.54	
* the non-magnetic product obtained in the magnetic separation test (No.31) was used as the feed material in No33 test to increase the Fe recovery.					
Exp. No	**Splitter (°)**	**Conveyor speed (Hz)**	**Magnetic product Amount (%)**	**Magnetic product Fe (%)**	**Fe recovery (%)**
No31	43	5	36.98	56.34	53.14
No34*		7	0.71	65.51	1.87
Total magnetic product (%)		**Total Fe (%)**		**Overall Recovery (%)**	
37.69		56.50		54.33	
* the non-magnetic product obtained in the magnetic separation test (No.31) was used as the feed material in No34 test to increase the Fe recovery.					
Exp. No	**Splitter (°)**	**Conveyor speed (Hz)**	**Magnetic product Amount (%)**	**Magnetic product Fe (%)**	**Fe recovery (%)**
No35	58	7	16.22	65.49	27.09
No36*		3	53.72	49.42	80.84
Total magnetic product (%)		**Total Fe (%)**		**Overall Recovery (%)**	
69.94		53.15		94.82	
* the non-magnetic product obtained in the magnetic separation test (No.35) was used as the feed material in No36 test to increase the Fe recovery.					
Exp. No	**Splitter (°)**	**Conveyor speed (Hz)**	**Magnetic product Amount (%)**	**Magnetic product Fe (%)**	**Fe recovery (%)**
No35	58	7	16.22	65.49	27.09
No37*		5	46.53	52.99	75.09
Total magnetic product (%)		**Total Fe (%)**		**Overall Recovery (%)**	
62.75		56.22		90.01	
* the non-magnetic product obtained in the magnetic separation test (No.35) was used as the feed material in No37 test to increase the Fe recovery.					
Exp. No	**Splitter (°)**	**Conveyor speed (Hz)**	**Magnetic product Amount (%)**	**Magnetic product Fe (%)**	**Fe recovery (%)**
No35	58	7	16.22	65.49	27.09
No38*		7	6.81	66.16	13.71
Total magnetic product (%)		**Total Fe (%)**		**Overall Recovery (%)**	
23.03		65.69		38.58	
* the non-magnetic product obtained in the magnetic separation test (No.35) was used as the feed material in No38 test to increase the Fe recovery.					

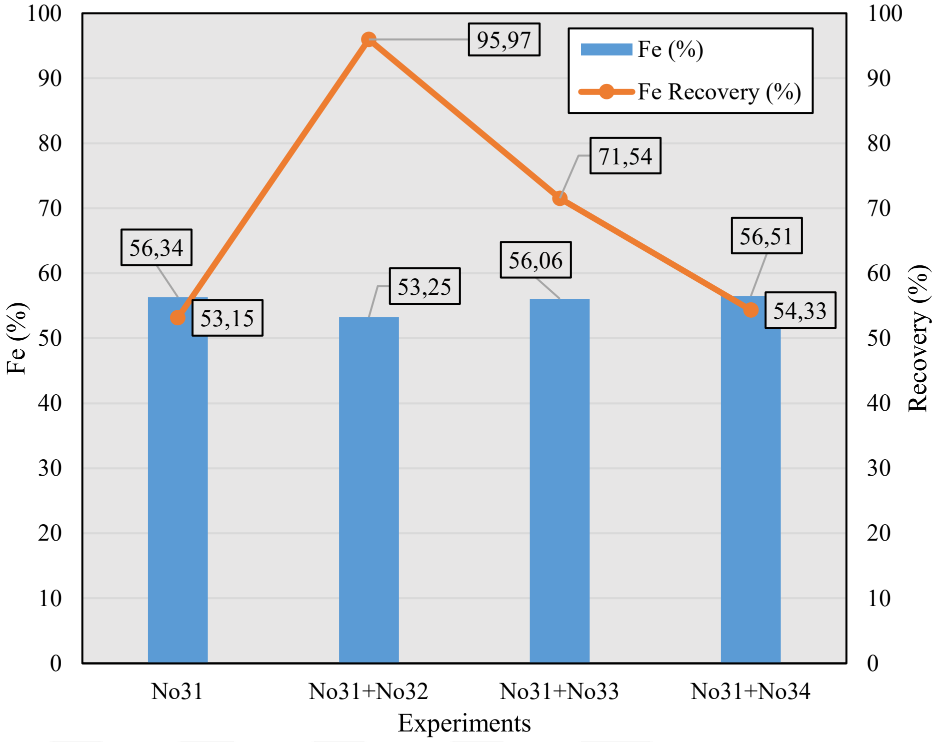

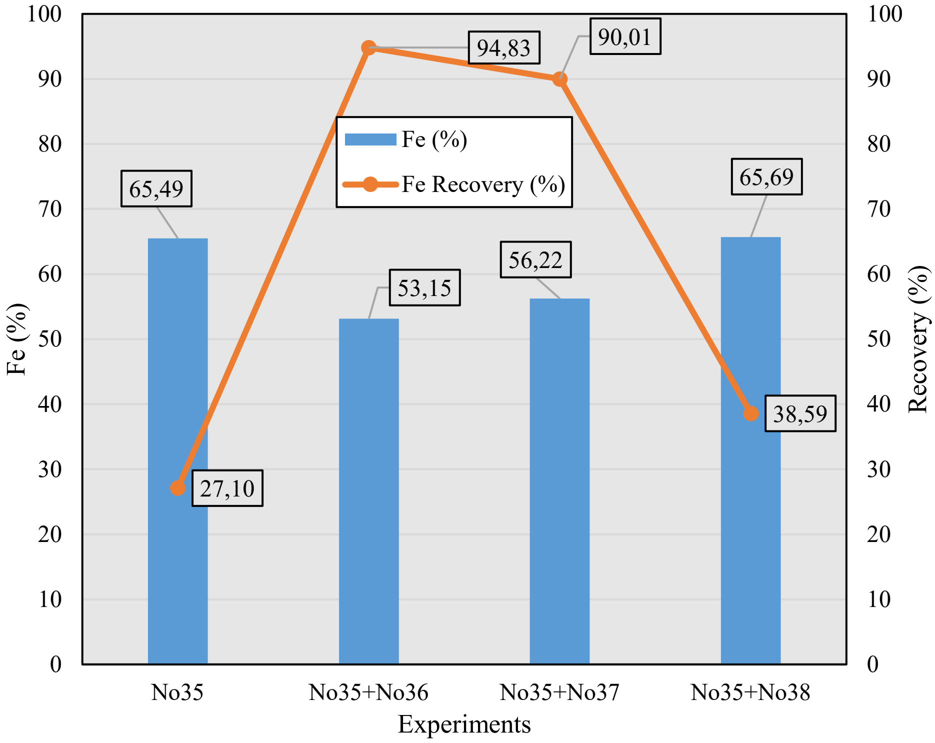

Figure 4.23. Effect of conveyor speed on the recovery of iron from the ore with a size of -1+0.500 mm: (a) splitter position: 43°, (b) splitter position: 58° [constant parameters: 0.4 T of magnetic field]

Sample 35 was subjected to experimentation using a splitter angle of 58° and a speed of 7Hz. The resulting concentrate, with a iron content of 65.49% and a recovery rate of 27.09%, was then utilized in subsequent experiments to determine if the desired objective could be achieved.

Experiment 36, conducted at 3Hz, yielded a iron content of 53.15% and a recovery rate of 94.82% when combined with the concentrate from sample 35. Increasing the speed to 5Hz in experiment 37, using the concentrate from sample 35, resulted in a iron content of 56.22% and a recovery rate of 90.01%. This outcome was found to be in line with the intended objective. However, when the speed was further increased for sample 38, which also utilized the concentrate from sample 35, the obtained mixture displayed a iron content of 65.69% and a recovery rate of 38.58%. These results fell significantly short of the desired goal.

4.4.2. Scenario – 2: [particle size: -0.500+0.300 mm]

For this scenario, it was decided to adjust the speed using the same sample (-500+0.300mm) while maintaining the same splitter position. Further adjustments were made to the splitter position and speed using the same sample to determine if it was possible to achieve an optimal iron content and recovery. Table 4.13 and Figure 4.25 show the obtained results in this stage. Experiment 46 was conducted with a splitter angle of 43° and a speed of 5Hz, resulting in a iron content of 52.25% and a recovery rate of 85.08%. The concentrate obtained from sample 46 was then used as sample 47, and a test was carried out with a speed of 3Hz. This combination, when combined with the result of sample 46, yielded a total iron content of 49.10% and a recovery rate of 99.99%.

Table 4.13. The results obtained from Scenario - 2

<table>
<tr><th rowspan="2">Exp. No</th><th rowspan="2">Splitter (°)</th><th rowspan="2">Conveyor speed (Hz)</th><th colspan="2">Magnetic product</th><th rowspan="2">Fe recovery (%)</th></tr>
<tr><th>Amount (%)</th><th>Fe (%)</th></tr>
<tr><td>No46</td><td rowspan="2">43</td><td>5</td><td>68.24</td><td>52.25</td><td>85.08</td></tr>
<tr><td>No47*</td><td>3</td><td>17.11</td><td>36.52</td><td>46.94</td></tr>
<tr><th colspan="2">Total magnetic product (%)</th><th colspan="2">Total Fe (%)</th><th colspan="2">Overall Recovery (%)</th></tr>
<tr><td colspan="2">85.35</td><td colspan="2">49.10</td><td colspan="2">99.99</td></tr>
<tr><td colspan="6">* the non-magnetic product obtained in the magnetic separation test (No46) was used as the feed material in No47 test to increase the Fe recovery.</td></tr>
<tr><th rowspan="2">Exp. No</th><th rowspan="2">Splitter (°)</th><th rowspan="2">Convery speed (Hz)</th><th colspan="2">Magnetic product</th><th rowspan="2">Fe recovery (%)</th></tr>
<tr><th>Amount (%)</th><th>Fe (%)</th></tr>
<tr><td>No48</td><td rowspan="2">58</td><td>7</td><td>34.84</td><td>49.71</td><td>30.99</td></tr>
<tr><td>No49*</td><td>3</td><td>58.14</td><td>36.83</td><td>78.40</td></tr>
<tr><th colspan="2">Total magnetic product (%)</th><th colspan="2">Total Fe (%)</th><th colspan="2">Overall Recovery (%)</th></tr>
<tr><td colspan="2">92.98</td><td colspan="2">41.65</td><td colspan="2">92.41</td></tr>
<tr><td colspan="6">* the non-magnetic product obtained in the magnetic separation test (No48) was used as the feed material in No49 test to increase the Fe recovery.</td></tr>
<tr><th rowspan="2">Exp. No</th><th rowspan="2">Splitter (°)</th><th rowspan="2">Convery speed (Hz)</th><th colspan="2">Magnetic product</th><th rowspan="2">Fe recovery (%)</th></tr>
<tr><th>Amount (%)</th><th>Fe (%)</th></tr>
<tr><td>No48</td><td rowspan="2">58</td><td>7</td><td>34.84</td><td>49.71</td><td>30.99</td></tr>
<tr><td>No50*</td><td>5</td><td>35.15</td><td>38.71</td><td>81.16</td></tr>
<tr><th colspan="2">Total magnetic product (%)</th><th colspan="2">Total Fe (%)</th><th colspan="2">Overall Recovery (%)</th></tr>
<tr><td colspan="2">69.99</td><td colspan="2">42.87</td><td colspan="2">94.21</td></tr>
<tr><td colspan="6">* the non-magnetic product obtained in the magnetic separation test (No48) was used as the feed material in No50 test to increase the Fe recovery.</td></tr>
</table>

Another test was performed by changing the splitter position to 58° and using a speed of 7Hz for sample 48. The results showed an iron content of 49.71% and a recovery rate of 30.99%. The concentrate obtained from sample 48 was used as sample 49 for a test in which the splitter position was maintained and the speed was changed to 3Hz. The combined results of samples 48 and 49 showed a total iron content of 41.65% and a recovery rate of 92.41%. It is evident that by decreasing the speed, the iron content decreases while the recovery rate increases. The decision was made to increase the speed while keeping the same splitter position for sample 50, which is the concentrate obtained from sample 48. The result showed a decrease in the iron content but not in the recovery rate. The mixture produced a total iron content of 42% and a recovery rate of 94.21%, indicating a high recovery rate.

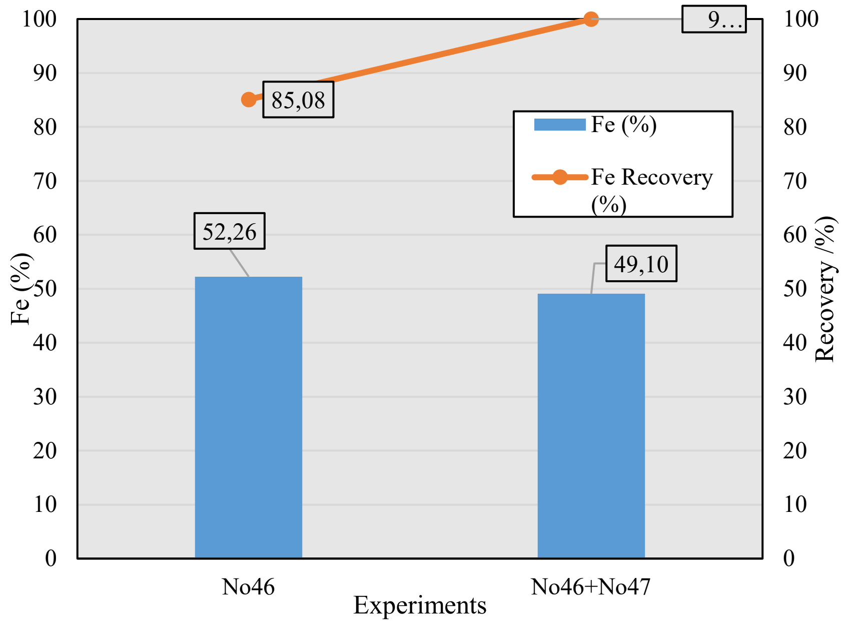

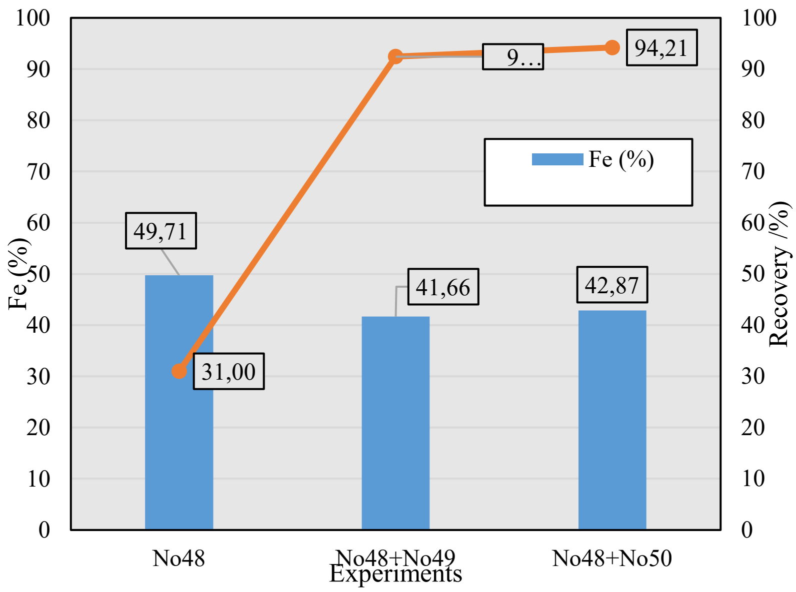

Figure 4.24. Effect of conveyor speed on the recovery of iron from the ore with a size of -0.500+0.300 mm: (a) splitter position: 43°, (b) splitter position: 58° [constant parameters: 0.4 T of magnetic field]

4.4.3. Scenario – 3 [particle size: -0.300+0.125 mm]

For this scenario, it was decided to adjust the speed using the same sample (-300+0.125mm) while maintaining the same splitter position. Subsequently, adjustments were made to the splitter position and speed using the same sample to determine if it was possible to achieve an optimal iron content and recovery. Table 4.14 and Figure 4.26 show the experimental results obtained in this stage.

Experiment 39 was conducted with a splitter angle of 43° and a speed of 5Hz, resulting in an iron content of 45.43% and a recovery rate of 88.84%. Samples 40, 41, and 43 were obtained as concentrates from sample 39 and were tested at speeds of 3Hz, 5Hz, and 7Hz, respectively, while maintaining the same splitter position as in sample 39. The combined results of these experiments, along with sample 39, yielded a total iron content of 42.07%, 45.89%, and 45.89%, and a recovery rate of 98.72%, 95.18%, and 95.17%, respectively. The splitter position was changed to 58° for samples 43, 44, and 45, with samples 44 and 45 being concentrates obtained from sample 43. The results of sample 43, with a speed of 7Hz, showed a iron content of 49.45% and a recovery rate of 66.97%. When combined with the result of sample 44, a total iron content of 39.67% and a recovery rate of 99.61% were obtained. The second combination, involving the results of samples 43 and 45, produced a iron content of 45.13% and a recovery rate of 92.25%.

It is observed that the best combinations are the ones obtained from the 1st scenario because of the large size particles. If we reduce the size of the particles the dry magnetic separation may not have a big impact on the result obtained. The results indicate that magnetic separation process is not efficient under dry conditions when the particle size of the sample was below <0.500 mm. These findings are in good agreement with those of a previous study (Dwari, Rao et al. 2013), which the iron content of the magnetic product with a size of -0.300 mm increased to 50.96% from 43.8% with a recovery of 95.30%. Moreover, it was stated that the separation efficiency under dry conditions was not good due to the dragging tendency of the fines particles. Finally, it was decided to conduct microwave treatment on the sample with a size of -0.500+0.300 mm and -0.300+0.125 mm to increase its magnetic susceptibility properties that may result in an increase the iron content of the magnetic product. The detailed information was explained in the following section.

Table 4.14. The results obtained from Scenario - 3

Exp. No	Splitter (°)	Conveyor speed (Hz)	Magnetic product		Fe recovery (%)
			Amount (%)	Fe (%)	
No39	43	5	77.43	45.43	88.84
No40*		3	15.46	25.29	43.75
Total magnetic product (%)		**Total Fe (%)**		**Overall Recovery (%)**	
92.89		42.07		98.72	

* the non-magnetic product obtained in the magnetic separation test (No39) was used as the feed material in No40 test to increase the Fe recovery.

Exp. No	Splitter (°)	Conveyor speed (Hz)	Magnetic product		Fe recovery (%)
			Amount (%)	Fe (%)	
No39	43	5	77.43	45.43	88.84
No41*		5	4.67	53.65	28.05
Total magnetic product (%)		**Total Fe (%)**		**Overall Recovery (%)**	
82.10		45.89		95.18	

* the non-magnetic product obtained in the magnetic separation test (No39) was used as the feed material in No41 test to increase the Fe recovery.

Exp. No	Splitter (°)	Conveyor speed (Hz)	Magnetic product		Fe recovery (%)
			Amount (%)	Fe (%)	
No39	43	5	77.43	45.43	88.84
No42*		7	4.67	53.65	4.17
Total magnetic product (%)		**Total Fe (%)**		**Overall Recovery (%)**	
78.12		45.89		95.17	

* the non-magnetic product obtained in the magnetic separation test (No39) was used as the feed material in No41 test to increase the Fe recovery.

Exp. No	Splitter (°)	Conveyor speed (Hz)	Magnetic product		Fe recovery (%)
			Amount (%)	Fe (%)	
No39	43	5	77.43	45.43	88.84
No42*		7	4.67	53.65	4.17
Total magnetic product (%)		**Total Fe (%)**		**Overall Recovery (%)**	
78.12		45.89		95.17	

* the non-magnetic product obtained in the magnetic separation test (No39) was used as the feed material in No42 test to increase the Fe recovery.

Exp. No	Splitter (°)	Conveyor speed (Hz)	Magnetic product		Fe recovery (%)
			Amount (%)	Fe (%)	
No43	58	7	53.61	49.45	66.97
No44*		3	45.80	28.22	70.38
Total magnetic product (%)		**Total Fe (%)**		**Overall Recovery (%)**	
99.41		39.67		99.61	

* the non-magnetic product obtained in the magnetic separation test (No43) was used as the feed material in No44 test to increase the Fe recovery.

Exp. No	Splitter (°)	Convery speed (Hz)	Magnetic product		Fe recovery (%)
			Amount (%)	Fe (%)	
No43	58	7	53.61	49.45	66.97
No45*		5	27.31	36.56	54.49
Total magnetic product (%)		**Total Fe (%)**		**Overall Recovery (%)**	
80.92		45.13		92.25	

* the non-magnetic product obtained in the magnetic separation test (No43) was used as the feed material in No45 test to increase the iron recovery.

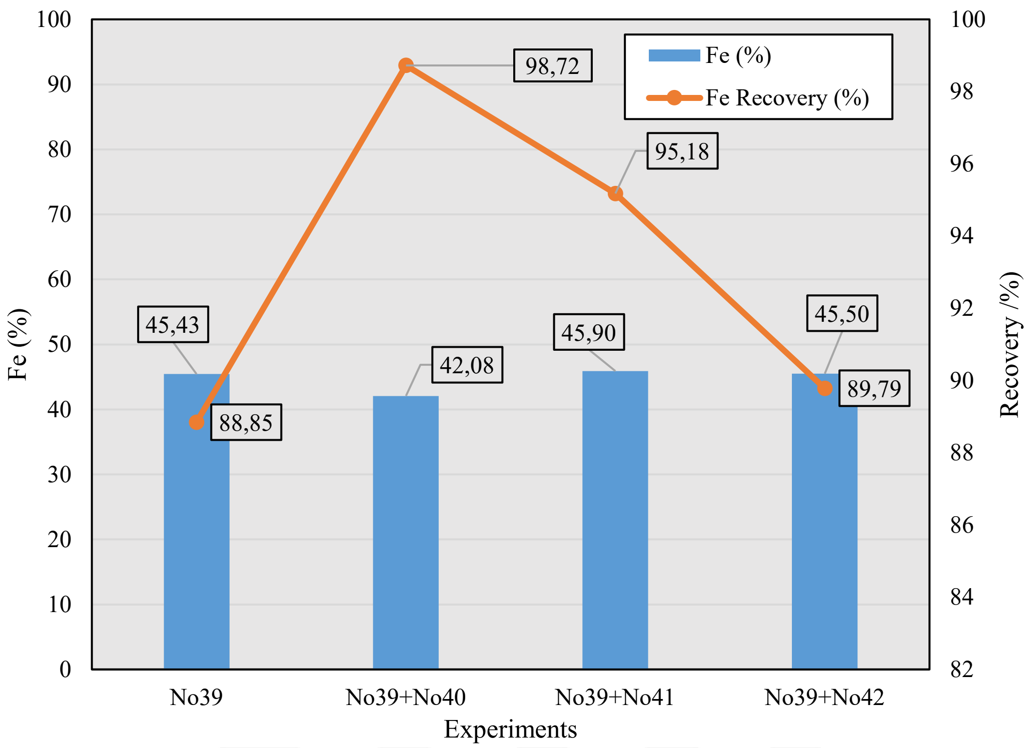

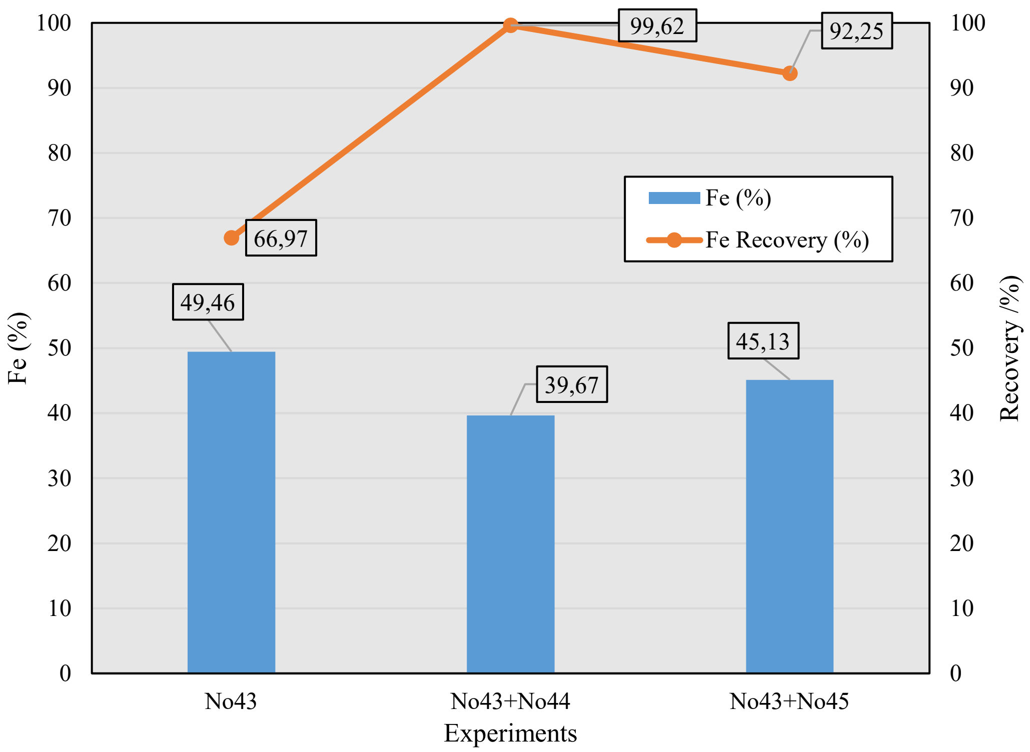

Figure 4.25. Effect of conveyor speed on the recovery of iron from the ore with a size of -0.300+0.125 mm: (a) splitter position: 43°, (b) splitter position: 58° [constant parameters: 0.4 T of magnetic field]

4.5. Heat Treatment

The utilization of microwave heating represents a potentially viable strategy for achieving energy conservation and presents a more efficacious option as compared to traditional thermal processing methodologies employed in mineral processing applications. This study examines the impact of microwave treatment on iron ore samples through varying levels of microwave exposure time and power. Furthermore, the effects of these treatment conditions on the magnetic properties of the iron ore before and after microwave treatment are analyzed. The photographs of the sample while exposing to microwave heating and after the microwave heating can be seen in Figure 4.26. (Omran et al. 2014)

Figure 4.26. Photographs of the ore (-1+0.500 mm) exposed to microwave treatment

Exposed to the microwave during a period of 8 minutes, the surface temperature of the sample with -1+0.500 mm of size showed an impressive change from 160 to 810 °C. However, an increase in the surface temperature of the sample with a size of -0.500+0.300 mm and -0.300+0.125 mm were not satisfactory. It was thought that the magnetic properties of these samples were not influenced by the microwave treatment. These findings are in good agreement with the results showing the magnetic hysteresis (MH) curves (Figure 4.27).

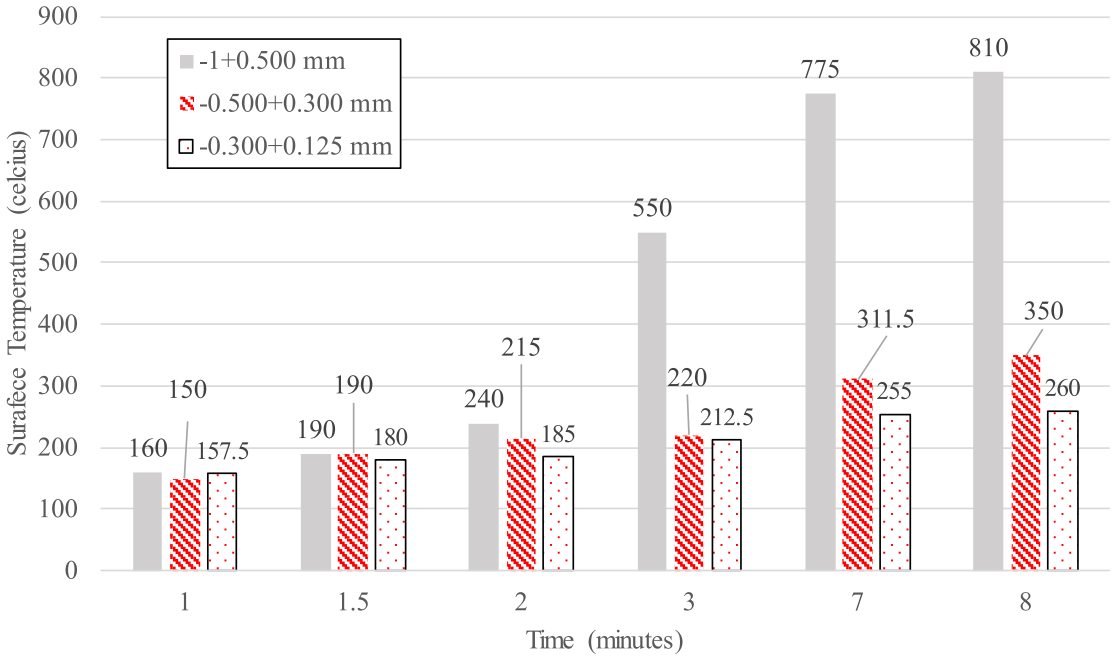

Figure 4.27. The surface temperature of the sample after exposing to microwave treatment

Figure 4.28 shows the magnetic hysteresis (MH) curves of the samples before and after the microwave treatment. It is possible to check the magnetic properties of the sample under the magnetic field strength by using this curve. There was no remarkable change determined in the magnetization value of the sample with a size of -0.500 +0.300 mm after the microwave treatment. When the sample with a size of -0.500+0.300 mm was exposed to 1.8 kW for 8 min, the magnetization value increased to 0.76 emu/g from 0.36 emu/g. On the contrary, the magnetization of the sample with a size of -1+0.500 mm was influenced by the microwave treatment. After the microwave treatment, the magnetization value of the sample with a size of -1+0.500 mm was found to be, 4.30 emu/g, which was quite higher than that of the sample with size of -0.300+0.106 mm (their value: 0.76 emu/g). Considering these results, it can be said that the sample with larger particle sizes. These results were checked by the microscope examination, which shows the microscope images of the sample before and after microwave treatment in Figure 4.29.

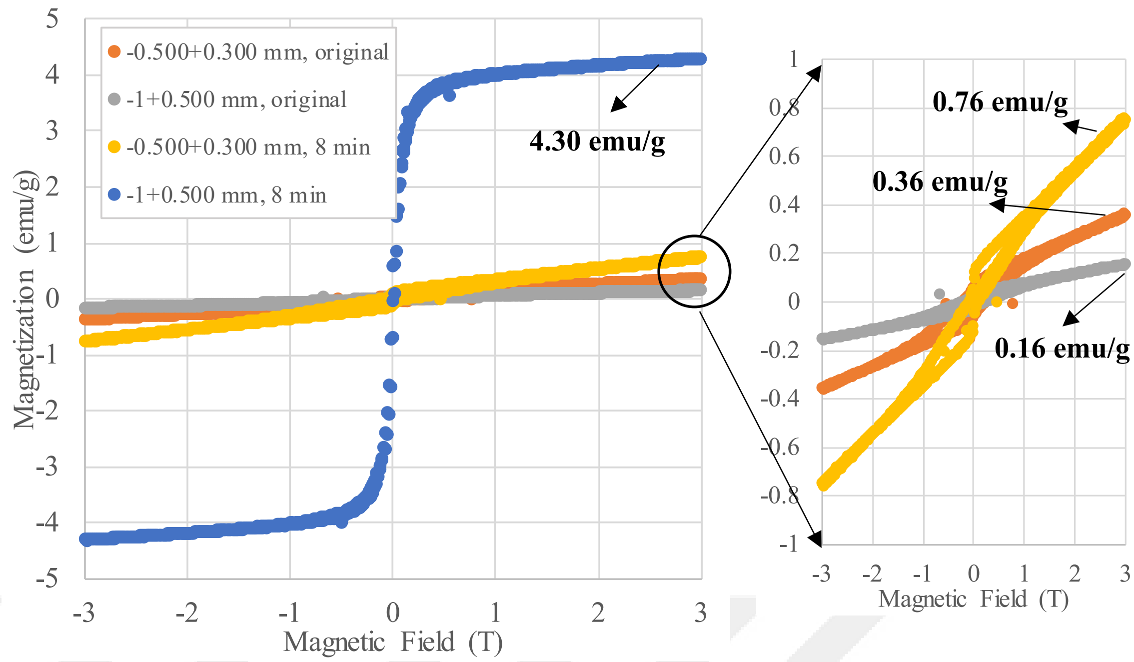

Figure 4.28. The magnetic hysteresis (MH) curves for original iron ores and microwave treated iron ores

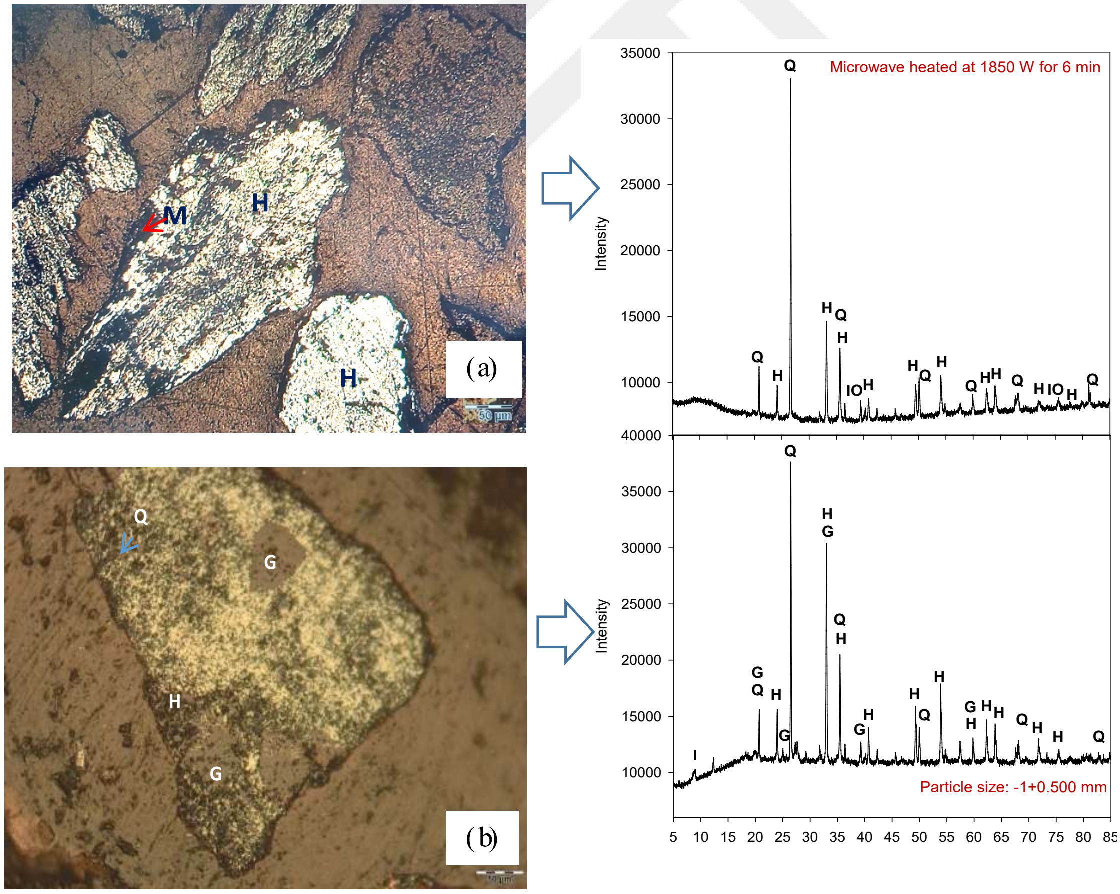

Figure 4.29. Microscope images and XRD analyses of the ore (-1+0.500 mm) (a) after the microwave treatment at a strength of 1800 W for 6 min (b) before the microwave treatment (G: Goethite “96-100-8768”, Q: Quartz “96-500-0036” , H: Hematite “96-900-0140”, IO: Iron Oxide “01-084-0308”)

It was observed in the bright section definitions that the main minerals were identified as were hematite, goethite minerals as ore paragenesis, and quartz as gangue mineral. In the mineralization observed in granular texture, goethite is found in the form of veins and inclusions. Hematite mineral is formed as a result of dehydration (water loss) processes of the Gothite mineral. It was determined that gothite mineral completely transformed into hematite, and hematite partially turned into magnetite. Magnetite formation started from hematite mineral walls. The formation is from the outer periphery to the center, as shown in Figure 4.29. Finally, as a result of combustion, porous texture and magnetite formation were observed in ore minerals (Figure 4.30).

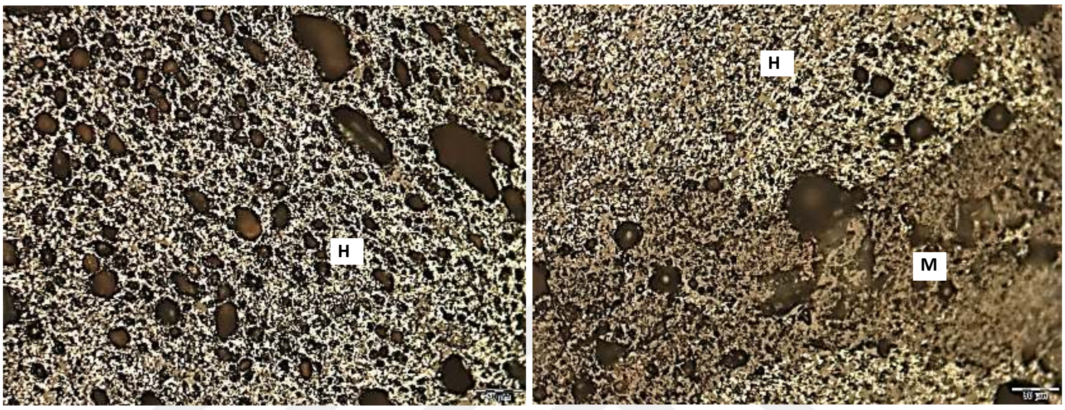

Figure 4.30. Hematite-Magnetite transformation and porous texture observed in hematite mineral.

However, it was understood from Figure 4.31 that when the sample with a size of -1+0.500 mm was exposed to microwave treatment at 1800 W for 4 min, the amount of hematite formation in the microwave-treated ore increased, but no magnetite mineral was determined. Goethite nodules are observed as fine grain size and present irregular texture due to the transformation of the ore after the microwave treatment. Goethite mineral appeared as small inclusions in hematite mineral. The exposure time of the microwave treatment was important parameter to transform goethite mineral into other iron-minerals (hematite or magnetite). XRD analysis shows that it was determined that there was no change observed in the sample with a size of -0.500+0.300 mm and -0.300+0.125 mm after the microwave treatment (Figure 4.32). The intensity of some peaks started to decrease, but these can be negligible.

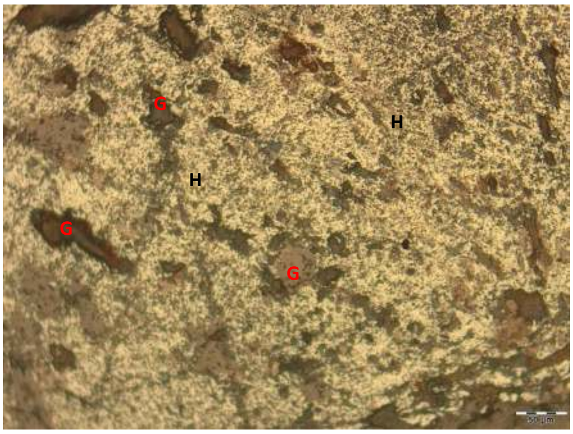

Figure 4.31. Goethite inclusions in hematite mineral present in the sample with a size of -1+0.500mm after the microwave treatment at 1800 W for 4 min (H: hematite, G: goethite)

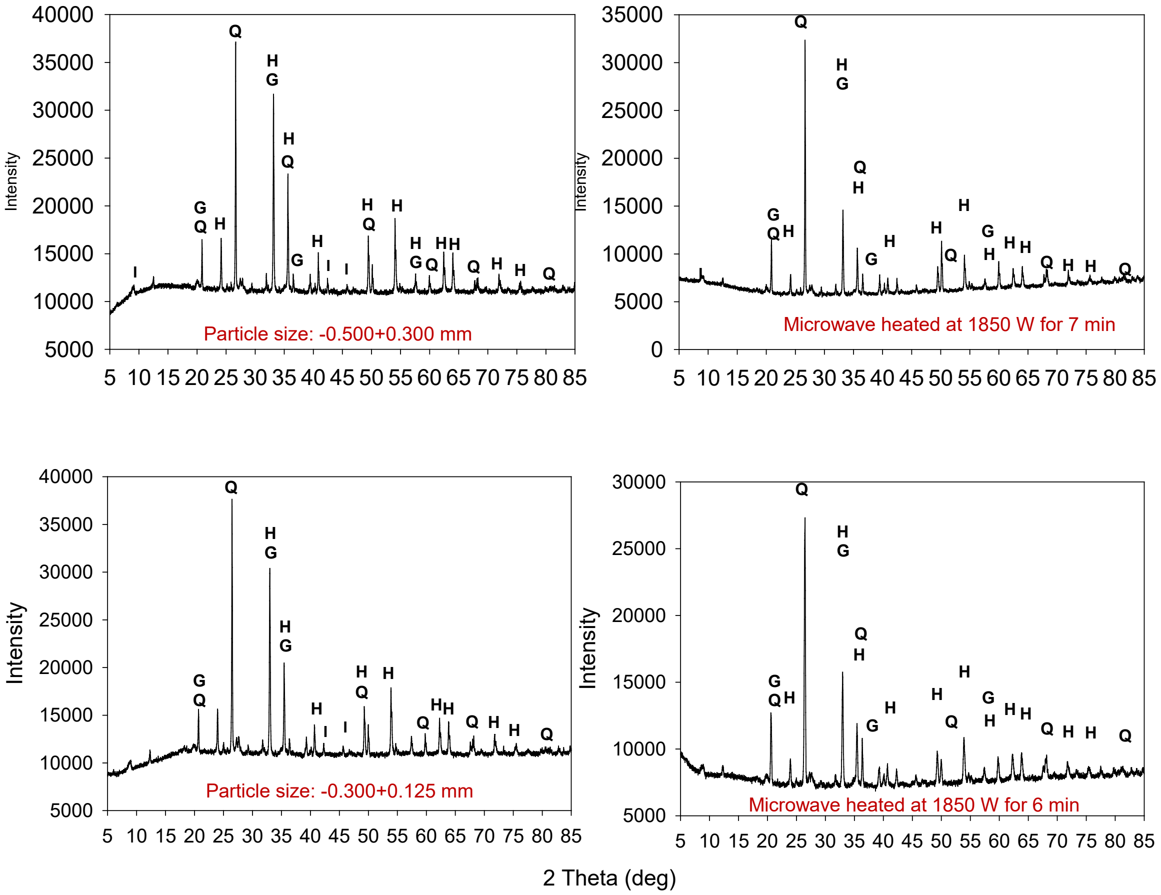

Figure 4.32. XRD patterns of the sample treated with microwave power

Considering all microwave treatment results, it is clear that there was no need to perform microwave treatment on the sample with size of <0.500 mm because the obtained results from the MH curves and microscope examinations were not satisfactory. Therefore, additional magnetic separation tests were not carried out to determine the effect of microwave treatment on the sample.

5. CONCLUSIONS

In this thesis, it was investigated to obtain an iron concentrate with desired qualities (high Fe content and high recovery) from a low-grade iron ore containing hematite and goethite minerals using a dry roll-magnetic separator. The ore used in this thesis was obtained from Feke/Adana region, Türkiye. The characterization of the ore was determined using different instrumental analysis techniques including, Mineral Liberation Analysis (MLA), X-ray Diffraction Analysis (XRD), X-ray Fluorescence Analysis (XRD), and Magnetic Hysteresis (MH) analysis.

MLA showed the properties of the ore such as; modal mineralogy, elemental content, elemental distribution based on mineral content, and mineral locking. It was understood from MLA that the ore was composed of iron-oxide (83.33%), quartz (9.63%), chlorite (2.30%), muscovite (0.84%), ilmenite (0.26%), kaolinite (0.04%) and Al-silicate minerals (0.01%). The presence of hematite and goethite minerals in the ore was confirmed by XRD analysis. The free surface of iron-oxide minerals found to be 32.84%. Furthermore, the liberated degree of iron-oxide minerals was calculated as 54.17%, a significant part of the ore (45.83%) was appeared to occur along with other mineral phases.

A magnetic separation test was carried out on the ore prepared with the following particle sizes: -1+0.500 mm, -0.500+0.300 mm, and -0.300+0.125 mm. therefore, the effect of particle size on the efficiency of magnetic separation test was determined. The effects of splitter position, magnetic field, conveyor speed on the iron content of the magnetic product and its recovery were investigated. The cleaning stage resulted in a decrease in the iron content of the magnetic product and its recovery and therefore there was no need to conduct cleaning stage process. Moreover, it was possible to obtain the magnetic product with a size of -1+0.500 mm with 64% iron content when the magnetic field was 0.2 T, however; its recovery was below <30%. In a follow up, an increase in the conveyor speed resulted in an increase the iron content of the magnetic product. Similarly, the recovery started to decrease with an increase of the conveyor speed. It is impossible to obtain the magnetic product with a size of -0.500+0.300 mm containing >56% iron content and also had a high recovery, except for the experiments which were conducted as the following conditions: cleaning stage:1, magnetic field: 0.4 T, conveyor speed: 7 Hz, splitter position: 43°. However, its recovery was found to be 35.25%. Similar results were found when the sample with a size of -0.300+0.125 mm was used in the magnetic separation test.

The Pearson correlation results showed that the effect of the parameters on the iron content was ordered as follows: the variable with the highest linear correlation was conveyor speed and the variable with the highest reverse correlation was particle size. In addition, the effect of parameters on the recovery was investigated and the Pearson correlation results were listed as follows: the variable with the highest linear correlation were particle size and splitter and the variable with the highest reverse correlation were conveyor speed and cleaning stage.

It was determined that all parameters conducted in this thesis played a key role to obtain satisfactory results. The efficiency of those parameters on the magnetic separation test (Fe content and recovery) was determined using the ANN method. Modeling studies were performed using three different training algorithms: (i) Bayesian Linear Regression (BR), (ii) Levenberg-Marquardt (LM), and (iii) Scaled Conjugate Gradient (SCG). The LM and SCG models for the estimation of iron value had respectively the highest R (0.996), the lowest RMSE (0.582), the lowest MSE (0.339), and the lowest MAE (0.194) at the training stage. However, when the prediction success in the test phase was evaluated, it was understood that the BR model had the highest R (0.887), the lowest RMSE (4.230), the lowest MSE (17.889) and the lowest MAE (3.477). The LM and SCG models for the estimation of the Recovery value had respectively the highest R (0.998), lowest RMSE (1.695), lowest MSE (2.872), and lowest MAE (0.582) at the training stage. However, when the prediction success in the test phase was evaluated, it was understood that the BR model had the highest R (0.972), the lowest RMSE (6.729), the lowest MSE (45.286) and the lowest MAE (5.418). The results demonstrate the successful application of ANN method in predicting the iron and recovery.

To improve the efficiency of dry magnetic separation process, different scenarios were performed. It was tried to increase the magnetic susceptibility of the ore by conducting microwave treatment at a field of 1800 W for different exposure times. Unfortunately, the changes in the magnetic susceptibility property of the ore was negligible and the use of microwave treatment before the magnetic separation test was found useless. However, the particle size of the sample was important and microwave treatment had a strong effect on the sample with a size of -1+0.500 mm, it was determined that the magnetic susceptibility of the microwave treated sample increased to 4.30 emu/g from 0.16 emu/g.

Considering all obtained experimental results, a flow-sheet was proposed to obtain the magnetic product from the low-grade ore (Figure 5.1). If 100 kg of the ore was used in the proposed magnetic separation process, iron content of the magnetic product with a size of -1+0.500 mm was found to be 56.65% and its weight was calculated as 19.62 kg. On the contrary, the results obtained from the dry magnetic separation test were not satisfactory when the sample with a size of below 0.500 mm. The final magnetic product with a size of -0.500 mm contained 51.14% iron and its weight was found to be 34.08 kg.

For future studies, the following topics are suggested: (i) The modeling of magnetic particles' behavior on the magnetic separator can be investigated. (ii) The sample with a size of <0.500 mm can be ground in a mill and its beneficiation by wet magnetic separator can be investigated.

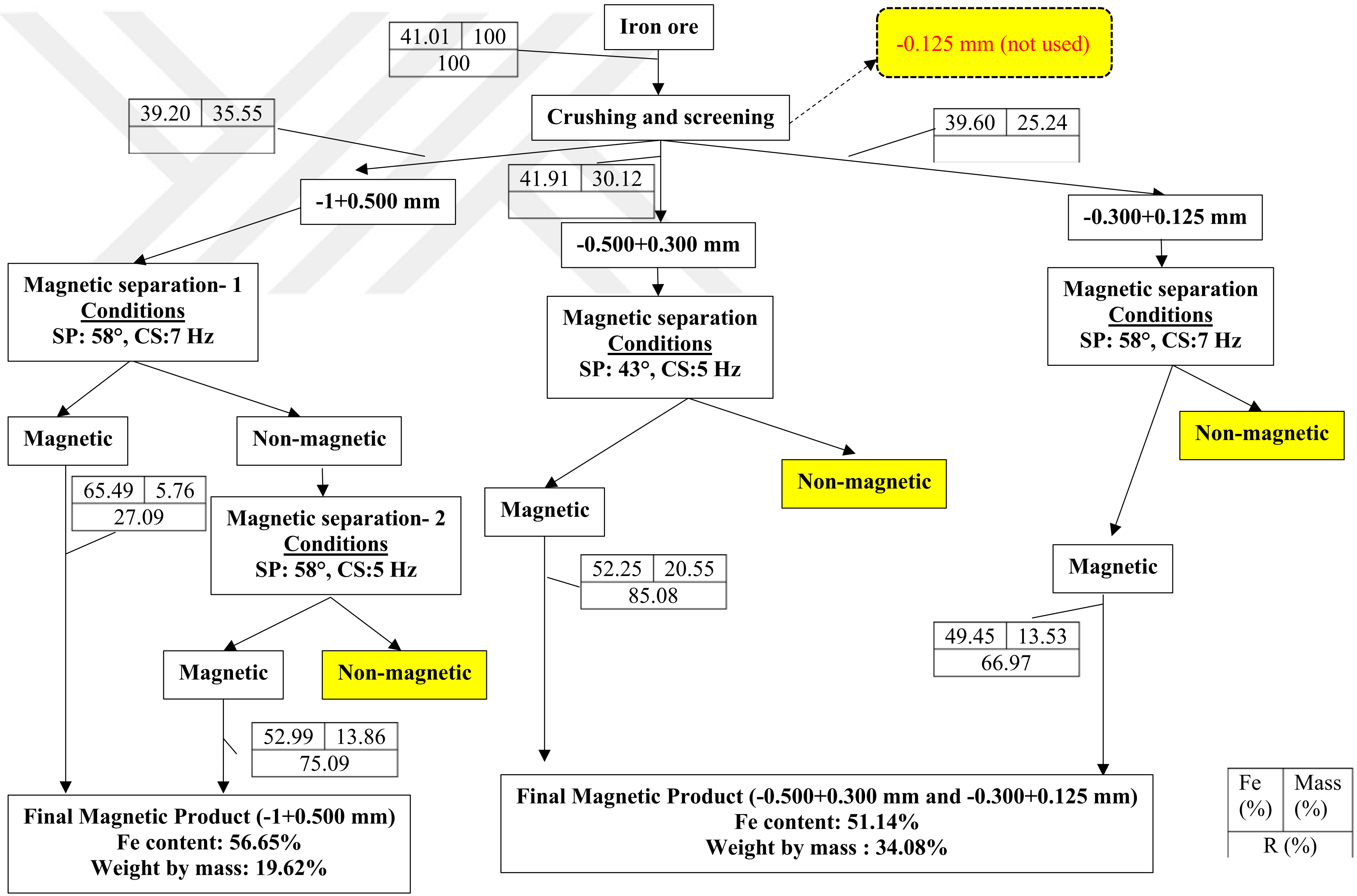

Figure 5.1. A flowsheet proposed for conducting magnetic separation tests to obtain iron concentrate with desired properties from the ore.

REFERENCES

Anonymous 1: https://pubs.usgs.gov/periodicals/mcs2023/mcs2023-iron-ore.pdf [Son erişim tarihi: 06.01.2023)

Ceryan, N. 2014. Application of support vector machines and relevance vector machines in predicting uniaxial compressive strength of volcanic rocks. Journal of African Earth Sciences, 100: 634-644.

Cheng, K. 2007. Development of dry weak magnetic field airflow suspension magnetic separator. . PhD Thesis, Kunming University of Science and Technology, China

Dobbins, M., Dunn, P. and Sherrell, I. 2009. Recent advances in magnetic separator designs and applications. The 7th International Heavy Minerals Conference "What next", The Southern African Institute of Mining and Metallurgy. South Africa

Dwari, R. K., Rao, D. S. and. Reddy, P. S. R. 2013. Magnetic separation studies for a low grade siliceous iron ore sample. International Journal of Mining Science and Technology, 23(1): 1-5.

Gharaei-Manesh, S., Fathzadeh, A., Taghizadeh-Mehrjardi R. 2016. Comparison of artificial neural network and decision tree models in estimating spatial distribution of snow depth in a semi-arid region of Iran. Cold Regions Science and Technology, 122: 26-35.

Gilan, S. S., Jovein H. B. and Ramezanianpour, A. A. 2012. Hybrid support vector regression–Particle swarm optimization for prediction of compressive strength and RCPT of concretes containing metakaolin. Construction and Building Materials, 34: 321-329.

Govindaraju, R.S. 2000. Artificial neural networks in hydrology. Journal of Hydrologic Engineering, 5(2): 124-137.

Hayer, H., Khosravi Nikou, M.R. 2014. Multi-component catalyst desing for oxidative coupling of methane using ANFIS and ANN. Petroleum Science and Technology, 32: 1357-1364.

Kabiru, O. A., Owolabi, T. O., Ssennoga, T. and. Olatunji, S. O. 2014. Performance comparison of SVM and ANN in predicting compressive strength of concrete, IOSR Journal of Computer Engineering (IOSR-JCE), 16(5), 88-94.

Ku, J., Lei, Z., Xia, J., Guo, B., Chen, H., Peng, X., Ran, H. and Deng, R. 2021. Dynamic behavior and separation prediction of magnetic ore bulks in dry medium-intensity magnetic separator. Minerals Engineering 171, 107113.

Levenberg, K. 1944. A method for the solution of certain problems in last squares. Quarterly of Applied Mathematics, 5: 164-168.

Liu, J., D. Lu, Y. Wang, X. Zheng, X. Li and Z. Cheng (2020). Effect of dry magnetic separator on pre-selection of magnetite under wind power. Chin. J. Nonferrous Met 30: 2482-2491.

Liu, L. 2022. The hematite ore liberation and separation properties in different comminution way. Separation Science and Technology, 57(1): 131-140.

Marquardt, D. 1963. An algorithm for least-squares estimation of nonlinear parameters. SIAM Journal on Applied Mathematics, 11(2): 431-441.

Messai, A., Idres, A. and Menendez-Aguado, J. 2020. Application of dry high-intensity magnetic separation in upgrading low-grade iron ore of Rouina deposit, Algeria. Journal of Mining and Metallurgy A: Mining, 56(1): 47-58.

Mishima, F., Yamazaki, S., Yoshida, K., Nakane, H., Yoshizawa, S., Takeda, S., Izumi, Y. and Nishijima, S. 2004. A study on the development of an open-gradient magnetic separator under dry condition. IEEE Transactions on Applied Superconductivity, 14(2): 1561-1564.

Mohanraj, G. T., Rahman, M. R., Joladarashi, S., Hanumanthappa, H., Shanmugam, B. K., Vardhan, H. and Rabbani, S. A. 2021. Design and fabrication of optimized magnetic roller for permanent roll magnetic separator (PRMS): Finite element method magnetics (FEMM) approach. Advanced Powder Technology, 32(2): 546-564.

Naik, P. K. 2002. Quantification of induced roll magnetic separation of mineral sands. Scandinavian Journal of Metallurgy, 31(6): 367-373.

Nunna, V., Hapugoda, S., Eswarappa, S. G., Raparla, S. K., Pownceby M. I. and Sparrow, G. J. 2020. Evaluation of dry processing technologies for treating low grade lateritic iron ore fines. Mineral Processing and Extractive Metallurgy Review, 43(3): 283-299.

Nunna, V., Hapugoda, S., Pownceby, M. I. and Sparrow, G. J. 2021. Beneficiation of low-grade, goethite-rich iron ore using microwave-assisted magnetizing roasting. Minerals Engineering 166, 106826.

Nunna, V., Suthers, S., Pownceby, M. and Sparrow, G. J. 2022. Beneficiation strategies for removal of silica and alumina from low-grade hematite-goethite iron ores. Mineral Processing and Extractive Metallurgy Review, 43(8): 1049-1067.

Omran, M., Fabritius, T., Elmahdy, A. M., Abdel-Khalek, N. A., El-Aref, M. and. Elmanawi, A. E.-H. 2014. Effect of microwave pre-treatment on the magnetic properties of iron ore and its implications on magnetic separation. Separation and Purification Technology, 136: 223-232.

Quast, K. and Skinner W. 2020. Influence of matrix type on WHIMS performance in the magnetic processing of iron ores. Minerals Engineering, 152, 106346.

Ravi Kiran, T. and Rajput, S.P.S.(2011. An effectiveness model for an indirect evaporative cooling (IEC) system: Comparison of artificial neural networks (ANN), adaptive neuro-fuzzy inference system (ANFIS) and fuzzy inference system (FIS) approach. Applied Soft Computing, 11: 3525-3533.

Singh, V., Nag, S. and Tripathy, S. K. 2013. Particle flow modeling of dry induced roll magnetic separator. Powder Technology, 244: 85-92.

Summerfield, D. (2020). Australian Resource Reviews: Iron Ore 2019, Geoscience Australia, Canberra.

Tripathy, S. K., Mohanty, I. and Filippov, L. O. 2020. Application of artificial neural networks to predict dry magnetic separation of low-grade hematite fines. Transactions of the Indian Institute of Metals, 73(7): 1797-1807.

Tripathy, S. K., Singh, V., Murthy R. Y., Banerjee, P. K. and Suresh, N. 2017. Influence of process parameters of dry high intensity magnetic separators on separation of hematite. International Journal of Mineral Processing, 160: 16-31.

Tuncel, S. A., N.Yoleri, B. Şahiner, M. (2017). Dünyada ve Türkiye'de Demir. Ankara, Maden Tektik ve Arama Genel Müdürlüğü, Fizibilite Etütleri Daire Başkanlığı.

Wang, J.; Yuan, Z. Sheng, H. Guangyu, Z. and Shiqing, W 2017. CTFG type dry magnetic separator for powder ore and its application. Mod. Min., 33: 159-161.

Xie, S., Hu, Z. Lu, D. and Zhao, Y. 2022. Dry permanent magnetic separator: present status and future prospects. Minerals, 12, 1251.

Xue, Z., Wang, Y. Zheng, X. Lu, D. and Li, X. 2020. Particle capture of special cross-section matrices in axial high gradient magnetic separation: A 3D simulation. Separation and Purification Technology, 237, 116375.

Yilmaz, I. and Yuksek, G. 2009. Prediction of the strength and elasticity modulus of gypsum using multiple regression, ANN, and ANFIS models. International Journal of Rock Mechanics & Mining Sciences, 46: 803-810.

Yu, H., Wilamowski, B.M. (2011). Levenberg-Marquardt Training. Intelligent Systems. pp. 610, Boca Raton.

Zhang, H., L. Chen, J. Zeng, L. Ding, L. and Liu, J. 2015. Processing of lean iron ores by dry high intensity magnetic separation. Separation Science and Technology 50(11): 1689-1694.

CURRICULUM VITAE

Abdourahman HASSAN BRAHİM FARİSS, graduated from Carmen Rosales science high school in Chad in 2012. He enrolled to Mining Engineering department of Çukurova University in 2016. He graduated from the department of Mining Engineering in 2020 and began his Master of Engineering in 2020 in Mining Engineering department. During his undergraduate studies, he did a compulsory internship about underground mining in AK METAL from July 2019 to August 2019 as a Mining Engineer trainee and another compulsory internship which led to a part-time job in MIRYILDIZ mining from 2020 to present as a Mining Engineer trainee in MIRYILDIZ mining from 2020 to present. He is currently doing some consultancy for some mining companies.